PROCEEDINGS

Chemistry Undergraduate Final Year Project Symposium

2014/2015

Department of Chemistry, Faculty of Science
Universiti Teknologi Malaysia

PROCEEDINGS
Chemistry Undergraduate Final Year Project Symposium 2014/2015

TABLE OF CONTENT

MODIFIED DESILICATED NATURAL ZEOLITE CATALYST FOR KNOEVENAGEL REACTION

Ainatul Mardiah Mat Rapi and Zainab Ramli
Department of Chemistry, Faculty of Science, Universiti Teknologi Malaysia, 81310 UTM, Johor Bahru, Johor

Abstract

Natural zeolite (NaZ) has wide range of usage in agriculture and waste water treatment. However, its application as catalyst has not been widely studied. In this research, natural zeolite was modified its property and applied as base catalyst in the Knoevenagel reaction. The modification was done by desilication in alkaline solution at different temperature followed by ion exchanged with calcium and barium ions of alkaline earth metal. The natural zeolite obtained characterized with XRD showed that desilication results in lowering crystallinity of zeolite crystal while FT-IR showed Si/Al ration of the zeolite framework decrease showing the increase of Al in the framework. The catalyst produced was then tested in Knoevenagel reaction and analyzed by gas chromatography (GC) which showed that barium exchanged desilicated NaZ is more active and highly selective than calcium exchanged NaZ due to its higher basicity.

Keywords: natural zeolite, mordenite, desilication, ion exchange and Knoevenagel reaction

INTRODUCTION

Zeolite is an inorganic crystalline, hydrated alluminosilicate of alkaline and alkaline earth cation consists of infinitely extending 3 dimensional networks of AlO_4^{5-} and SiO_2^{4-} tetrahedral which is linked by oxygen [1]. It has been discovered as a potential material in various industrial applications because it can prevent pollution, environmental friendly substance, conserve raw material and low in production. It can be found in naturally and can be synthesized. Zeolite has a varied application due to its unique characteristic which are the microporous structure that give uniform pore dimension. It allows the hydrocarbon molecule to enter the crystal based on the molecular size. Besides that, zeolite also can develop internal acidity which able to function as catalyst material. In fact, it has high ion exchange capacity and high thermal stability [2]. Therefore, zeolite is able to perform ion exchange reaction and catalyze many reactions which applied in many industrial fields.

The objective of this work is to determine the potential of natural zeolite and modified desilicated natural zeolite as base catalyst in Knoevenagel reaction. Knoevenagel reaction is used in organic synthesis to produce alkenes. Since the reaction can be catalyzed by a variety of solid bases, it could be used as probe reaction to compare basic character of different solids [3]. In this research, the natural zeolite are modified by desilication in alkaline solution and ion exchanged in order to increase the basic properties of the mordenite structure and the catalytic properties or reactivity is investigated using the modified natural zeolite. Both products obtained are characterized using a few instruments. Desilication or base leaching is a selective extraction process of silicon framework by treatment in alkaline solution. In this process, the controlled leaching of Si by OH⁻ form intracrystalline mesopores will facilitate the access and diffusion of molecule in zeolite [4].It will increase the activity, selectivity and lifetime of modified zeolite in catalysis. This modification process will lead to the mesoporosity development of the zeolite structure without distinct modification

EXPERIMENTAL

Desilication with sodium hydroxide solution (NaOH)

Firstly, the solution of sodium hydroxide (3M, Qrec) was prepared by dissolving NaOH pellet (12g) with 10mL distilled water. Then, it was transferred into volumetric flask (100mL) and diluted to the mark. While, the natural zeolite (mordenite, Indonesia) was ground to obtain fine powder using mortar and pestle. Next, the powder was sieved using Laboratory testing sieve of the size 160 μm. Then, the alkaline treatment (desilication) was carried out at room temperature (RT) and 60 °C.

For reaction at room temperature natural zeolite (5g) is added into NaOH solution (100mL, 3M). Next, the mixture was shaken using orbital shaker at the speed of 160 rpm for 24hours. While for the reaction at 60 °C, the mixture of natural zeolite (5g) in NaOH solution (100mL) was stirred with an electrothermal heater using oil bath. The mixture was then separated by filtration using Hirsch funnel. The solid sample obtained was washed with distilled water and dried overnight at 100 °C. The samples were denoted as NaZ-RT and NaZ-60

Ion Exchanged process

For ion exchange process, the barium and calcium solution of 1 M was prepared by dissolving of barium nitrate, $Ba(NO_3)_2$ (26.13g, Bendosen) and calcium nitrate, $Ca(NO_3)_2.4 H_2O$ (26.315g, Qrec) with 10 mL distilled water. Then, each mixture was transferred into the 100 mL volumetric flask and diluted to the mark. After that, the natural zeolite of 60°C (NaZ-60) was added into 250 mL round bottomed flask containing 100 mL prepared solution. The mixture was heated at 60 °C in an oil bath for 24 hours with stirring. Next, the product of barium and calcium exchanged natural zeolite (Ba-NaZ and Ca-NaZ) obtained were filtered with Hirsch funnel and dried in oven. The product obtained were weighed and recorded

Characterization

The modified desilicated natural zeolites and ion-exchanged desilicated natural zeolite were characterized using X-ray Diffraction (XRD, model Brucker Advance D8 diffractometer) to determine the crystalinity and phase of structure. Besides, Fourier Transform Infrared Spectroscopy (FT-IR, Perkin Elmer 1600) was used to measure the bond vibration frequencies and determine the functional group that are presence in the structure. While elemental analysis of sodium, calcium and potassium was carried out by using Atomic Absorption Spectroscopy (AAS, Perkin Elmer) to determine the single element concentration present in the zeolite sample.

Reactivity of the modified natural zeolites catalyst in Knoevenagel Reaction

The Knoevenagel reaction was carried out between benzaldehyde (0.05mol, 2.5g) with the dimethyl maloanate (0.05mol, 4.0g) in the presence of catalyst. The catalyst was first activated at 500°C for 5 hour. After the catalysts added, the mixture was placed in the round bottom flask equipped with condenser. The mixture was heated in oil bath at 120 °C for 24 hours with stirring. The reaction was carried out under nitrogen gas. Then, 1μL of sample before and after the reaction was taken to be analyzed by gas chromatography. When the reaction complete, the product are allowed to cool down and the catalyst was separated out from the solution by filtration. In the Knoevenagel reaction, the sample taken was characterized with the gas chromatography (HP-5 column, Agilent 6890 Series). The components from the chromatogram GC obtained was identified by GC-MSD (Agilent 6890 Series)

RESULTS AND DISCUSSION

The natural zeolite, mordenite undergone modification by desilication and the ion exchange process with barium and calcium ions of alkaline earth metal. Figure 1 presents the XRD of natural zeolite NaZ and the desilicated samples.
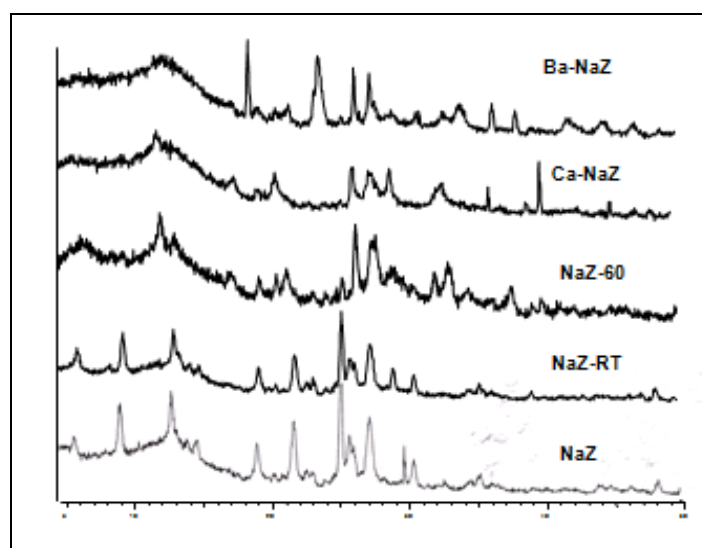
Figure 1 X-ray diffractograms of natural zeolite mordenite (NaZ) and the desilicated modified NaZ samples

From the XRD result, it was confirmed that the natural zeolite used has mordenite phase structure. From the diffractogram, it showed that for desilicated NaZ at room temperature (NaZ-RT) show similar pattern with that

of NaZ. This indicates that there is no significance change to the structure. However, there a slightly change to lower intensities of the peaks after desilication under 60°C was observed. It showed the some zeolite framework structure has collapsed and preferred orientation of atom has changed. The XRD pattern of the barium ion and calcium exchanged desilicated natural zeolite (Ba-NaZ and (Ca-NaZ), shows decreased intensities the peaks and became broader, indicated that some amorphous parts started to form exist in the structure. It can be concluded that the crystalinity of the zeolite decreases from the NaZ > NaZ-RT.> NaZ-60> Ca-NaZ> Ba-NaZ.

Table 1: Percentage of crystallinity and concentration of ions in the natural zeolite and modified natural zeolite samples

Sample	% of Crystalinity	Concentration ion(ppm)				% ion exchanged
		Na^+	K^+	Ca^{2+}	Ba^{2+}	
Natural Zeolite (NaZ)	100	0.2526	0.2844	12.28	-	-
Desilicated natural Zeolite 60°C(NaZ-60)	25.39	2.171	0.1443	4.982	-	100
Calcium ion exchange Natural Zeolite(Ca-NaZ)	18.90	0.3044	0.0527	43.42	-	86
Barium ion exchange natural Zeoite (Ba-NaZ)	16.89	0.4624	0.1688	7.507	0.0020	79

The IR spectra in the Figure 2 support the XRD data. It was observed that there are no significant different between NaZ, and desilicated NaZ-RT and NaZ-60 samples in term of vibration bonding pattern. However, the asymmetric stretching bands for desilicated natural zeolite have shifted to the lower wavelength from the original natural zeolite (1046 cm^{-1}) to 1038 cm-1 for NaZ-RT and 993 cm^{-1} for NaZ-60. This indicates that the amount of framework aluminium has increased in the framework of zeolite.
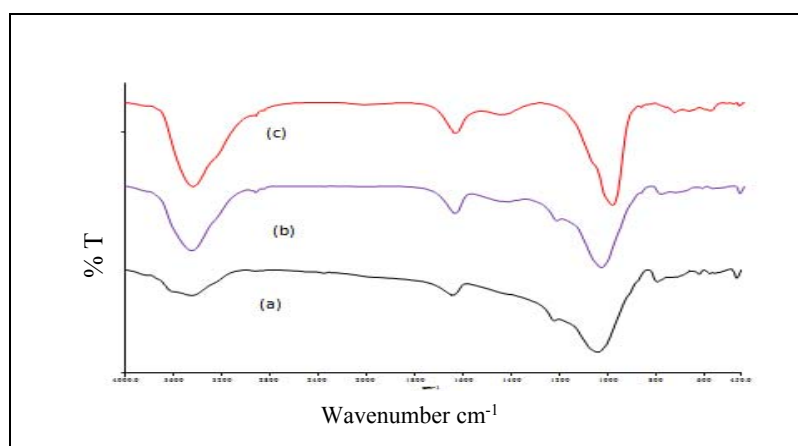
Figure 2 FT-IR spectra of (a) Natural zeolite (NaZ), (b) Desilicated natural zeolite a room temperature (NaZ–RT) and (c) Desilicated natural zeolite at 60 °C (NaZ-60)

From the elemental analysis, it can be calculated that the percentage of ion exchange of NaZ- 60 toward Ca-NaZ and Ba-NaZ are 86% and 78.7%. It showed that the ion exchanged process have been successfully be carried out by replacing sodium with barium and calcium ions.

In order to test the catalytic activity of the modified desilicated zeolite, Knoevenagel reaction had been carried out. The reaction is between benzaldehyde and dimethyl maloanate as illustrated in the equation 1 below:

Results showed that Ca-NaZ catalyst, it gave 20.8% conversion and 63.2% selectivity, while the Ba-NaZ catalyst gave 55.8% of conversion and 100 % of selectivity toward the formation of the dimethyl-2-benzylidenemaloanate (main product). It showed that the barium exchanged natural zeolite (Ba-NaZ) is active than calcium exchanged natural zeolite (Ca-NaZ) as expected since Ba has stronger basicity character than Ca based on its higher conversion. As for the selectivity, highly strength basic property facilitated for higher percentage of selectivity as was shown by the 100% selectivity obtained by Ba-NaZ catalyst.

a) Benzaldehyde
b) Dimethyl maloanate
c) Di methyl 2-benzylidenemaloanate
d) Methyl 3- phenylpropanoate
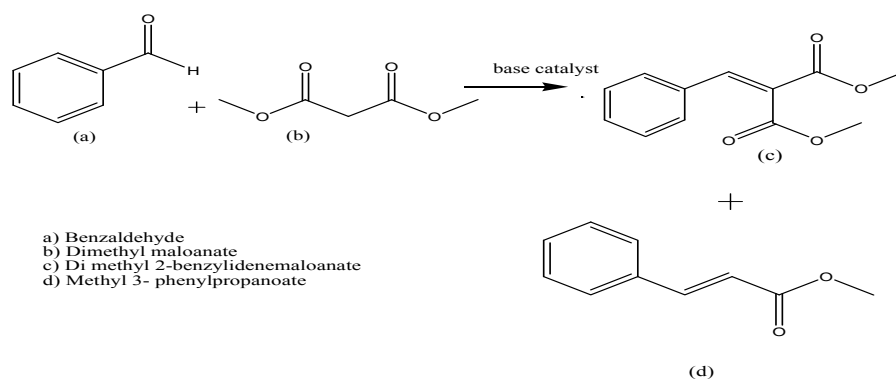
Figure 3 shows the percent conversion and selectivity for Ca-NaZ and Ba-NaZ samples.   This result was obtained from analyzing the chromatogram of the liquid.
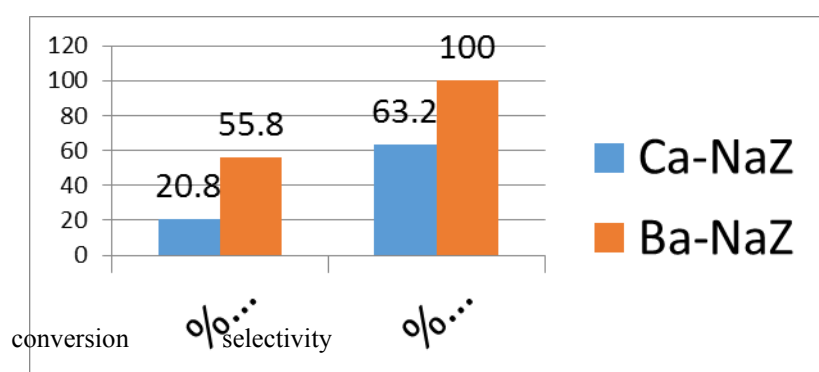
Figure 4 :   Percent conversion and selectivity of Ca-NaZ and Ba-NaZ catalysts for Knoevenagel reaction between benzaldehyde and dimethyl maloanate.

CONCLUSION

The modifications of the natural zeolite are successfully done by the desilication followed by ion exchanged process. Characterization on the desilicated NaZ shows the increased of Al in the zeolite framework which then enhanced the number of ions balancing the anionic zeolite framework hence increased the basicity of the ion exchanged desilicated NaZ catalysts. Reactivity of the catalysts for Knoevenagel reactions showed that the barium exchanged desilicated NaZ was more reactive than calcium exchanged desilicated NaZ with higher selectivity due the higher basicity of barium than calcium ion.

REFERENCES

1.   L.S.Gadekar, Katakar, S. S., & K.N.Vidahate. (2008). Modification, characterization and catalytic potency of modified natural zeolite Knoevenagel reaction. *Buletin of Catalysis Society of India*, 76-83.
2.   Bekkum, H. V., Flanigen, & Jansen, J. C. (1991). Introduction to Zeolite Science And Practice 58: Elsevier Science Amsterdam.
3.   Linares, C. F., Goldwasser, M. R., Machado, F. J., Rivera, A., Rodriguez-Fuantes, G., & Barrault, J. (2000). Advantages of base exchanged Natural Clinoptilolite as Catalyst for Knoevenagel Reaction. *Microporous and Mesoporous Materials, 41*, 69-77
4.   Bonilla, A., Baudouin, D., & Pérez-Ramírez, J. (2009). Desilication of ferrierite zeolite for porosity generation and improved effectiveness in polyethylene pyrolysis. *Journal of Catalysis*, 170-180

CHEMICAL CONSTITUENTS AND ANTIOXIDANT ACTIVITY OF *GARCINIA PARVIFOLIA* MIQ. STEM BARK

Muhammad Aizam Hassan, NorazahBasar, Farediah Ahmad
Department of Chemistry, Faculty of Science, UniversitiTeknologi Malaysia, 81310 Johor Bahru.

Abstract

The chemical constituents of *Garciniaparvifolia*Miq.stem bark have been studied. The dried samples have been extracted using Soxhlet apparatus to give the crude products. The constituents were separated and purified by using vacuum column chromatography, gravity column chromatography and recrystallisation. The chemical compounds obtained were elucidated by infrared (IR) and nuclear magnetic resonance (NMR) spectroscopy. Two compounds namely as 1,6,7-trihydroxy-3-methoxyxanthone and 3,8"-binaringenin were isolated from the ethyl acetate crude extracts of *G. parvifolia*Miq. The free-radical scavenging activity of the crude extracts were determined by the 2,2-diphenyl-1-picrylhydrazyl (DPPH) assay. The ethyl acetate extract was found to be the most active free radical scavenger with IC_{50} value of 4.2 ppm, followed by methanol extract (IC_{50} 96 ppm) and petroleum ether extract (IC_{50} 200 ppm).

Keywords: *GarciniaparvifoliaMiq.,stem bark, 1,6,7-trihydroxy-3-methoxyxanthone, 3,8"-binaringenin.*

INTRODUCTION

*Garciniaparvifolia*Miq.is one of the species from Clusiaceae (Guttiferae) family distributed widely in the tropical region of the world and has high potential as spice and value medicinal plants. Clusiaceae family have 36 genera and 1,600 species with a pan tropical distribution. Four genera and 16 species are native to Australia and three genera and five species are found in the Northern Territory, Australia. Three genera were reported as *Calophyllum*L., *Garcinia*L., and *Hypericum*L. The Clusiaceae (Guttiferae) family is part of Malpighiales and Clusioideae as the subfamily [1]. In peninsular Malaysia there are 49 Garcinia species out of 350 species estimated, which include *Garciniaatroviridis*, *G. cowa, G. morella, G. lanceaefolia, G. hombroniana, G. prainiana*and *G. mangostana* [2,3].

   GarciniaparvifoliaMiq is known as "asamkandis" and it has white colour with taste like mangosteen which is the most famous fruit in Malaysia [4]. Previous study on *G. parvifolia*Miq.reportedthe presence of xanthones as the major chemical constituents together with triterpenes, bioflavonoids and benzophenones. Moreover, *G. parvifoliaMiq*showed *several* biological activities *included antioxidant, antibacterial, cytotoxicand antiplasmodial activities [5]. In this paper, we report the isolation of two chemical constituents from the stem bark of GarciniaparvifoliaMiq. and the antioxidant assay on the crude extracts.*

EXPERIMENTAL

General Experimental Procedures

Thin layer chromatography (TLC) analysis was done using Merck 60 F_{254} pre-coated silica gel aluminium sheet with thickness of 0.20 mm with different polarity of solvent system. The spots on the TLC plate was visualized by UV lamp (254 nm) and sprayed with vanillin-sulphuric acid spraying reagent. Fractionation and purification process was carried out by using vacuum liquid chromatography (VLC) and gravity column chromatography (CC) with different size of silica gel as stationary phase. Silica gel 230-400 mesh was used for VLC, while silica gel 70-230 mesh was used for gravity column chromatography (CC) with different polarity of solvent as the mobile phase. Elucidation of pure compounds was obtained by infrared (IR) and Nuclear Magnetic Resonance (NMR) spectroscopies. The IR spectra were measured using Perkin-Elmer Spectrum Two (ATR), while ^{1}H NMR spectra were recorded by BrukerAvance Spectrometer 400 MHz with deuterated chloroform (CDCl$_3$) and acetone (acetone-d$_6$) as solvents.

Plant Material

The stem barks of *G. parvifolia*Miq. with voucher specimen number SK 1961/11 was obtained from Sekayu Forest Reserved in Kuala Berang, Terengganu, Malaysia in June 2011.

Extraction and Isolation

Soxhlet extraction method was performed on the dried stem bark (800 g) of *G. parvifolia*with three different solvent starting with petroleum ether, ethyl acetate and methanol for 8 hours each. The extracts were filtered out and concentrated using rotary evaporator to afford the petroleum ether, ethyl acetate, and methanol crude extracts.

The ethyl acetate crude extract (7.29 g) was fractionated by using VLC to give ten fractions (1-10). The crude extract was eluted with *n*-hexane, ethyl acetate and methanol. Fraction 6 (1.41 g) was further purified using CC and eluted with *n*-hexane and chloroform to give seventeen subfractions (1-17). Subfraction 14 give yellow solid of 1,6,7-trihydroxy-3-methoxyxanthone (**1**) (1.3 mg, 0.02%). While, subfraction 17 was then further purified using Sephadex LH-20 which resulted the isolation of 3,8"-binaringenin (**2**) (30 mg, 0.41%) as light brown amorphous powder.

1,6,7-Trihydroxy-3-methoxyxanthone (1)

Yellow solid, m.p. 212-214°C (Ref: 213-216°C), R_f= 0.58 (*n*-hexane:acetone = 1:1): IR (neat) v_{max} cm^{-1}: 3332.3 (O–H), 2922.1 (sp^3 C–H), 1646.4 (C=O), 1608.3 and 1485.0 (C=C aromatic), 1159.5 (C–O); ^{1}H NMR (acetone-d$_6$, 400 MHz) : 13.18 (1H, br s, 1-OH), 6.25 (1H, d, *J*= 2.0 Hz, H-2), 6.41 (1H, d, *J* = 2.0 Hz H-4), 6.95 (1H, s, H-5), 7.56 (1H, s, H-8), 3.99 (3H, s, OCH$_3$), 9.85 (1H, br, s, 6-OH, 7-OH).

3,8''-Binaringenin (2)

Light brown amorphous powder, m.p. 220-225°C (Ref: 220-225°C), R_f= 0.5 (*n*-hexane:acetone = 2:3); IR (neat) v_{max} cm^{-1}: 3180.2 (O–H), 2924.7 (sp^3 C–H), 1630.6 (C=O), 1596.4 and 1442.8 (C=C aromatic), 1158.7 (C–O), ^{1}H NMR (acetone-d$_6$, 400 MHz): 5.87 (1H, m, H-2), 4.72 (1H, m, H-3), 12.20 (1H, m, 5-OH), 5.98 (1H, br s, H-6, H-8), 7.23 (1H, br s, H-2', H-6'), 6.75 (1H, br s, H-3', H-5'), 5.33 (1H, m, H-2''), 2.69 (1H, m, H-3''a), 2.78 (1H, m, H-3''b), 12.31 (1H, m, 5''-OH), 5.93 (1H, br s, H-6''), 6.82 (1H, br s, H-2''', H-6'''), 6.91 (1H, m, H-3''', H-5''').

Free Radical Scavenging Activity (DPPH) Assay

The free radical scavenging activity with 1,1-diphenyl-2-picrylhydrazyl (DPPH) was tested on petroleum ether, ethyl acetate and methanol crude extracts and butylated hydroxytoluene (BHT) which used as a positive control. A volume 170 µL sample solution (1000 ppm) of all crude extract and BHT were diluted into 1000, 500, 250, 125, 62.5 and 31.8 µg/mL solution using methanol. A volume 30 µL of DPPH in methanol solution (300 µM) was added to different concentrations of sample solutions and was reacted until 30 min. at room temperature.

The absorbance of the reaction mixtures was recorded at wavelength 517 nm. Measurements of all samples were performed in triplicates and the average values were calculated. The percentage of antioxidant activity was calculated using the equation below:

$$\% \text{Scavenging} = \frac{[\text{Abs}（\text{control}) - \text{Abs}（\text{DPPH} + \text{sample})]}{\text{Abs(control)}} \times 100\%$$

The significant radical scavenging activities of extracts can be determined when a reduction greater than that produced by 10 µM BHT and were evaluated for IC$_{50}$ (the concentration of the sample at 50% inhibition). The concentration of the sample at 50% inhibition (IC$_{50}$) was obtained from the graph percentage inhibition against concentration in µg/mL.

RESULTS AND DISCUSSION

Soxhlet extraction method using non-polar to polar solvents was carried out on the stem bark of *Garciniaparvifolia*. The extraction process was started with petroleum ether, ethyl acetate and methanol for 8 hours each. Methanol was used to ensure that all compounds were extracted from the stem bark of *G. parvifolia.* The extracts were filtered out and concentrated using rotary evaporator to afford yellow petroleum ether, brown ethyl acetate and dark brown methanol of crude extracts with yield of 2.85 g (0.36%), 8.62 g (1.08%) and 13.26 g (1.66%), respectively.
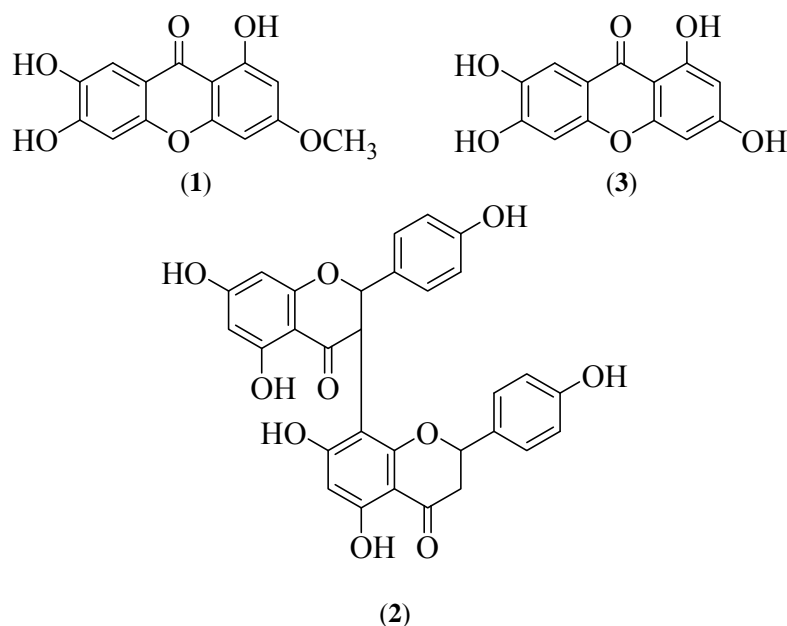
1,6,7-Trihydroxy-3-methoxyxanthone (**1**) (1.3 mg, 0.02%) was yielded as yellow solid and the TLC spot shows green after sprayed with vanillin-sulphuric acid spraying reagent and this compound was predictable to have xanthone moiety. The compound had R_f= 0.30 (*n*-hexane:Et_2O = 3:2) and melting point value 212-214°C (Ref: 213-216°C). Based on IR and ^{1}H NMR, the compound was identified as 1,6,7-trihydroxy-3-methoxyxanthone (**1**).The absorption at 2922.1 cm^{-1} and 1646.4 cm^{-1} were attributed to sp^3 C–H and conjugated C=O ketone, respectively. The absorption at 1608.3 cm^{-1} and 1485.0 cm^{-1} indicated to C=C aromatic and 1159.5 cm^{-1} for C-O band. The ^{1}H NMR spectrum showed characteristics of xanthone pattern based on a chelated hydroxyl group presence at the downfield region. A singlet signal observed at δ 3.99 was assigned to a methoxy group, 3-OCH_3 while singlet at δ 13.18 was due to a chelated hydroxyl group, 1-OH. A doublet at the downfield region of δ 9.85 was assigned to two hydroxyl groups attached to the aromatic ring, 6-OH and 7-OH. While, two doublet peaks at δ 6.25 and δ 6.41 with *J* value of 2.0 Hz corresponded to the presence of two *meta*-coupled aromatic protons, H-2 and H-4. The comparison with literature data show that 1,6,7-trihydroxy-3-methoxyxanthone (**2**) provide similar pattern of ^{1}H NMR spectrum with norathyriol(**3**) which was isolated previously from the twigs of *G. hombroniana*and *G. parvifolia*[6]. ^{1}H NMR spectra of 1,6,7-trihydroxy-3-methoxyxanthone(**1**) and norathyriol(**3**) were very similar except for the different substituents (hydroxyl and methoxy) bonded to the aromatic ring. Norathyriol(**3**) had four hydroxy groups whereas 1,6,7-trihydroxy-3-methoxyxanthone(**1**) had three hydroxy groups and one methoxy groups. Table 1 shows comparison of ^{1}H NMR data between 1,6,7-trihydroxy-3-methoxyxanthone (**1**) andnorathyriol(**3**).

Table 1:   Comparison of the ^{1}H NMR Data 1,6,7-trihydroxy-3-methoxyxanthone(**2**) with Norathyriol(**3**)

Carbon	1,6,7-Trihydroxy-3-methoxyxanthone(**2**) $δ_H$ (ppm)	Norathyriol(**3**) $δ_H$ (ppm)
1	13.18 (1H, br s, OH)	13.26 (1H, br s, OH)
2	6.25 (1H, d, *J* = 2.0 Hz)	6.18 (1H, d, *J* = 1.7 Hz)
3	3.99 (3H, s, OCH_3)	-
4	6.41 (1H, d, *J* = 2.0 Hz)	6.37 (1H, d, *J* = 1.7 Hz)
4a	-	-
5	6.95 (1H, s)	6.85 (1H, s)
6	9.85 (1 H, br s, OH)	-
7	9.85 (1 H, br s, OH)	-
8	7.56 (1H, s)	7.39 (1H, s)
8a	-	-
9	-	-
9a	-	-
10a	-	-

3,8"-Binaringenin (**3**), a light brown amorphous powder which gave an orange spot on the TLC after sprayed with vanillin-sulphuric acid spraying reagent was recognised having a biflavonoid skeleton. The compound had R_f= 0.50 (*n*-hexane:Et_2O = 3:2) and melting point value m.p 220-225°C (Ref: 220-225°C). The compound was identified as 3,8"-binaringenin (**4**) based on previous study on *Garciniagriffithi*T.Anderson [7]. The IR spectrum showed a broad absorption band of OH group at 3180.2 cm^{-1}. The absorption of C-H sp^3 and conjugated C=O ketone were observed at 2924.7 cm^{-1} and 1630.6 cm^{-1}. Strong absorption band at 1596.4 and 1442.8 cm^{-1} was corresponded to the C=C aromatic while, absorption at 1158.7 cm^{-1} attributed to the presence of C-O bond. Analysis of the ^{1}H NMR spectrum showed characteristics of bilavonoids pattern based on a chelated hydroxyl group presence at the downfield region. The ^{1}H NMR spectrum showed the most deshielded peaks resonated at δ 12.20 and 12.31 corresponded to two chelated hydroxyl groups, 5-OH and 5"-OH, respectively which indicative a biflavonoid compound. Six sets of multiplets resonated at δ 2.69, 2.78, 4.72, 5.33, 6.91 were assigned for H-3", H-3, H-2", H-5'", H-2, respectively. Five singlet peaks were observed at δ 5.98, 7.23, 6.75, 5.93, 6.82 were assigned to protons bonded to the aromatic rings H-6, H-8, H-2', H-6', H-3', H-5', H-6", H-2'", H-6'", respectively.

Antioxidant activities of the crude extracts were tested using radical scavenging DPPH method. The ethyl acetate extract was found to be the most active free radical scavenger with IC_{50} value of 4.2 ± 0.61 ppm, followed by methanol extract (IC_{50} 96 ± 4.93ppm) and petroleum ether extract (IC_{50} 200 ± 11.55 ppm). The ethyl acetate extract display the most active antioxidant property due to the existence of bulk polar compounds in the extract such as xanthones and bioflavonoids which contribute to the antioxidant activity [8].

(1)

(3)

(2)

CONCLUSIONS

Purification of the crude extracts from the stem bark of *G. parvifolia*were successfully isolated two chemical compounds, identified as 1,6,7-trihydroxy-3-methoxyxanthone (**1**) and 3,8"-binaringenin (**2**)from the ethyl acetate crude extract.

Antioxidant activity was tested by 2,2-diphenyl-1-picrylhydrazyl (DPPH) assay on the petroleum ether, ethyl acetate and methanol crude extracts. The ethyl acetate extract was found to be the most active free radical scavenger with IC_{50} value of 4.2 ± 0.61 ppm due to the bulk amount of phenolic compounds present in the extract, followed by methanol extract (IC_{50} 96 ± 4.93 ppm) and petroleum ether extract (IC_{50} 200 ± 11.55 ppm).

REFERENCES

1. R.A. Kerrigan, I. D. C. and D. J. D. (2011). Flora of The Darwin Region. Vol. 1. Australia: National Library of Australia. 1-7
2. Borthakur, S. B. and S. K. (2012). Studies on Morphology and Ethnobotany of Six Species of *Garcinia*L. (Clusiaceae) Found in the Brahmaputra Valley, Assam, India. *Journal of Natural Product Plant Resources* **2**(3): 389-396.
3. Khare, C. P. (2007). *Indian Medicinal Plants*. India: Springer Science Business Media. 277-280
4. Ali Hassan, S. H., Fry, J. R., & Abu Bakar, M. F. (2013). Phytochemicals Content, Antioxidant Activity and Acetylcholinesterase Inhibition Properties of Indigenous *Garciniaparvifolia* Fruit. *BioMed Research International*, *2013*.
5. Kumala, S., &Sutaryo, B. (2007). Screening of some extracts from Garciniaparvifoliamiq.(Guttiferae) for antiplasmodial, antioxidant, cytotoxic and antibacterial activities. *Asian Journal of Plant Sciences*.
6. Nargis Jamila (2013) Phytochemical and Biological Activity Studies of *Garciniahambroniana*UniversitiSainsMalaysia : Thesis of Doctor of Philosophy.
7. NikSyazwaniAfifahNikSazali (2014). Chemical Constituents and Bioactivities of *Garciniagriffithi*T.AndersonUniversitiTeknologiMalaysia : Thesis of Degree of Master.
8. Zhao, Y., Liu, J.-P., Lu, D., Li, P.-Y., and Zhang, L.-X. (2010). A New Antioxidant Xanthone from the Pericarp of *Garciniamangostana* Linn. *Natural Product Research* **24**(17): 1664-1670.

CHEMICAL CONSTITUENTS AND ANTIOXIDANT ACTIVITY FROM THE RHIZOMES OF *ZINGIBER CASSUMUNAR*

Nurul Amila Fadhlin Baharuddin and Hasnah Mohd Sirat
Department of Chemistry, Faculty of Science, Universiti Teknologi Malaysia, 81310 Johor Bahru

Abstract

Zingiber cassumunar is one of the species belongs to the genus of *Zingiber* in the Zingiberaceace family. Hydrodistillation of fresh rhizomes afforded 2.83% of essential oil as a pale yellow liquid with pungent smell. Chemical compositions of the oils were determined by gas chromatography and gas chromatography-mass spectrometry techniques. Twenty-nine compounds were found in the rhizome essential oil which contributed to 78.74% of the total oil. The compounds have been classified as monoterpenes (75.9%), sesquiterpenes (1.8%) and ester (0.8%). The major constituents were found to be terpinen-4-ol (31.35%) **(1)** and sabinene (23.37%)**(2)**. The dried rhizome of *Z. cassumunar* was also extracted with chloroform using Soxhlet extraction for twenty hours. Fractionation of the crude extract using silica gel vacuum liquid chromatography, followed by repeated purification using silica gel gravity column chromatography afforded two compounds. The structure of these compounds were elucidated by infrared and nuclear magnetic resonance spectroscopies as *trans*-1-(3,4-dimethoxyphenyl)butadiene **(3)**and *trans*-4-(3,4-dimethoxyphenyl)but-3-en-1-yl acetate**(4)**. DPPH antioxidant screening using DPPH free radical scavenging activity showed that the essential oil of the rhizome of *Z. cassumunar* gave weak antioxidant property and chloroform crude extract gave positive antioxidant result at higher concentration.

Keywords: Zingiberaceace, Zingiber cassumunar, essential oil, crude extract, DPPH

INTRODUCTION

Herbs have long been used in traditional medicine in various cultures throughout the world [1]. The phytochemicals constituents of herb plants play an important role as a prevention and therapy in human health and development [2]. Zingiberaceace is one of the largest families of plant kingdom that established traditional forms of medicine to treat various kinds of diseases [3, 4]. This species is native to East Asia and it is one of the herbaceous ground floras of the rainforest component in Peninsular Malaysia [5]. The members from this family provide many useful food products, perfumes, medicines, ornamentals and other economic uses [4].

*Zingibercassumunar*is one of the genus fromZingiberaceace familythat has been widely known as a medicinal plant and folklore remedies [6]. This plant is native plant of India and is now widely cultivated in tropical Asia. It occurs widely as a home-garden plant in Southeast Asia [7]. *Z. cassumunar* has a pungent odour, and foul-smelling flowers. It is common to be known as *'bonglai'* in peninsular Malaysia, *'bangle'* in Java and *'Plai'* in Thailand [8]. The rhizomes are very rich in essential oil. The oil has a pale amber color, cool scent and a green peppery odour with a touch of a bite [9]. *Z. cassumunar*was claimed to have various functions in folklore medicine as its essential oil has medicinal properties which is used in medical field for various treatment. The pungent components are proven beneficial in treating health problems and protection against certain diseases. Another pharmacological study had discovered that the rhizome of *Z. cassumuna r*provide an antioxidant activity which gave useful usage in medical field [10].Within the scope of continuation search for bioactive compounds from natural plants, the rhizomes of *Z. cassumunar* were further investigated. In this paper, we report the isolation and structural elucidation of chemical constituents of the essential oil as well as the crude extract from the rhizome of *Z. cassumunar*. In addition, both essential oil and the crude extract were evaluated for their antioxidant activity.

EXPERIMENTAL

Vacuum liquid chromatography (VLC) was carried out on Merck silica gel 230-400 mesh using distillated petroleum ether 60-80ºC and diethyl ether as eluent system with increasing polarity to give of fractions. Purification of the compounds were carried out by using column chromatography which used Merck silica gel 70-230 nm as the stationary phase, eluted with a eluents mixture of petroleum ether and diethyl ether and mixture of *n*-hexane and diethyl ether. Thin layer chromatography (TLC) was carried out using aluminium sheet coated with 0.20 mm Merck silica gel plates (60 F_{254}). The spots on the TLC plates were visualised by Ultraviolet (UV) radiation with wavelength of 254 nm and 365 nm. Vanillin sulphuric acid reagent was used to spray the TLC plate in the TLC analysis. This reagent was sprayed on the TLC plate and heat at 100ºC to visualise the spots. Gas chromatography was carried out using Hewlett-Packard gas chromatography with Ultra 1 column (dimethylpolysiloxane) (0.2 mm internal diameter, 0.32 μm thickness and 25 m long). The carrier gas used is Helium with rate flow 1.0 mL/min. Operating temperature for GC was 50ºC to 300ºC with rate by 4ºC

per minute. The type of detector used was Flame Ionization detector (FID). The chemical composition from the essential oil of the rhizome was identified using gas chromatography-mass spectrometry (GC-MS) equipped with Wiley/NIST Registry of Mass Spectral Library, 7th edition 1999. HP 19092A-102 Hewlett-Packard gas chromatography was used with Ultra 1 capillary column (0.2 x 0.32 x 35 mm). Helium gas is the carrier gas with flow rate 1.0 mL/min and the oven temperature was programmed to increase after 5 minutes to 50% and continuously heated until 250ºC at a rate of 5ºC /min. The end temperature was held for 5 minutes. The chromatogram was compared with the Kovats Indices reference and MS libraries. Infrared (IR) spectra were measured using Perkin-Elmer Series 1600 using (NaCl) pellet for liquid samples. The ^{1}H NMR spectra were recorded on BrukerAvance 400 MHz with $CDCl_3$ as solvent. Residual proton in $CDCl_3$ was used as standard.

Plant Material

The fresh rhizome of *Z. cassumunar* was purchased from a wet market in Larkin, Johor Bahru. The rhizomes were washed and chopped into small pieces. The rhizomes were kept in dried conditions.

Extraction of Essential Oil

The fresh rhizomes of *Z. cassumunar*(310 g) were hydrodistilled in an all glass apparatus using Dean-Stark apparatus for 8 hours. The essential oil collected was extracted with ether (3 x 5 mL), dried over anhydrous magnesium sulphate and filtered. The ether was then evaporated at room temperature overnight to give essential oil (8.78 g) as pale yellow liquid with pungent smell. The essential oil was stored at 4ºC in the air- tight container until further analysis.

Extraction of Chloroform Crude Extract

The air-dried rhizomes (214.6 g) were ground and extracted in a 2 L Soxhlet extractor using chloroform (1.5 L) for 20 hours. The resulting extract was filtered and concentrated using rotary evaporator to yield crude extract (27.6 g) as brownish yellow viscous liquid with pungent smell. The extract *Z. cassumunar*(14.1 g) was fractionated using vacuum liquid chromatography on Si gel (200 g) and eluted with increasing polarity of the solventsto give twenty six fractions. Fraction 10 (0.28 g) from the VLC was further purified using column chromatography with Si gel 70-230 (7.0 g) and eluted using *n*-hexane and ether with increasing polarity to give 60 fractions. Fractions with similar TLC profile were combinedto afford**(3)**(0.025 g) as a pale yellow viscous liquid with R_f value 0.70 in *n*-hexane: ether (1:1). Fractions 19 to 21 (1.4) g were combined and further purified by column chromatography using petroleum ether: ether with increasing polarity to give 190 fractions. Fractions that showed similar TLC profile were recombined and evaporated to afford**(4)** (0.106 g) as a pale brown viscous liquid, $R_f$value0.38 in PE: E (3:2).

Free Radical Scavenving Activity (DPPH) Assay

The radical scavenging activity using1,1-diphenyl-2-picryhydrazyl (DPPH) was carried out on the sample essential oil and $CHCl_3$ crude extract with the ascorbic acid as the positive standard. Sample stock solution (1.0 mg/mL) of sample essential oil and $CHCl_3$ crude extract were diluted to final concentration using methanol (CH_3OH) solvent. Methanolic solution was added to different concentration sample solutions and was to react for 30 minutes at room temperature.After 30 minutes, the absorbance of the reaction mixtures was recorded at 517nm. All test and analysis were run triplicates and average values were calculated. Percentage of antioxidant activity was calculated using the following equation:

$$\% \text{ Scavenging} = \frac{|Abs (control) - Abs (DPPH) + sample|}{Abs (control)} \times 100\%$$

RESULTS AND DISCUSSIONS

Chemical Composition of essential oil

The hydrodistillation extraction of the fresh rhizome of *Z. cassumunar* (310 g) using Dean-Stark apparatus for 8 hours gave the essential oil (8.78 g) a pale-yellow liquid. The essential oil was analysed using the GC and GC-

MS with an Ultra 1 GC capillary column. The mass spectrum of each peak was compared with Wiley Library Data and Kovat Indices with literature values. Table 1 shows twenty four constituents in the rhizome oil which contributed 78.47% of the oil. The oil comprised of monoterpenes 75.9%, sesquiterpenes 1.8% and ester 0.8%. The major constituents were found to be terpinen-4-ol **(1)**(31.35%) and sabinene**(2)**(23.37%).
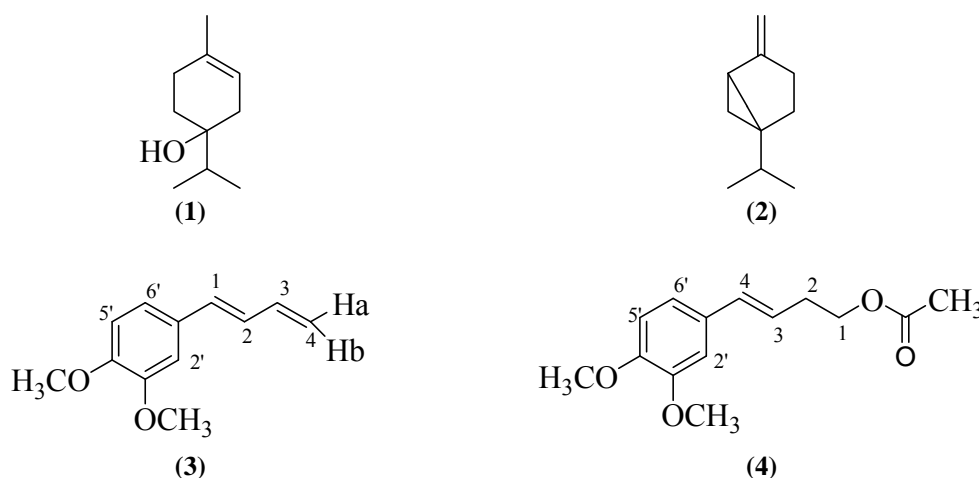
Table 1: Chemical composition of essential *Zingibercassumunar* from GC

No	Retention Time, t_R	KI	Compound	MW	Molecular Formula	% Area,
1	9.68	923	α-Thujene	136	$C_{10}H_{16}$	0.49
2	9.87	929	α-Pinene	136	$C_{10}H_{16}$	1.20
3	10.28	942	Camphene	136	$C_{10}H_{16}$	0.06
4	11.20	968	Sabinene	136	$C_{10}H_{16}$	24.37
5	11.26	970	β-Pinene	136	$C_{10}H_{16}$	2.72
6	11.81	985	Myrcene	136	$C_{10}H_{16}$	0.58
7	12.59	1006	α-Terpinene	136	$C_{10}H_{16}$	2.92
8	12.71	1011	*p*-Cymene	136	$C_{10}H_{16}$	0.98
9	12.92	1018	β-Phellandrene	136	$C_{10}H_{16}$	0.74
10	12.20	1020	Limonene	136	$C_{10}H_{16}$	0.61
11	13.96	1051	γ-Terpinene	136	$C_{10}H_{16}$	5.58
12	14.08	1054	*cis*-Sabinene hydrate	154	$C_{10}H_{18}O$	1.46
13	14.90	1079	Terpinolene	136	$C_{10}H_{16}$	0.58
14	15.02	1082	2,6-dimethyl-2,7-octadiene-6-ol	154	$C_{10}H_{18}O$	1.09
15	15.79	1105	*trans*-Menth-2-en-1-ol	154	$C_{10}H_{18}O$	0.65
16	16.32	1124	*cis*-Menth-2-en-1-ol	154	$C_{10}H_{18}O$	0.43
17	17.57	1166	Terpene-4-ol	154	$C_{10}H_{18}O$	31.35
18	17.92	1177	(Z)-4-Hexenyl Butyrate	170	$C_{10}H_{18}O_2$	0.02
19	17.96	1179	α-Thujanol	150	$C_{10}H_{14}O$	0.02
20	28.09	1572	Caryophellene Oxide	220	$C_{15}H_{24}O$	0.14
21	26.19	1491	Zingibrene	204	$C_{15}H_{24}$	0.56
22	26.72	1513	β-Sesquiphellandrene	204	$C_{15}H_{24}$	1.11
23	27.77	1559	(E)-1-(3,4-dimethoxyphenyl)but-1-ene)	190	$C_{12}H_{14}O_2$	0.04
24	28.709	1598	(E)-1-(3,4-dimethoxyphenyl)buta-1,3-diene)	190	$C_{12}H_{14}O_2$	0.78

Chemical components of chloroform crude extract

The dried powder rhizomes of *Z. cassumunar* (214.6 g) were extracted by Soxhlet extraction using chloroform as the solvents for 20 hours. Evaporation of the solvent yielded (27.6 g, 12.8%) as a brown viscous liquid with pungent smell crude extract.

Trans-1-(3,4-dimethoxyphenyl)butadiene **(3)**was obtained from the purification of the chloroform crude extract as a pale yellow viscous liquid with R_f values 0.70 in *n*-hexane: ether (1:1) which suggested as a non-polar compound. The IR spectrum of the *trans*-1-(3,4-dimethoxyphenyl)butadiene **(3)** showed characteristic bands for *sp²* =CH at 3019 cm⁻¹, *sp³* C-H stretching at 2962 and 2936 cm⁻¹ strong absorption of C-O stretching at 1265 and 1216 cm⁻¹, strong absorption at 1597 cm⁻¹ showed conjugation of C=C alkenes stretching, 1508 and 1465 cm⁻¹ aromatic stretching. Analysis of ¹H NMR spectrum revealed the characteristic signals of two methoxyl groups (OCH₃) in compound **(3)** as two singlet signals at δ 3.90 and 3.93. The peaks for H-1 and H-3 were overlapping to each other at δ 6.51 which showed the coupling between olefenic protons. A doublet signals (*J* = 9.6 Hz) at δ 5.15 indicated the *cis*position H-4a and δ 5.31 (*J*= 16.5 Hz) H-4b to the H-3 resonance at δ 6.45. The signal for H-2 which is *trans* position to H-1 (*J* = 15.9 Hz) at δ 6.52 and coupling in acyclic dienes to H-3 (*J* = 10.8 Hz) at δ 6.45 was demonstrated by a doublet of doublet multiplicity at δ 6.70. A doublet with (*J*= 8.1 Hz) at δ 6.85 was assigned to H-5' that showed an *ortho*-coupling with H-6'. A doublet of doublet with (*J*= 8.1 and 1.8 Hz) at δ 6.95 was attributed to H-6', while *meta*-coupled proton with (*J*= 1.8 Hz) was assigned to H-2.
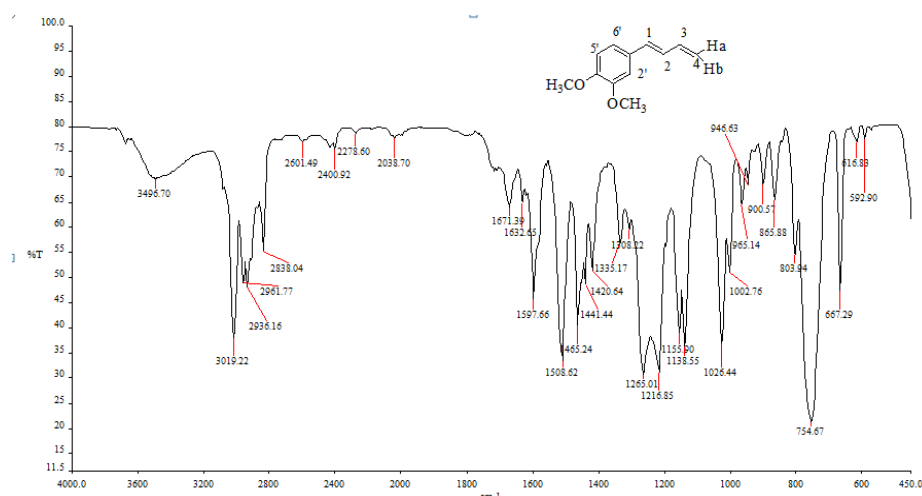
Figure 1: IR spectrum for trans-1-(3,4-dimethoxyphenyl)butadiene **(3)**
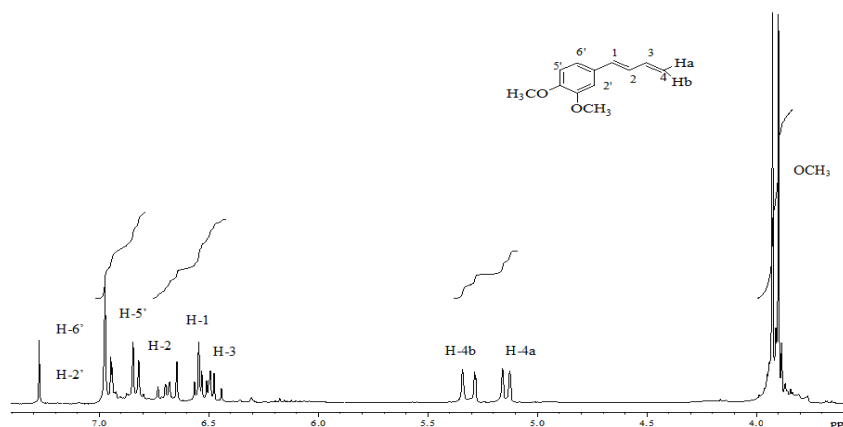
Figure 2: ¹H NMR spectrum for trans-1-(3,4-dimethoxyphenyl)butadiene **(3)**

Trans-4-(3,4-dimethoxyphenyl)but-3-1-yl acetate **(4)** was obtained from the purification of the chloroform crude extract as a pale yellow viscous liquid with R_f value 0.38 in PE: E (3:2). The IR spectrum of *trans*-4-(3,4-dimethoxyphenyl)but-3-en-1-yl acetate **(4)** showed characteristic bands for =CH *sp²* at 3020 cm⁻¹, C-H *sp³* stretching at 2960 and 2838 cm⁻¹. A strong absorption bend at 1734 cm⁻¹ for C=O stretching together with C-O stretching bands at 1240 and 1216 cm⁻¹ suggested the presence of ester moiety. The IR also showed stretching υ for conjugated alkene C=C at 1586 cm⁻¹ and 1465 cm⁻¹. The analysis of ¹H NMR spectrum of *trans*-4-(3,4-dimethoxyphenyl)but-3-en-1-yl acetate **(4)** revealed the presence of a singlet signal integrating for three proton at δ 2.08 was assigned to acetoxyl group (CH₃CO) group. A quartet signal at δ 2.53 with *J* = 6.9 Hz integrating for two protons was attributed to methylene proton of carbon two for H-2. Two singlet signals integrating for

three protons each at δ 3.90 and 3.98 were attributed to methoxyl groups (OCH$_3$). A triplet peak with *J*= 6.9 Hz at δ 4.19 was assigned to methylene protons bearing the acetoxy group. Two olefinic protons at δ 6.04 and 6.42 were mutually coupled with a coupling constant of *J*= 15.9Hz, which indicated that the geometry of the double bond was in *trans* configuration. A doublet of doublets with *J*= 8.1 and *J*= 1.8 Hz at δ 6.89 was assigned to H-6' showing an *ortho*-coupling with H-5', while a *meta*-coupled proton *J*= 1.8 Hz at δ 6.92 was assigned to H-2'. The comparison of the *trans*-1-(3,4-dimethoxyphenyl)butadiene **(3)**and*trans*-4-(3,4-dimethoxyphenyl)but-3-en-1-yl acetate **(4)** obtained from the experiment showed a similarities in pattern of ^{1}H NMR spectrum of compound from the previous research based on the ^{1}H NMR spectrum and IR data [11]. Figure 1, Figure 2, Figure 3 and Figure 4 showed the IR and ^{1}H NMR spectrum for both compound.
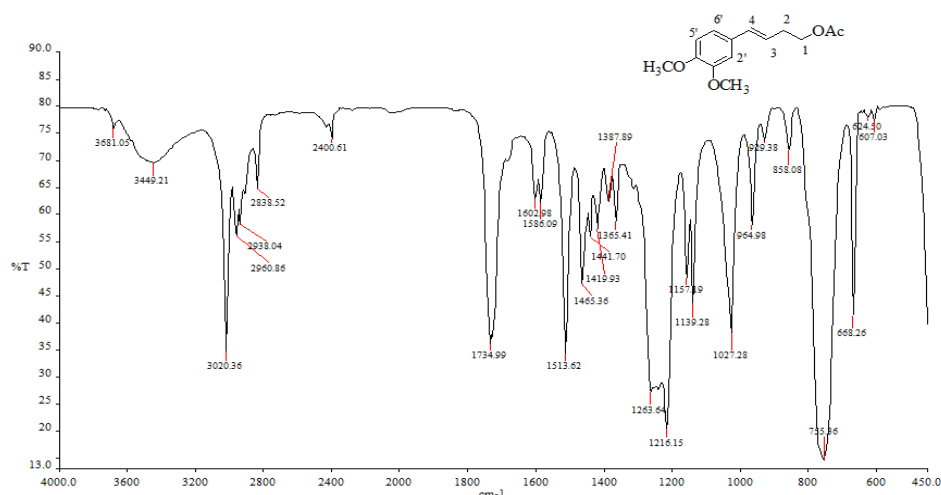
Figure 3: IR spectrum for *trans*-4-(3,4-dimethoxyphenyl)but-3-en-1-yl acetate **(4)**
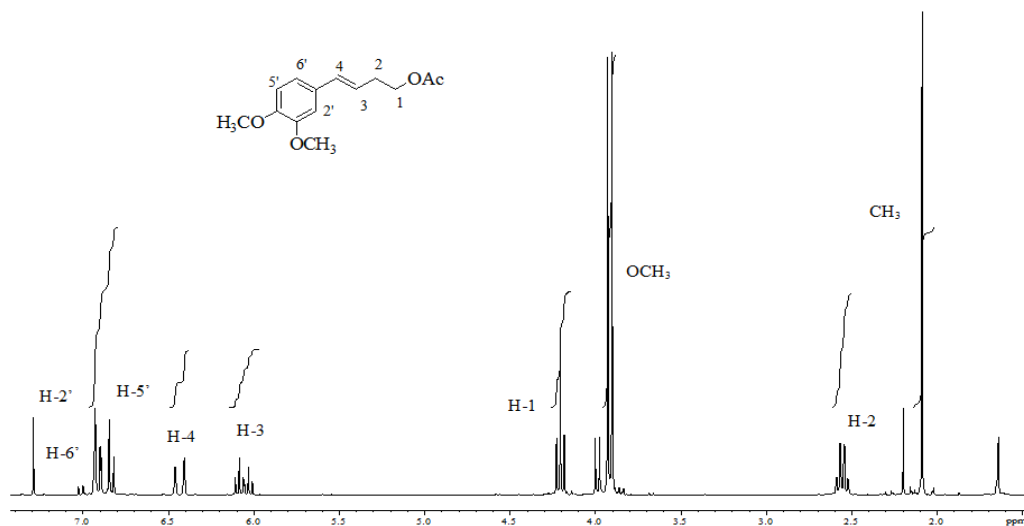
Figure 4: ^{1}H NMR spectrum for *trans*-4-(3,4-dimethoxyphenyl)but-3-en-1-yl acetate **(4)**

DPPH Free radical Scavenging Activity Assay

The DPPH system is a stable radical scavenging-generating procedure because it can accommodate a large number of solid or liquid samples in a short period, and it is sensitive enough to detect active principles at low concentration [10]. The structure of DPPH and its reduction by an antioxidant are shown in **Scheme 1.**
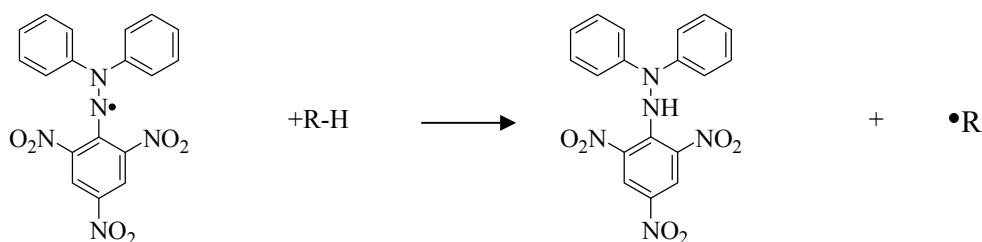
Scheme 1: The reduction reaction of DPPH

The radical electron in the DPPH free radical is purple in color and gave a strong absorption at 517 nm. The color changes when it reacts with an antioxidant compound from purple to light yellow. The color changed was due to molar absorptivity of DPPH radical at 517 nm decreased due to the odd electron of DPPH radical becomes paired with hydroxylated benzene to form the reduced DPPH [10]. Based on the experiment, the purple color of DPPH solution changed when the sample of essential oil and $CHCl_3$ crude extract were added into the DPPH solution at concentration (1000 µg/mL) and (600-1000 µg/mL) respectively. This indicated that the $CHCl_3$ crude extract was active as radical scavengers against DPPH radical at higher concentration. However, in essential oil it showed that the antioxidant activity was almost inactive. At lower concentration,both essential oil and $CHCl_3$ crude extract remain purple in colour of DPPH solution which indicated inactive radical scavengers against DPPH radical. IC_{50} shows effectiveness of the compound to inhibit biological or biochemical function and be obtained from the graph percentage inhibition against concentration in µg/mL. The percentage of scavenging (*I %*) was plotted versus concentration of sample in ppm. Ascorbic acid was used as standard ($r^2 = 0.8672$) gave $IC_{50} = 10.77$ µg/mL. The IC_{50} value for ascorbic acid, essential oil and $CHCl_3$ crude extract were obtained by using equation from the most similar curve as the plot. **Table 2**showed IC_{50} value for the samples, essential oil and $CHCl_3$ crude extract.

Table 2: IC_{50} values for the Samples

Sample	IC_{50} (µg/mL)
Ascorbic Acid	10.77
Essential Oil	700.65
$CHCl_3$ crude extract	77.31

It was suggested the antioxidant property was presence in both sample but it was expected to be very weak in essential oil whereas, in crude showed higher possibilities to be a strong antioxidant. Samples acts as an antioxidant property due to the presence of phenolics groups (hydroxyl substituents next to their aromatic structures), which enable them to scavenge free radicals [10]. Therefore, it was suggested that the crude have the compounds with phenolic group such *trans*-4-(4-hydroxy-3-methoxyphenyl) but-2-en-l-ol **(33)**, *trans*-2-hydroxy-4-dimethoxyphenyl) but-3-en-l-ol **(34)**, *trans*-2-methoxy-4-(3,4dimethoxyphenyl)but-3-en-l-ol **(35)** that make it to have antioxidant property [12].
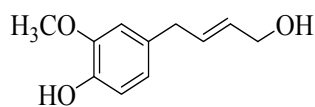
(33)
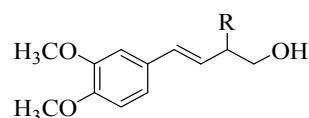
(34) R = OH

(35) R = OCH₃

CONCLUSIONS

Hydrodistillation of the rhizomes of *Zingiber cassumunar* produced essential oil in (2.83%) as a yellow pale liquid with pungent smell. A total of (78.47%) of the essential oil compositions with fifteen compounds were identified, consisting of monoterpenes (75.90%) and sesquiterpenes (1.80%) and ester 0.8%. Terpinen-4-ol **(1)**(31.35%) and sabinene**(2)** (23.37%) were found to be the main constituents in the essential oil. Soxhlet extraction of the dried rhizomes of *Z. cassumunar* using chloroform followed by purification using several chromatographic techniques afforded *trans*-1-(3,4-dimethoxyphenyl)butadiene **(3)**and *trans*-4-(3,4-dimethoxyphenyl)but-3-en-1-yl acetate **(4)**.The structures of compounds were elucidated by using spectroscopic methods as methoxyphenyl derivatives using IR and nuclear magnectic resonance (^{1}H NMR). The CHCl$_3$ crude extract gave antioxidant properties at higher concentration which more than 600 µg/mL in the DPPH assay whereas the essential oil extract showed almost inactive or very weak antioxidant activity.

REFERENCES

1. Ghasemzadeh, A., Jaafar, H. Z., andRahmat, A. (2010). Antioxidant activities, Total phenolics and flavonoids content in two varieties of Malaysia young ginger (*Zingiberofficinale* Roscoe). *Molecules*. **15**, 4324-4333.
2. Mohamad, R. (2013). Quality control methods for some Zingiberaceous plants from Indonesia using liquid chromatography combined with chemometrics. *Doctoral dissertation*. 1-53.
3. Ubonnuch, C., Ruangwises, S., Gritsanapan, W., andRuangwises, N. (2013). Total and Inorganic Arsenic Contents in Some Edible Zingiberaceous Rhizomes in Thailand. *Evidence-Based Complementary and Alternative Medicine*. **13**, 1-7.
4. Ubonnuch, C., Ruangwises, S., Gritsanapan, W., &Ruangwises, N. (2013). Total and Inorganic Arsenic Contents in Some Edible Zingiberaceous Rhizomes in Thailand. *Evidence-Based Complementary and Alternative Medicine*. **13**, 1-7.
5. Habsah, M., Amran, M., Mackeen, M.M., Lajis, N.H., Kikuzaki, H., Nakatani, N., Rahman, A.A., Ghafar, and Ali, A.M. (2000). Screening of Zingiberaceace Extracts for Antimicrobial and Antioxidant Activities. *Journal of Ethnopharmacology***72**, 403-410.
6. Parthasarathy, V.A., Zachariah, T.J., andChempakam, B. (2008). Ginger. *Chemistry of Spices*. **5**, 70-96.
7. Bua-In, S., Paisooksantivatana, Y., Weimer, B. C., andChowpongpang, S. (2014). Molecular cloning and expression levels of the monoterpene synthase gene (ZMM1) in Cassumunar ginger (*Zingibermontanum* (Koenig) Link ex Dietr.). *Archives of Biological Sciences*. **4**, 1321-1331.
8. Hamirah, M.N., Sani, H.B., Boyce, P.C., andSim, S.L. (2010). Micropropagation of red ginger (*Zingibermontanum Koenig*), a medicinal plant. *In Proceedings Asia Pacific Conference on Plant Tissue and AgribiotechnologyJournal of MolecularBiology&Biotechnology*.**18**, 127-130.
9. Sukatta, U., Rugthaworn, P., Punjee, P., Chidchenchey, S., and Keeratinijakal, V. (2009). Chemical composition and physical properties of oil from Plai (*Zingibercassumunar*Roxb.) obtained by hydro distillation and hexane extraction. *Kasetsart Journal. (National Science.)***43**, 212-217.
10. Bua-in, S., andPaisooksantivatana, Y. (2009). Essential oil and antioxidant activity of *cassumunar*ginger (Zingiberaceae: *Zingibermontanum* (Koenig) Link ex Dietr.) collected from various parts of Thailand. *Kasetsart Journal: (Natural Science)*. **43**, 467-475.
11. Saat, R., (1999). *Kandungan Kimia danbioaktivititiga species Zingiberaceace*. (Master's Thesis, Faculty of Science,UniversitiTeknologi Malaysia,).
12. Masuda, Toshiya, and Akiko Jitoe. (1995). Phenylbutenoid monomers from the rhizomes of *Zingibercassumunar*. *Phytochemistry*.**39**, 459-461.

PHOTODEGRADATION SCREENING ON CHLORPYRIFOS AND BENZOIC ACID USING TITANIA-BASED PHOTOCATALYST SUPPORTED ON PULASAN PEEL ACTIVATED CARBON

Anisaturrahmah Bt Mohd Yussof and Rusmidah Ali
Department of Chemistry, Faculty of Science, UniversitiTeknologi Malaysia, 81310 Johor Bahru.

Abstract

Chlorpyrifos and benzoic acid are harmful and toxic organic compounds which contribute to the damage of the environment and human health. Therefore, any organic or inorganic pollutants present in water system should be treated in an appropriate way and low-cost before they can be safely disposed to the environment. In this research, TiO_2 modified with PPW activated carbon, TiO_2/AC was synthesized. The pulasan peel was treated with sulphuric acid to obtain activated carbon. Various ratios of TiO_2/AC (90:10, 50:50, 10:90) with various calcination temperatures (500, 600 and 700℃) were prepared by physical mixing. Titania-silver oxide was also prepared with various ratios (90:10, 50:50 and 10:90) and calcined at 500℃ and prepared by wet-impregnation method. All the prepared photocatalysts were screened on chlorpyrifos and benzoic acid degradations under UV irradiation (λ=365 nm), monitored by UV-Vis spectrophotometer. The main absorption measured at wavelength λ_{max}=210 nm for chlorpyrifos and λ_{max}= 227 nm for benzoic acid were recorded. Among the photocatalysts prepared, the catalyst which gave maximum percent degradation was 5T/3SAC (50:50) compared to single TiO_2 and other modified photocatalysts. The best photocatalyst was assessed on the effect of various catalysts loading (0.1, 0.2 and 0.3 g) on the benzoic acid solution and result shows that as catalyst loading increase, the rate of degradation was also increased. The prepared photocatalysts were characterized by X-ray diffractometer (XRD), Brunauer-Emmett-Teller (BET) and field emission scanning electron microscopy-energy dispersive X-ray (FESEM-EDX). It is proven that (5T/3SAC 50:50) is the most efficient photocatalyst with the presence of anatase phase, and homogenous distributed porous surface with average size (1.48 μm) and from BET surface area of 4SAC showed highest surface 228.49 m^2/g.

Keywords: Pulasan peel waste, activated carbon, photodegradation, chlorpyrifos, benzoic acid

INTRODUCTION

Environmental pollution is a common issue in this century. Most of the pollution present is due to the disposal of organic and inorganic substances into water sources such as rivers. Besides that, aquatic environment, underground water layer, and the surface of the habitat is often contaminated by waste which are mostly disposed by various source such as industrial, agricultural chemicals, agricultural runs off and others.

The types of chemicals that are difficult to degrade naturally by biological method are comes from the group of dyes, aromatic carboxylic acid group, and pesticides. Therefore, the materials are accumulated for a long time and will cause harm to the environment and living things.

In recent years, photocatalytic degradation has become a promising techniques for wastewater treatment and removal of organic pollutants. Photocatalytic degradation is actually an Advance Oxidation Process (AOP) which can degrades and mineralizes most organic contaminants into carbon dioxide and water without any formation of any stable intermediate species. The process operates by the presence of heterogeneous semiconductor as a catalyst, and also in the presence of source of light such as UV light radiation or high intense of sunlight. The process occurs at ambient temperature and pressure. The most outstanding and stable photocatalyst which shows tremendous activity is titanium dioxide. However, zinc oxide also shows a high efficiency in photocatalysis but it has low stability which makes its aqueous suspensions stable only at basic pH. The efficiency of photocatalysis process depends on several characteristic of semiconductor particles, such as their surface properties, the position of their band gap potentials, mobility and recombination rate of the charge carriers generated by UV-light absorption [1]. However, a few drawbacks were investigated by researchers such as low degradation due to recombining process of positive holes and generated electron. As responds to these problems, support materials with large surface areas were used on TiO_2 such as activated carbon from pulasan peel waste to increase the absorption of substare and metal oxide as co-dopant was also added to retard the recombination process. This development would be great significance to enhance the photodegradation effieciency [2].

EXPERIMENTAL

Reagent and materials

Previously synthesized activated carbon from pulasan peel waste was used in this work as adsorbent for titania. The dried pulasan peels were soaked in 20% sulphuric acid solution with 1:4 ratio (pulasan peel (g): v H_2SO_4) for 24 hours. Then, the acid was poured off and the pulasan peel was dried in the hot air oven at 95℃ and left for two days. Next, the sample was washed with hot distilled water and the sodium bicarbonate (1% w/v) was used to remove the acid until the precursor was fully free of acid and dried in hot oven at 95℃. Then, the activated carbon was activated in a muffle furnace with different temperatures which were 300, 400 and 500℃ for 2 hours. Coupled of titania-activated carbon was prepared with various ratios and calcination temperatures by physical mixing.TiO_2/AgO was also prepared by wet-impregnation method. Photocatalysts prepared were screened on chlopyrpyrifos (a) and benzoic acid (b) to get an optimum photocatalytic activity.

(a)　　　　　　　　　　　　　　　(b)
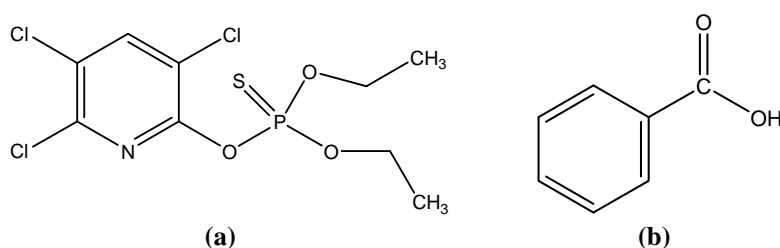
Instruments

The evaluation of photocatalysts efficiency on chlorpyrifos and benzoic acid were monitored using UV-Visible spectrophotometer, Shimadzu UV-250000PC model and to obtain information on structural properties and crystalline phase of the prepared photocatalyst, it was analyzed by using Siemens D5000 X-ray diffractometer equipped with Cu-Kα (λ = 1.54 Å, 40 kV, 30 mA) radiation. The morphology of several photocatalysts were examined using FESEM- Zass Supra 35 VP with Gemini Column and to determine surface area of the prepared activated carbon, single point BET was used. The specific surface area was determined by single point BET using nitrogen as the adsorption gas.

Plant Material

Nephelium Mutabile (Pulasan) bought from Tampoi Market and was used to prepare activated carbon.

RESULTS AND DISCUSSION

Characterization

X-ray Diffraction (XRD) Techniques

X-ray diffraction is a technique to identify and determine the crystallinity or phase transformation of powdered compounds. The effect of TiO_2/AC ratios and calcination temperature was studied in this study. The phase and structural of photocatalysts were identified by matching the 2θ with the powder diffraction file (JCDPS) obtained and studied on both anatase and rutile phases of TiO_2 to determine the peak crystallinity from its peak intensity.

Figure 3.1 shows the XRD diffractograms of TiO_2/3SAC with ratio 50:50 calcined at 500℃ (a) (5T/3SAC 50:50), while (b) was single TiO_2calcined at 500℃ (T-500) and (c) titania-activated carbon calcined at 700℃ (7T/5SAC 10:90) photocatalysts. The result indicates that the synthesized TiO_2/AC consists of pure phase and no other characteristic peak can be found from other phase or impurities. The XRD patterns of single TiO_2 and coupled TiO_2 photocatalysts showed the presence of peaks at 2θ values of 25.6, 37.9, 48.1, 55.2, 62.6, 68.9 and 75.2˚ corresponding to the anatase phase (JCDPS No. 21-1272). However, peaks at 2θ values of 54.2, 69.0 and 70.2˚are characteristic of TiO_2 rutile phase ((JCDPS No. 21-1276).

Based on Figure 3.1 5T/3SAC 50:50 (a) and single TiO_2 (b) calcined at 500℃ consists of anatase phase with small amount of rutile phase while TiO_2/AC calcined at 700℃ (7T/5SAC 10:90) consist of rutile phase with

small amount of anatase phase. The phase transformation of TiO_2/AC photocatalyst occurs at the temperature of 500°C where anatase shifts gradually to rutile phase during calcination process [4].

It is apparent that thermal annealing greatly affects the structure and the size of the resulting TiO_2 crystal. The crystal sizes for both anatase and rutile increased with increasing of calcination temperature, indicating aggregation of TiO_2 nanoparticles upon annealing. The fraction of rutile becomes greater with increasing reaction temperature accelerates phase transformation from thermodynamically metastable anatase to most stable and more condense rutile phase [4].

Lastly, a rough baseline was obtained as shown by Figure 3.1 (c) when 90% AC present in the photocatalyst. This result obtained was due to the highly content of amorphous activated carbon in the photocatalyst.

Single Point BET Surface Area

The surface area of activated carbon after calcination at various temperatures (300, 400, 500°C) was determined and was shown in Table 3.1. Activated carbon that was calcined at 400°C (4SAC) has the highest surface area compared to AC that were calcined at 300 and 500°C. BET specific surface area increases with activation temperature (See Table 3.1) with the most significant increase being between 300 and 400°C. When the activation temperature was increased from 400°C to 500°C, the effect of activation temperature on BET specific surface area was dramatically decreased. This can be attributed to high activation temperatures allowing easier removal of organic matter, formation of more micropores, and an increase in specific surface area, but also easier collapsed of micropores, backfilling, and formation of graphite-like carbon structures, thus decreasing the BET specific surface area [5].

Table 3.1: Surface area for prepared activated carbon (activated with sulphuric acid)

LabelActivation	Temperature (°C)	Surface Area (m^2/g)
3SAC	300	96.20
4SAC	400	228.49
5SAC	500	41.83

Field Emission Scanning Electron Microscope (FESEM)

In this research, FESEM micrographs (Figure 3.2 -3.4) were used to study the morphology and composition of single TiO_2 which were calcined at various temperatures, 500, 600 and 700°C. Besides that, the coupled photocatalysts morphologies were also studied using this instrument. Figures 3.2 shows the micrographs of single TiO_2 calcined at 500°C, 600 and 700°C with magnification of 5000x respectively. The energy bombardment applied was 10 kV and working distance was 8.5 and 8.6 mm.

From the results shown, the particles size of TiO_2 increase after calcined at 600 and 700 °C. The formation of tetragonal shape was clearly observed at these calcination temperatures due to the rutile phase that started to form at these temperatures. The increase of size was due to the agglomeration process which involves combination of primary particles and secondary particles that occur at high temperature. TiO_2 calcined at 500°C and 600°C were considered as mesopores category due to its mean size was 20.87 nm and 38.22 nm. It was spherical in shape and homogenous. However, TiO_2 calcined at 700°C was in macropores category because its mean size of particle was 128.94 nm. The size of particles was measured using J image software. According to IUPAC recommendation, total porosity usually classified into micropore (< 2 nm) mesopores (2-50 nm) and macropores (> 50 nm).

Figure 3.3 shows the surface micrograph of activated carbon calcined at 300 and 400°C. From Figure 3.2, the morphological structure of 3SAC shows highly defined pores that the surface was rough and dented [6]. There was major development of internal pores that could be seen and the pore size distributions were non-uniform. However, 4SAC morphology shows cleaner and smooth surface. The pore development was larger and it was an external pores [5]. This explained why BET surface area value (see Table 3.1) for 3SAC was lower than 4SAC. The quality of the activated carbon seemed to be deteriorated as the calcination temperature was increased. This might be a result of the collapse of micropores as it was heated at higher temperature [7].

Based on Figure 3.4, the 5T/3SAC (50:50) photocatalyst obviously have larger surface area and pore size (1.48 μm) suitable for the degradation. This type of titania-activated carbon shows the highest percent of degradation due to ability of activated carbon acts as adsorbent to enhance the photocatalytic activity. The

calcination temperature of 500℃ also plays as important role because calcinations at higher temperature might destroy the pore structures, as well as change the active phase of anatase to more rutile which is inactive.

Photodegradation of Chlorpyrifos Using Single TiO₂Photocatalyst

Degradation rates for all single TiO_2 that were calcined at various temperatures (500, 600, 700℃) on chlorpyrifos (see Figure 3.5) showed that 500 TiO_2 gave the highest percentage of photodegradation with 71.47 followed by 46.43 and 49.9% for 600 TiO_2 and 700 TiO_2. The best performance of 500 TiO_2 is due to the presence of anatase phase at temperature 500℃ which was more stable than the other phase. From the results obtained it was shown that the crystallinity, crystal phase and crystallite size were influenced by varying the calcination temperature. Calcination temperature was important for removing the organic molecules from the final products and completing the crystallization. However, very high calcination temperature will results in aggregation and phase transformation and affect the microstructure as well as the properties of TiO_2. Photocatalytic activity of TiO_2 strongly depends on its crystal structure. Anatase phase TiO_2 crystallite are generally found to be more active than rutile. Therefore, 500 TiO_2 gave the highest percent of degradation on chlorpyrifos.

Effect of Calcination Temperature On Activated Carbon Preparation

The results obtained in Figure 3.6 showed that the titania coupled with activated carbon calcined at 300 and 400℃ gave the higher activity compared to 500℃. Activated carbon calcined at 300℃ gave high porosity which can help an adsorption of benzoic acid on the surface or pores when the active species of ●OH radical was available in high concentration that help to degrade the substrate. However, at high calcination temperature the pores might collapse and reduce the adsorption acitivity.

Photodegradation of Benzoic Acid using Various Ratio of TiO₂/AC Photocatalysts

Among all the photocatalysts with ratio (90:10) and (10:90), TiO_2/4SAC with ratio (90:10) that was calcined at 500℃ shows the highest percentage of degradation (46.85%) followed by 500 TiO_2/3SAC that gave percentage degradation of 29.20%. According to the results shown by titania-acitvated carbon with ratio (10:90), as the calcinations increased, the degradation of benzoic acid was also decreased. This is due to agglomeration of particles that will reduce the surface area. The similar trend observed with ratio (90:10). Ratio (90:10) gave higher degradation due to the high contents of titania can provide higher active site to generate more hydroxyl radicals. However the high contents of activated carbon in the catalysts can increase the adsorption but lack of active site of TiO_2 that make the benzoic acid degradation become less effective. As a photocatalyst, the presence of titania in TiO_2/AC composites will increase the surface area of adsorption and photocatalytic reaction so it can serve as hydroxyl radicals source that significantly increase the benzoic acid degradation [8]. An excessive amount of activated carbon might also blocked the TiO_2 surface.

In addition the result also showed that the degradation 5T/4SAC (90:10) (46.38 %) was higher than 5T/3SAC (90:10) (29.2%). In this case, 4SAC activated carbon which was calcined at 400℃ has higher surface area than 3SAC which were 228.49 and 96.2 m^2/g respectively. The larger surface area of 4SAC contributed to the higher degradation of 500 TiO_2 rather than 5T/3SAC (90:10). As reported by Patnukao *et. al* [7], the surface area of activated carbon leads to high adsorption of pollutants on the catalyst surface, and therefore it might accelerate the process of decomposition through the transfer of the adsorbed molecules to the surface of the photoactive titania.

Effect of TiO₂/AgO on Photodegradation of Benzoic Acid

In order to improve the photocatalytic activity of benzoic acid, the coupled photocatalysts of titania-silver oxide (AgO) was prepared in different ratios (90:10, 50:50 and 10:90) which were calcined at 500℃. Results showed TiO_2/AgO (90:10) gave 31.40% degradation on benzoic acid but for TiO_2/AgO with ratio 50:50 and 10:90 did not show good degradation activities. The small adsorption band gap energy of 1.02 – 2.07 eV for AgO make the excitation of electrons from valence band to conduction band easier and thus the photocatalyst can achieve a higher photocatalytic activity but the recombination process might also occurs faster [9]. The impregnated photocatalyst can prevent the recombination of electrons with h^+ holes in valence band by transferring the electrons from the conduction of catalyst to the conduction band of co-catalyst. Therefore, the recombination process is delayed [10]. The coupling of AgO as co-catalyst is expected to give higher result due to the delay of electron hole recombination process but not observed in this research. It might due to the other factors such as the properties of the substrate, pH of the reaction mixture and the co-catalyst chosen is not active.

Effect of Loading 500 Ti/3SAC (50:50) On Benzoic Acid

The amount of photocatalyst can play an important role in influencing the degradation rate. Due to this, the optimum amount of catalyst used to degrade benzoic acid was studied in order to achieve the maximum photocatalytic activity. Figure 3.7 shows effect the of different loading of the best photocatalyst among all the sets of photocatalysts 5T/3SAC with ratio 50:50 was chosen to test its efficiency on benzoic acid when used in different loading. Range between 0.1 to 0.3 g were used to investigate the effect loading of the catalyst. The photodegradation efficiency increasing with loading was increased from 51.20% to 65.14% . This results can be explained by the fact that, when larger amount of photocatalyst was used in the reaction, the availability of active site on the surface of the catalyst for reaction to occur increased. Thus, the photodegradation rate was higher [11].
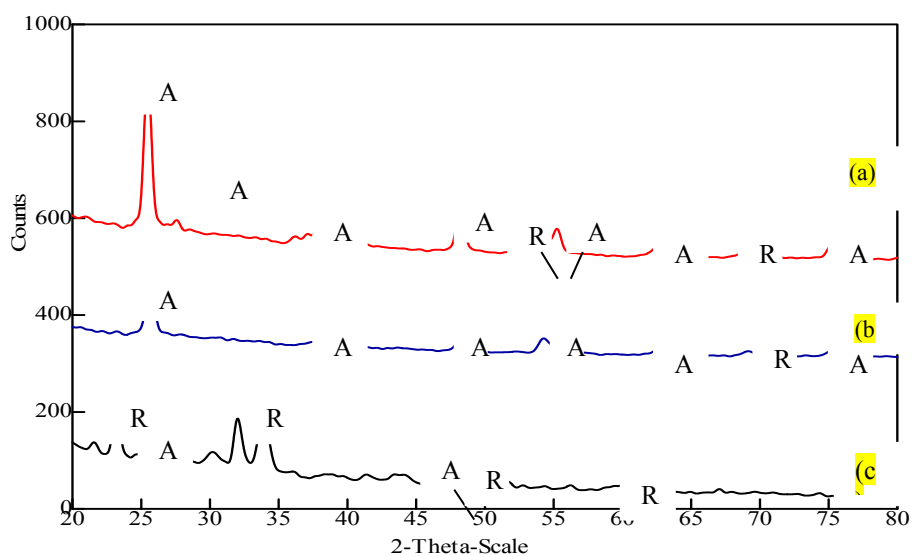
Figure 3.1: XRD patterns of (a) 5T/3SAC (50:50) (b) sol gel TiO_2 (T-500) and (c) 7T/5SAC (10:90)
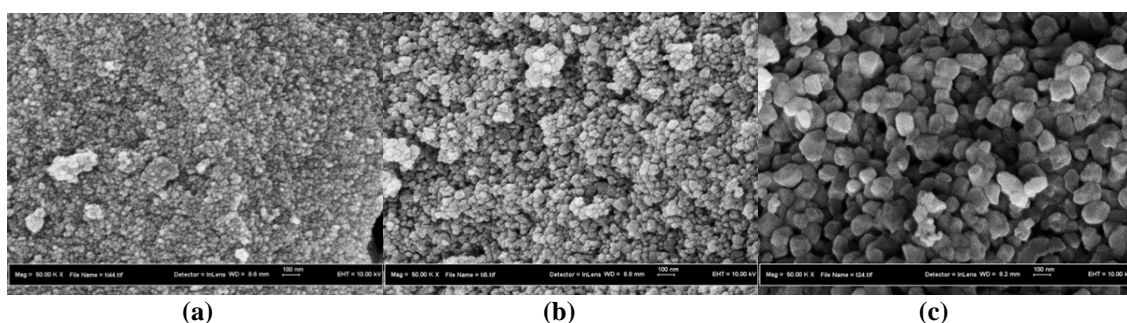
Figure 3.2: FESEM micrograph single TiO_2 calcined at 500℃ (a), 600℃ (b)and (c) 700℃ with 5000x magnification.
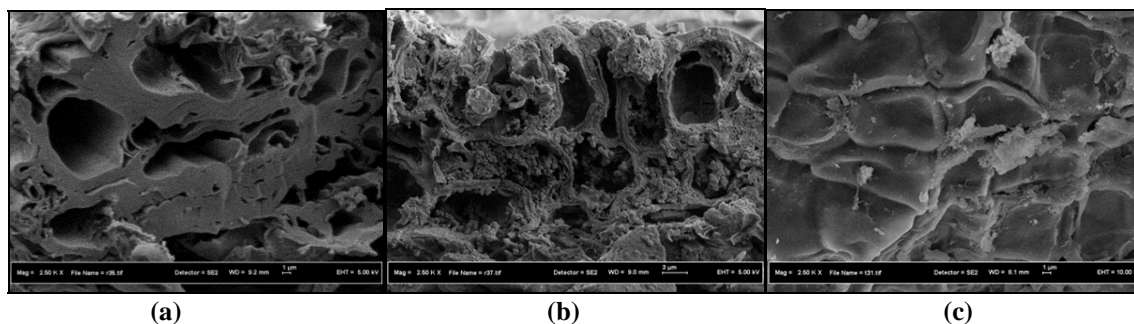
Figure 3.3: FESEM micrographs of activated carbon (a) and (b) calcined at 300℃ (3SAC) while (c) was 4SAC with the magnification 2500x.

(a)   **(b)**   **(c)**
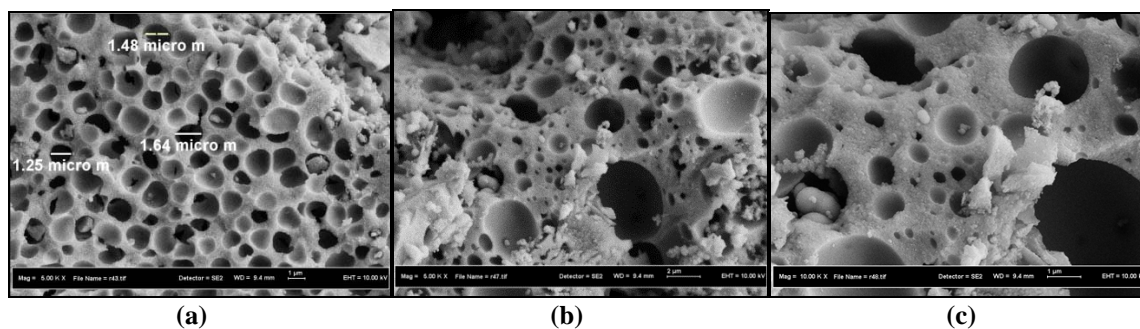
Figure 3.4 : FESEM micrographs of 500 TiO_2/3SAC (50:50) (a) with magnification 5000x while (b) and (c) 10000x magnification
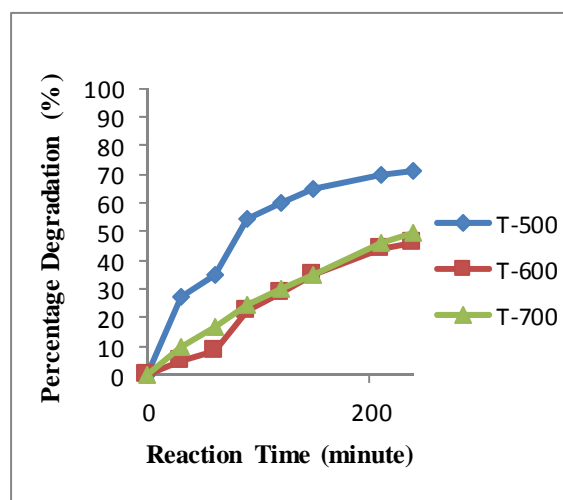
Figure 3.5: Percentage of degradation for chlorpyrifos using sol gel TiO_2 photocatalysts calcined at 500℃, 600℃ and 700℃.
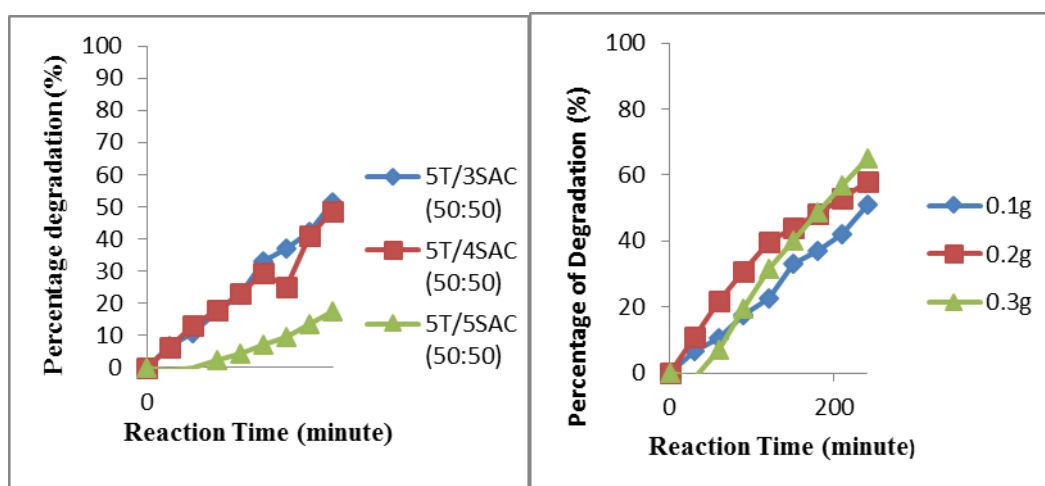
Figure 3.6: Effect of calcination temperature of activated carbon in TiO_2/AC photocatalystscalcined at 500℃ towards degradation of benzoic acid.

Figure 3.7: Percentage degradation of benzoic acid using various amount loading of catalysts.

CONCLUSION

Various photocatalysts supported on rambutan peel activated carbon were successfully synthesized. The best photocatalyst that can be applied to degrade benzoic acid was $TiO_2/3SAC$ (50:50) calcined at 500℃ which gave 51.20% degradation compared to single TiO_2 and photolysis which degrade only 37.92 and 9.93% respectively. The addition of activated as an adsorbent increase the photoactivity of TiO_2 catalyst. However, for chlorpyrifos, the highest percentage of degradation was using single TiO_2 photocatalyst calcined at 500. The addition of AgO as co-catalyst slightly decreased the activity.

REFERENCES

1. Vione, D., Minero, C., Maurino, V., Carlotti, E., M., Picatonotto, T., Pelizzetti, E. (2005). Degradation of Phenol and Benzoic Acid In The Presenceof a TiO_2-Based Heterogeneous Photocatalyst. *Applied Catalysis B: Environmental*,**58**, 79-88.
2. Mrowetz, M., Selli, E. (2006). Photocatalytic Degradation of Formic and Benzoic Acids and Hydrogen Peroxide Evolution in TiO_2 and ZnO Water Suspensions. *Journal of Photochemistry and Photobiology A:Chemistry*, **180**, 15-22.
3. Torimoto, T., Okawa, Y., Takeda, N., Yoneyama. H. (1997). Effect of Activated Carbon Content in TiO_2-Loaded Activated Carbon on PhotodegradationBehaviours of Dichloromethane. *Journal of Photochemistry and Photobiology A:Chemistry*,**103**, 153-157.
4. Lo, S.C., Lin, C.F., Wu, C.H., and Hsieh, P.H. (2004). Capability of Coupled $CdSe/TiO_2$ForPhotocatalytic Degradation of 4-Chlorophenol. *Journal of Hazardous Materials B*, **114**, 183-190.
5. Huang, P., H., Cheng, H. H., Lin, S. H. (2015). Adsorption of Carbon Dioxide onto Activated Carbon Prepared From Coconut Shells, 2015, 1-10.
6. Yacob, A. R., Majid, Z. A., Dasril, R. S. D., Inderana, V. (2008). Comparison of Various Sources of High Surface Area Carbon Prepared by Different Types of Activation. *The Malaysian Journal of Analytical Sciences*,**12(1)**, 264-271.
7. Patnukao, P. and Pavasant, P. (2008). Activated Carbon From*Eucalyptus camaldulensisDehn* BarkUsing Phosphoric Acid Activation.*Bioresource Technology*,**99**, 8540-8543.
8. Slamet, Bismo, S., Fasa, A. F., Jabbar, A., Putera, A. (2010). Performance Test of a Novel Tubular V-Collector for Phenol Removalfrom Aqueous Solutions over TiO_2-Activated Carbon Composites. *World Applied Sciences Journal*,**8(6)**, 672-679.
9. Barone, P., Stranges, F., Barberio, M., Renzelli, D., Bonanno, A., Xu, F. (2014). *Study of Band Gap of Silver Nanoparticles-Titanium Dioxide Nanocomposites.* **2014**, 1-6.
10. Saravanan, R., Karthikeyan, S., Gupta, V.K.,Sekaran, G., Narayanan, V., Stephen, A.(2013). Enhanced Photocatalytic Activity of ZnO/CuONanocomposite For the Degradation of Textile Dye on Visible Light Illumination. *Materials Science and Engineering*,**33**, 91-98.
11. Ariffin, M. F. M. (2014). Degree of Master ofScience (Chemistry). UniversitiTeknologi Malaysia.

DEACETYLATION OF CHITIN ISOLATED FROM FERMENTED PRAWN WASTE TO PRODUCE CHITOSAN USING AUTOCLAVE METHOD

Zainoha Zakaria*, Bong Tze Song, Marshifah Jamaludin
Department of Chemistry, Faculty of Science, Universiti Teknologi Malaysia, 81310 Johor Bahru, Malaysia

Abstract

A partially purified chitin was isolated from fermented prawn waste. Chitin was further deacetylated using autoclave method under condition of 121 C and 101.kPa to form chitosan with the objective of reducing the deacetylation time and cost of production. The effect of NaOH concentrations and various steeping modes on the degree of deacetylation (DD) of chitosan were evaluated. Degree of deacetylation of chitosan was determined using FTIR spectroscopy. Chitosan film was not formed when chitin was deacetylated in 40% and 45% (w/w) NaOH solution. Effective chitosan film formation was observed only when 50% (w/w) NaOH was used. Result showed that chitin was successfully deacetylated using autoclave and reaction time of 20 minutes to form chitosan of up to 84% DD. The DD also increases with steeping time and a double steeping mode was able to increase up to 91% DD of chitosan.

Keyword: chitin, steeping time, deacetylation, chitosan, autoclave

INTRODUCTION

The recent expansion of Malaysian shrimp industry due to global demand is contributing to the increase in shrimp waste production locally as nearly 50% of the whole prawn are discarded as waste [1-2]. Major compositions of prawn waste are chitin, protein and minerals. An economical way to minimize environmental impacts due to shrimp waste disposal is to extract chitin from the shrimp shell waste and put it to good use such as conversion to a more versatile derivatives chitosan. Chitin can be extracted from shrimp waste using chemical method through strong acid and alkali treatment. Alternatively, lactic acid bacterial fermentation has also been applied in our laboratory to extract protein [3] for aquaculture purposes and produces chitin by-product.

Chitin is often deacetylated under strong alkali and high temperatures to produce chitosan which is of higher economic value than its starting material chitin. Deacetylation of chitin can be done by boiling, autoclaving (boiling under pressure), or boiling by microwave method [4]. Degree of deacetylation (DD) is used as an indication of how much chitin has been converted to chitosan through the removal of acetyl group from chitin. It is envisaged that steeping or soaking prior to deacetylation process may assist in increasing the DD of chitosan [5]. Chitosan with higher DD will have more amine groups (more basic) and is therefore expected to be of higher reactivity. In this study, chitosan is produced by deacetylation of chitin using autoclave method at temperature of 121°C, and pressure of 101.3 kPa and the effect of steeping time, mode of steeping and concentration of sodium hydroxide (NaOH) used are discussed. To date, no data has been reported on using chitin from fermented prawn waste to produce chitosan.

MATERIALS AND METHODS

Chitin source

Chitin was obtained from fermented tiger prawn waste from our laboratory (Biochemistry Laboratory, Faculty of Science, Universiti Teknologi Malaysia). After three days fermentation, chitin was separated from the proteinaceous liquor, washed and dried.

Effect of steeping on DD of chitosan

Steeping process prior to autoclaving to improve deacetylation process was evaluated. In this study, two steeping modes were conducted.

Single Steeping: Chitin (2.00 g) was mixed with NaOH (50% w/w), in an autoclave bottle (50mL) with solid to liquid ratio of 1:10. Samples were left soaking in the solution for various durations (1, 2, 3, 4 and 5 days) before being deacetylated in an autoclave.

Double Steeping: The double steeping mode is similar to single steeping method. However, after steeping time was completed, NaOH solution was replaced with fresh NaOH (50% w/w) and again steeped for similar durations (1, 2, 3, 4 and 5 days respectively) before being deacetylated.

Deacetylation of chitin to chitosan using autoclave

Chitin which has been steeped in NaOH (50%, w/w) for the required durations, was deacetylated in an autoclave under pressure of 102.3 kPa, 121 °C for 20 minutes using Hirayama Autoclave (HVE-50). After autoclaving, the cooled mixture was centrifuged at 4500 rpm for 15 minutes (Hettich Zentrifugen) to separate the solid product. After thoroughly washing under running tap water to remove excess NaOH, the product was dissolved in a constantly stirred acetic acid solution (1%, v/v) in a ratio of 1:15 (w/v). The dissolved chitosan solution was centrifuged at 4500 rpm for 15 minutes for degassing and to separate impurities and unreacted chitin as chitin does not dissolve in acetic acid. Chitosan films were prepared according to the method of Mayachiew and Devahastin [6]. The obtained chitosan solution (20mL) was poured into a petri dish, and oven dried (Memmert) at temperature of 60°C for 24h. The thin chitosan film formed was further treated by immersing the chitosan film in NaOH (1% w/w) solution for 30 minutes to neutralize the acetic acid present in the chitosan film [7]. The treated chitosan film was then washed with distilled water to remove excess NaOH (1% w/w) followed by absolute ethanol and dried in desiccator for 2 days before analyses using FTIR spectrophotometer. The degree of deacetylation were calculated using three methods for comparioson, Domszy and Robert (1985), Baxter *et al.* (1992), and Sabnis & Block (1997) [8, 9, 10 respectively]. It is interesting to note that these three methods were chronologically developed and all of them had used the same values of OH and C=O of amide bonds.

Determination of degree of deacetylation

The treated chitosan film was analysed using FTIR spectroscopy and the DD was calculated by applying the formula which was proposed by Domszy and Robert (1985)(Eq. 1), Baxter *et al.* (1992) (Eq. 2), and Sabnis & Block (1997) (Eq. 3) for comparison.

$$\text{Degree of Deacetylation} = 100 - \frac{\frac{A_{1655}}{A_{3450}} \times 100}{1.33} \qquad \text{(Eq. 1)}$$

$$\text{Degree of deacetylation} = 100 - \frac{A_{1655}}{A_{3450}} \times 115 \qquad \text{(Eq. 2)}$$

$$\text{Degree of deacetylation} = 97.67 - (26.486 \times \frac{A_{1655}}{A_{3450}}) \qquad \text{(Eq. 3)}$$

Where,
A_{1655} = the absorption band of amide at 1655 cm^{-1}
A_{3450} = the absorption band of hydroxyl at 3450 cm^{-1}

RESULTS AND DISCUSSION

Effect of concentration of NaOH solution on the formation of chitosan film

The result showed that 40% and 45% (w/w) NaOH solution were unable to form film when casted on a petri dish (Figure 1) which indicates that not enough chitosan was formed. Although several studies have indicated that DD of chitosan is proportionally related to the concentrations of NaOH solutions, most results also suggested that the minimum concentration of NaOH solution to produce chitosan from chitin is by using concentrations higher than 40% (w/w). In this work, the efficiency of NaOH to effect deacetylation is probably reduced further due to the presence of some impurities in the fermented chitin as reported by Zakaria *et al.*, (1998) that chitin obtained through a 72h fermentation process of scampi waste had minimal protein left (6%) and small amount of minerals (20%) [11]. It may therefore be suggested that if chitin from fermented shrimp is to be used for deacetylation processes, minimal pre-treatment by acid and alkali treatment to remove remaining protein and impurities before undergoing deacetylation process would be highly recommended.

Determination of DD of chitosan by FTIR spectroscopy

Samples of chitosan formed were analysed using FTIR spectroscopy. All samples showed absorbance peaks at 1655cm^{-1} and 3450cm^{-1} (Table 1). The absorption band of N-H stretching (3270 cm^{-1}) was not observed as it

overlaps with the broad absorption band for O-H stretching at a region of 3200-3400 cm^{-1}. Table 1 also shows the calculated DD using the three equations (Eq 1, 2 and 3). The results showed that equation 3 (Eq 3) by Sabnis and Block (1997) showed the highest DD while equation 2 the least.

Chitosan is a hygroscopic material and thus the hydroxyl (OH) groups of the chitosan are sensitive to atmospheric humidity. As a result, the absorption band for O-H stretching in FTIR spectrum may increase in intensity if the sample is not properly dried. Precautions had been taken to reduce the effect of water moisture by keeping the chitosan film in desiccators prior to FTIR analyses.
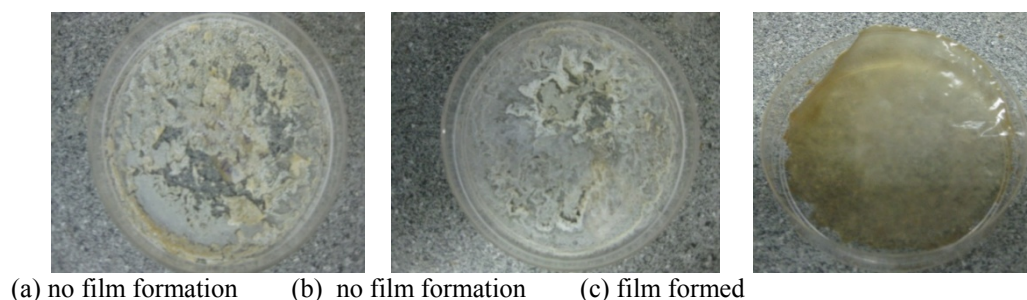

(a) no film formation   (b) no film formation   (c) film formed

Figure 1: Effect of concentration of NaOH solution on film formation. (a) 40% NaOH, (b) 45% NaOH, and (c) 50% NaOH.

Chitin with (1 → 4)-2-acetamido-2-deoxy-D-glucan (GlcNAc) as structural units, and (1 → 4)-D-glycoside linkages, forms a linear chain through the many inter- and intramolecular hydrogen bonds. The hydroxyl groups in chitin contribute strong intra- and intermolecular hydrogen bonds. Both hydrophobic and hydrophilic interactions may also occur between macromolecular chains. If these hydrogen bondings in chitin can be broken prior to deacetylation process, it will improve the degree of deacetylation of chitosan. Concentrations of NaOH solution used and steeping of the chitin in NaOH solution prior to hydrolysis by autoclaving is envisaged to promote higher degree of deacetylation of chitosan. It has also been suggested that cleavage of hydrogen bonds by acid can be done to improve DD of chitosan [12].

Effect of steeping on degree of deacetylation of chitosan

Single steeping time

Table 1 shows that DD in all three equations increases with steeping time. In equation 3, after 120h of steeping, the value of DD increases to 84% DD of chitosan. Hence, it can be suggested that various DD of chitosan can be easily produced by using appropriate steeping time. This is important as certain applications of chitosan may only require certain amount of purification of chitin. Efforts have been made in our laboratory to find usage for low grade chitin or chitosan for various applications since this work produces chitin as a by-product of fermentation of prawn waste for protein extraction. Low grade chitin or chitosan may potentially be used as fillers or reinforcing materials in forming biocomposites.

Table 1: Effect of duration of single steeping time on DD of Chitosan.

Single steeping time (h)	Absorbance		% DD of chitosan			
	1655 cm^{-1}	3450 cm^{-1}	Eq. 1[a]	Eq. 2[b]	Eq. 3[c]	Average
24	0.58	0.69	37.07	3.75	75.50	38.78
48	0.69	0.98	47.06	19.03	79.02	48.37
72	1.70	2.35	45.61	16.81	78.51	46.98
96	1.40	2.11	50.11	23.70	80.10	51.30
120	1.75	3.45	61.86	41.67	84.24	62.59

Reaction condition: NaOH (50%w/w), 101.3 kPa and 121°C. [a]Domszy and Roberts (1985), [b]Baxter et al.(1992), [c]Sabnis and Block (1997).

Visual observations on the colour of the chitosan produced from partially purified chitin changes from dark brown to light brown with increasing number of steeping days. This shows that NaOH (50% w/w) purifies the

protein residue from the partially purified chitin and the amount of protein removed increases as steeping time increases. This further demonstrates the necessity of minimal acid and alkali treatments prior to steeping and decetylation process if fermented chitin is to be used.
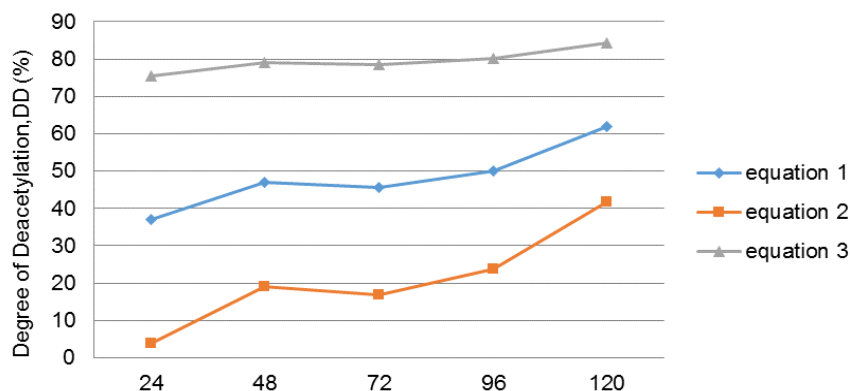

Figure 2: Effect of duration of single steeping time on DD of chitosan. Eq. 1: Domszy and Roberts(1985), Eq. 2:Baxter *et al*.(1992), Eq.3: Sabnis and Block

Steeping time (hours)

Double steeping time

The result shows that double steeping mode with 120h steeping in NaOH (50% w/w) produced high DD chitosan (average of 74.87%) (Table 2). Results using equation 3 shows that DD of chitosan are all above 80%. It is interesting to note that using a 120 days of double steeping had only increased the DD by 6% from 83% (at 24hr) to 89%(at 120hr) (equation 3) compared to an 8% increase (76% at 24hr to 84% at 120hr) when using single steeping for the same duration of reaction time (refer Table 1).

Table 2: Effect of double steeping time on DD of Chitosan

Double steeping time (h)	Absorbance		% DD of chitosan			
	1655 cm^{-1}	3450 cm^{-1}	Eq. 1	Eq. 2	Eq. 3	Average
24	1.75	3.07	57.14	34.45	82.57	58.05
48	1.59	3.60	68.67	52.08	86.63	69.12
72	1.33	2.34	60.63	39.78	83.80	61.40
96	0.00	4.22	100.00	100.00	97.67	99.20
120	0.59	1.75	74.65	61.23	88.74	74.87

Reaction condition: NaOH (50%w/w), 101.3 kPa and 121°C.

Similar to single steeping effect shown in Figure 2, results of equation 3 by Sabnis and Block (1997) shows the highest DD of chitosan throughout the 120h (Figure 3). Interestingly however, all equations showed a maximum DD of 98% - 100% after 96h of double steeping time which suggested that no further treatment is needed to enhance DD of chitosan beyond this point. However, beyond 96h of steeping time, chitosan showed only a slight decrease in DD. Similar trend was also noted by Baskar and Sampath Kumar (2009), during deacetylation of chitin by boiling method at 107°C whereby DD of chitosan decreases after 6h of boiling treatment [6]. They suggested that when DD is high or as the amino groups increases within the molecular chain of chitosan, it forms cations which combine with the water in the alkaline solution, rendering the solution to be more viscous. This hinders the stirring rate thus reducing the DD values.

Effect of steeping mode and steeping time on DD of chitosan

Figure 4 shows a comparison between the effect of mode of steeping (double and single steeping) and steeping time (24h to120 h) on DD of chitosan. In both modes of steeping, DD increases with time except for double steeping whereby DD decreased slightly after 96h.

Comparing the increase in DD when double mode was used shows that the increase in DD reduces with time. There is a 7% increase when steeped for 24h and only 4.5% increase when steeped for 120h (Table 3). This shows that although double steeping method may be useful in improving DD of chitosan, longer periods of double steeping is not economical. It is therefore appropriate to suggest that a double steeping mode is cost effective when used in shorter durations such as a 48h double steeping which had produced a DD of 86.63% (Table 3) which is similar to commercial chitosan of 85%. Yaghobi and Hormozi (2010) also suggested that a multistage deacetylation might be effective for increasing the degree of deacetylation of chitin [15].
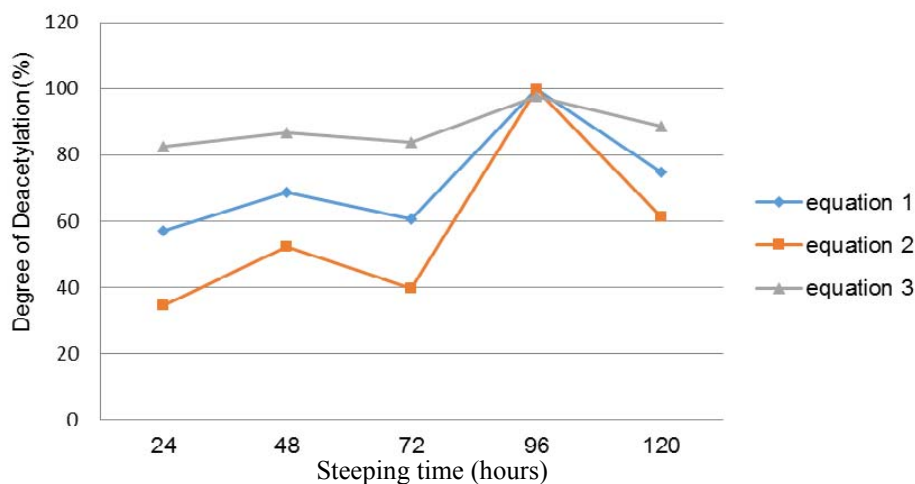
Figure 3: Effect of double steeping time on DD of chitosan. Eq.1: Domszy and Roberts (1985), Eq 2: Baxter et al.(1992), Eq.: Sabnis and Block (1997).
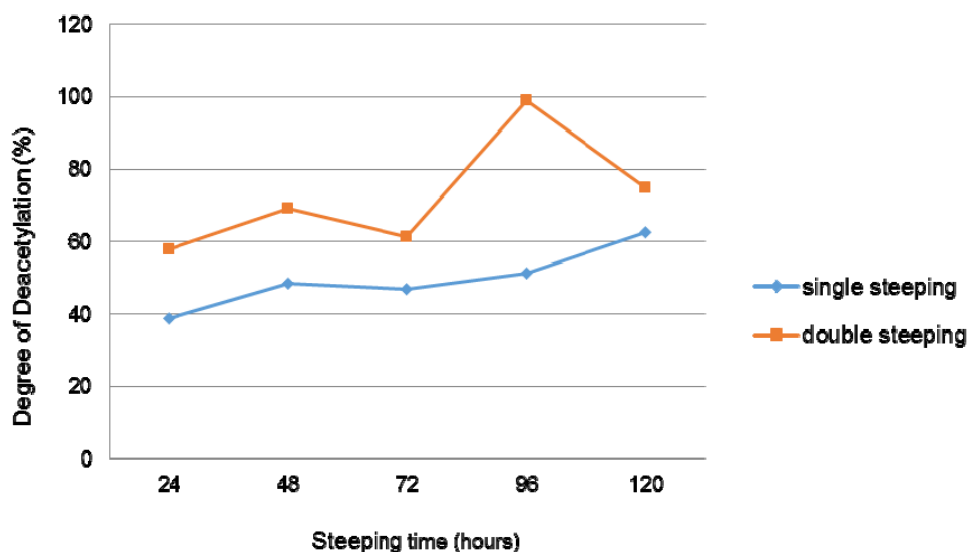
Figure 4: Effect of steeping mode on DD of chitosan.

Table 3: Comparison between the increase in DD by single and double steeping method using equation 3 of Sabnis and Block (1997) [**10**].

Steeping time (h)	24	48	72	96	120
Single steeping (%)	75.50	79.02	78.51	80.10	84.24
Double steeping (%)	82.57	86.63	83.80	97.67	88.74
Increase in DD (%)	**7.07**	**7.61**	**5.29**	**17.57**	**4.50**

CONCLUSIONS

Chitosan was produced from chitin isolated as by-products of fermented shrimp waste. Characterization of chitosan using FTIR spectroscopy showed that DD of chitosan increased with increasing number of steeping time and double steeping mode demonstrate better DD compared to single steeping mode. A limited double steeping mode shows a promising method to economically produce chitosan. This study which involved deacetylation using steeping and autoclave method together with using fermented chitin as a starting material could provide a more cost effective methods of producing high DD chitosan. However further investigation needs to be conducted to evaluate true cost of production.

ACKNOWLEDGEMENTS

REFERENCES

1. Samin, S. (2002). The status of the Fish Marine Cage Culture Industry in Sabah, Department of Fishery Sabah.
2. Shahidul Islam, Md., Saleha Khan, Masaru Tanaka. (2004). Waste loading in shrimp and fish processing effluents: potential source of hazard to the coastal and nearshore environments. *Marine Pollution Bulletin*. 49, 103-110.
3. Nor, N. M. , Zakaria, Z. , Manaf, M. S. A. and Salleh, M. M .(2011). The Effect of Partial Replacement of Dietary Fishmeal with Fermented Prawn Waste Liquor on Juvenile Sea Bass Growth, *Journal of Applied Aquaculture*, Volume 23, Issue 1, 51-57.
4. Singh, S, Tripathi, D. N., Tiwari, A., Sanghi, R. (2006). Microwave synthesized chitosan-graft-poly(methylmethacrylate): An efficient Zn^{2+} ion binder. *Carbohydrate Polymers*. 65, 35-41.
5. Abdou, E.S., Nagy, K.S.A., Elsabee, M.Z.(2008). Extraction and characterization of chitin and chitosan from local sources. *Bioresource Technol.*, *99*, 1359-1367.
6. Mayachiew, P. and S. Devahastin (2010). Effects of drying methods and conditions on release characteristics of edible chitosan films enriched with Indian gooseberry extract. *Food Chemistry*. 118, 594-601
7. Baskar, D. and T. S. Sampath Kumar (2009). Effect of deacetylation time on the preparation, properties and swelling behavior of chitosan films. *Carbohydrate Polymers*. 78, 767-772.
8. Domszy, J. G. and G. A. F. Roberts (1985). Evaluation of infrared spectroscopic techniques for analysing chitosan. Die Makromolekulare Chemie. 186, 1671-1677.
9. **Baxter, A. Dillon, M, Taylor,** K.D.A**., Roberts, G.A.F.,** (1992). Improved method for i.r. determination of the degree of N-acetylation of chitosan. *International Journal of Biological Macromolecules*. 14, 166-169.
10. Sabnis, S. and L. Block (1997). Improved infrared spectroscopic method for the analysis of degree of N-deacetylation of chitosan. *Polymer Bulletin*. 39, 67-71.
11. Zakaria,Z., G.M. Hall and G. Shama. (1998). Lactic Acid Fermentation of Scampi Waste in a Rotating Horizontal Bioreactor for Chitin Recovery, *Process Biochemistry*, 33, 1-6.
12. Theruvathil K Sini, Sethumadhavan Santhosh, Paruthapara T Mathew. (2007). Study on the production of chitin and chitosan from shrimp shell by using Bacillus subtilis fermentation. *Carbohydrate Research*. 342, 2423-2429.
13. Yaghobi, N. and F. Hormozi (2010). Multistage deacetylation of chitin: Kinetics study. *Carbohydrate Polymers*. 81, 892-896.

FABRICATION OF *Rhizomucormiehei*LIPASE REINFORCED NANOBIOCONJUGATES AS BIOCATALYSTS FOR A STATISTICALLY OPTIMIZED PRODUCTION OF EUGENOL BENZOATE

Fatin Myra Abd Manan dan Roswanira Abdul Wahab
Department of Chemistry, Faculty of Science, Universiti Teknologi Malaysia, 81310 Johor Bahru.

Abstract

The chemical synthesis ofeugenol benzoate is associated with numerous environmentally unfavorable practices *viz.* the use toxic chemicals, tedious separation process and liberation of harmful by-products. On this standpoint, an alternative approach utilizing *Rhizomucormiehei*lipase (RML) immobilized onto activated chitosan-multiwalled carbon nanotubes (RML/CS/MWCNTs) is suggested. The properties of the biocatalyst were characterized using Fourier-Transform Infrared Spectroscopy (FTIR), Field Emission Scanning Electron Microscopy (FESEM) and thermogravimetric analysis (TGA). Response surface methodology employing central composite design (CCD) based on four relevant parameters (incubation time, temperature, substrate molar ratio, and enzyme loading) was used to optimize the experimental conditions for the enzymatic synthesis to produce eugenol benzoate. The study found the high conversion of eugenol benzoate is greatly affected by temperature and incubation time. The highest yield of eugenol benzoate was 56.13 %, under optimized conditions of 60 °C, incubation time of 6 hr, enzyme loading of 150 IU and molar ratio of eugenol/benzoic acid of 4:1. The findings suggest that the RML/CS/MWCNTs biocatalyst developed here is a promising alternative to overcome shortcomings associated with the chemically produced esters.

Keywords: esterification, eugenol benzoate, Rhizomucormieheilipase, nanobioconjugates, Response Surface Methodology.

INTRODUCTION

Eugenol (4-allyl-2-methoxyphenol) is a member of phenylpropanoids, and it is commonly found in some essential oils especially in clove leaf oil, cinnamon oil, nutmeg, bay and basil leaf (Chaibakhsh*et al.,* 2012). Eugenol exists as a clear to pale yellow oily liquid and is commonly used in cosmetics and food products as a flavoring agent.Conventionally, esters of eugenol such as eugenol benzoate are acquired through the chemical route of the esterification process which is concomitant with a myriad of shortcomings (Radzi*et al.,* 2011). Such approach to synthesize the eugenol esters incurs the use of strong acidcatalysts and hazardous chemical such as halogenated metals. Apart from low conversion and extensive reaction time, the chemical route has been associated with tedious separation process and emancipation of harmful unwanted by-products (Charpe and Rathod., 2011). These problems can be overcome by opting for the biotechnological route utilizing specific biocatalysts such as lipases. Lipases (triacylglycerol ester hydrolysis EC 3.1.1.3) are enzymes that catalyze esterification reactions under ambient conditions and do not require conditions of high temperature and pressure. The biotechnological route is relatively straightforward when compared with the chemical synthesis (Charpe and Rathod., 2011).

In this context, *Rhizomucormiehei* lipase (RML) is the biocatalyst of choice owing to its versatility, strong specificity, and its suitability for ester synthesis has been evaluated under different conditions of temperature, pressure, water content, and substrates (Skoronski*et al.,* 2014). In order to improve the properties of the lipase, RML was immobilized onto a suitable solid support; in this case an activated chitosan/multiwalled carbon nanotube and used as catalyst. The immobilized enzymeallows reuse of the biocatalysts for better productivity (Zou*et al.,* 2010), improve stability and activity of enzymes (Cesar *et al.,* 2007). Currently, many materials have been explored for purposes of immobilizing lipases such as polymer resins, silica, chitin, chitosan, carbon nanotubes, and microspheres. Among these polymers, chitosan and carbon nanotubes are often favored by researchers. Chitosan (CS) is a natural cationic biopolymer that offers the benefits of biocompatibility, non-toxicity, and has high mechanical strength. This is due to the presence of amino and hydroxyl groups in CS that facilitates attachment of enzymes via covalent bonding or crosslinking (Solanki*et al.,* 2009). Likewise, carbon nanotubes (CNTs) have extraordinary mechanical strength, good electrical and thermal properties (Mubarak *et al.,* 2014). Once the surfaces of the CNTs are functionalized, the functional groups afford good sites of linkage with enzyme proteins.

The current conventional method of optimization requires screening of large number of variables, requires a large number of experiments, and involves lots of time and resources (Chaibakhsh*et al.,* 2012). Hence, response surface methodology (RSM) is employed as a fast and economical statistical technique that can be used to determine the optimal conditions of a multivariable system. RSM has been extensively applied for optimization of enzymatic processes (Chaibakhsh*et al.,* 2012). This present study was aimed at investigating the applicationof covalently bonded of RML ontoactivated chitosan/multiwalled carbon nanotube as potential economical biocatalysts. The RML/CS/MWCNTs beads were then used in synthesizingeugenol benzoate. In

addition, the enzymatic synthesis is then optimized by employing RSM, and the parameters investigated are incubation time, temperature, molar ratio of acid to alcohol, and enzyme loading.

EXPERIMENTAL

Materials

Commercial lipase of *Rhizomucor miehei*, activity of $\geq$20,000 U/g was purchased from Sigma-Aldrich (St. Louis, USA). Eugenol (>99% purity) and benzoic acid (>99% purity) were used as reagents for esterification reactions. Sodium hydroxide (NaOH) pallet, chloroform, glacial acetic acid, and nitric acid (65%), sodium phosphate buffer (pH 5.6), phenolphthalein were also purchased from Sigma-Aldrich. Meanwhile, powdered chitosan and MWCNTs were a gift from Dr. Zainoha and Dr. See Hong Heng, respectively. Other chemicals such as 2-(N-morpholino)ethanesulfonic acid (MES) salt, 1-Ethyl-3-[3-dimethylaminopropyl]carbodiimide hydrochloride (EDAC), and *N*-hydroxysuccinimide (NHS) were purchased from Tokyo Chemical Industry (Korea).

Purification and Functionalization of MWCNTs

Commercial MWCNTs (1.5 g) were refluxed with concentrated HNO_3 (4M, 90 mL) at 80°C for 5 h to completely remove the amorphous carbon phase and to oxidize the raw material. After cooling to room temperature, the mixture was centrifuged at 6000 rpm for 5 mins. The MWCNTs suspension was washed thouroughly with distilled water until the pH is neutral. Then, the suspension was filtered and dried in the oven (60°C) for 8 h. For the functionalization process, purified MWCNT (1.5 g) was refluxed in 1:3 v/v a mixture of H_2SO_4 (10ml, 95-97%) and HNO_3 (30ml, 65%). Then, the purified MWCNTs were oxidized under reflux at 100°C for 6 h to introduce functional carboxylate group. After the mixture is completely cooled, the suspension of functionalized MWCNTs (f-MWCNTs) was centrifuged at 6000 rpm for 5 mins and the liquid decanted. The f-MWCNTs were washed for several times with distilled water until the pH 7.0 was attained. The f-MWCNTs was precipitated by centrifugation (6000 rpm) and dried in vacuum oven at 60°C (Mohamad*et al.,* 2015).

Preparation of MWCNT/Chitosan Beads

MWCNT/chitosan (CS) beads were prepared by mixing 500 mg of powdered CS into 25 mL acetic acid solution (2.0% v/v) and stirred for 10 min at room temperature. The f-MWCNTs (5% w/w) was added into the CS mixture and homogenously stirred to afford the CS-MWCNTs suspension. The CS-MWCNTs mixture was slowly dropped into 1M sodium hydroxide (NaOH) solution using a pipette under continuous stirring.The initial beads were formed in the mixture and stirred for an additional 30 mins. CS-MWCNTs beads were washed several times with distilled water till neutrality. The beads were left to dry at room temperature overnight (Campos Carneiro*et al.,* 2014).

Covalent immobilization of Rhizomucormiehei on CS-MWCNTs beads and its characterization

Attachment of free FRML using EDAC as cross linker was performed according to the method described by Raghavendra*et al.* (2013) with some modifications. MWCNTs/CS beads (400 mg) were suspended in 20 mL 50 mM 2-(N-morpholino)ethanesulfonic acid (MES buffer at pH 6.1) and the mixture was stirred at 150 rpm for 5 mins before addition of NHS (8.0 mL of 50 mg/mL) followed by continuous stirring for another 5 mins. Under fast stirring, 4.2 mL of EDAC (10 mg/mL) was added and the mixture was stirred magnetically at room temperature for 60 min. The CS-MWCNTs beads were washed with 50 mM MES buffer (pH 6.1) to remove excess EDAC, NHS and urea by-product. The activated MWCNTs/CS beads were dispersed in 9.2 mL of 50 mM MES buffer (pH 6.1) containing 0.8 mL (20,000 IU/g) RML. The mixture was stirred at 4°C for 16 h to afford the CRL-CS-MWCNTs beads. The CRL-MWCNTs/CS beads were washed with 50 mM MES buffer (pH 6.1) to remove any unbound protein until no activity was detected in the washings and vacuum dried. The RML-CS-MWCNTs beads were stored at 4 °C until further use.

    Attenuated Total Reflectance (ATR): An aliquot amount of beads is placed onto the small crystal area. By using the Spectrum 100 Series, the vibrational spectrum of RML-CS-MWCNTs beads was recorded. The spectrumwas obtained using model in transmission mode between 400 -4000 cm^{-1}. ***Field emission scanning electron microscope (FESEM):*** A field emission scanning electron microscope (FESEM) (Brand: Hitachi, Model:SU8020) was used to study the morphology RML-CS-MWCNTs beads.

RML-CS-MWCNTs Catalyzed Synthesis of Eugenol Benzoate

The esterification reactions were performed in 50 mL screw-capped bottles which consisted of varying molar ratios of eugenol and benzoic acid and, stirred in chloroform as solvent. The RML-CS-MWCNTs beads (1 mg/mL) were added to initiate the reaction and stirred in a horizontal paraffin oil bath at 200 rpm at variable temperatures and incubation time (Table 3.1) (Horchani*et al,* 2010).

Experimental Design and Statistical Analysis

A four-factor-five-level central composite rotatable design (CCRD) was employed in this study, requiring 30 experiments. The fractional factorial design consisted of 16 factorial points, eight axial points, and six centre points. The parameters and their levels used for the optimization of RML-CS-MWCNTS catalysed synthesis of eugenol benzoate were reaction time (2-18 hr), temperature (30-70°C), enzyme loading (50-45- IU) and molar ratio of alcohol:acid (1:1-5:1). The experiments were randomized for statistical reasons and each experiment was run in triplicates.A software package, Design Expert Version 7.0 (Stat-Ease, Statistical Made Easy, Minneapolis, MN, USA) was used for designing and analysing the experimental data. The model equation was used to predict the optimum value and subsequently to elucidate the interaction between the factors. The quadratic equation model for predicting the optimal point was expressed as below:

$$y = b_0 + \sum_{i=1}^{4} b_i\,x_i + \sum_{i=1}^{4} b_{ii} x_i + \sum_{i=j}^{3} \sum_{j=i+1}^{4} b_{ij} x_{ij} + e \qquad \text{(Eqn.1)}$$

where y is the dependent variable (% yield) to be modelled; x_i and x_j are the independent variables (factors), b_0, b_i, b_{ii}, and b_{ij} are the regression coefficients of the model and *e* is the error of the model. Next, analysis of variance (ANOVA) was used to determine the adequacy of the constructed model to describe the observed data. R^2 value presents statistical points to the percentage of the variability of the optimization parameters explained by the model. Three-dimensional surface plots were generated to illustrate the main and interactive effects of the independent variables on the dependent ones.

RESULTS AND DISCUSSION

Rationale on covalent immobilization of RML onto activated MWCNTs/CS beads

Surface functionalization of carbon nanotubes plays an essential role for improving the solubility and dispersion of the nanotubes in aqueous solutions and to design new materials (Yudianti*et al.,* 2011). The functional groups (COO⁻) grafted onto the MWCNTs (f-MWCNTs) can potentially increase their interactions with CS, thus resulting in significant improvement in mechanical properties of the MWCNTs/chitosan beads.In this study, carbon nanotubes were proposed as fillers within the polymeric biomaterials of CS and serve to strengthen structure of CS and improve mechanical and biological properties compared to neat CS (Kroustalli*et al.*2013). Covalent attachment of RML to the CS/MWCNTs beads provide powerful link between the lipase and its carrier matrix. The nucleophilic groups (COO⁻) will interact strongly with electrophiles on the RML protein. The resultant RML-CS/MWCNTs nanobioconjugates are more desirable and beneficial in terms of reusability and robustness.

Characterization of Immobilized Lipase (RML/CS/MWCNTs)

Field emission scanning electron microscope (FESEM)

CS beads were incorporated with MWCNTs to enhance their mechanical structure. The inclusion of MWCNTs changed the morphology of the beads, as shown in **Figure 1(i).** The CS/MWCNTs bead had a more rigid and spherical structure and its FESEM image shows a spiky structure that resulted from the inclusion of MWCNTs nanoparticles, which could further enhance its mechanical strength (Lau *et al.,* 2014). In addition, the change in the roughness of the beads can be observed **Figure 1(ii)** and it is increased upon N-hydroxysuccinimide (NHS)and EDAC treatment and subsequent RML immobilization on the activated surface (Hedge and Veeranki, 2014).It can be seen that the reactivity of beads was increased due to the formation of amide bonds between carboxylic acid groups on the functionalized MWCNTs, and amine groups from the RML. This process was catalyzed by the activation of carboxyl groups by the EDAC coupling reagent, resulting in successful enzyme immobilization (Alkhatib et al., 2012).
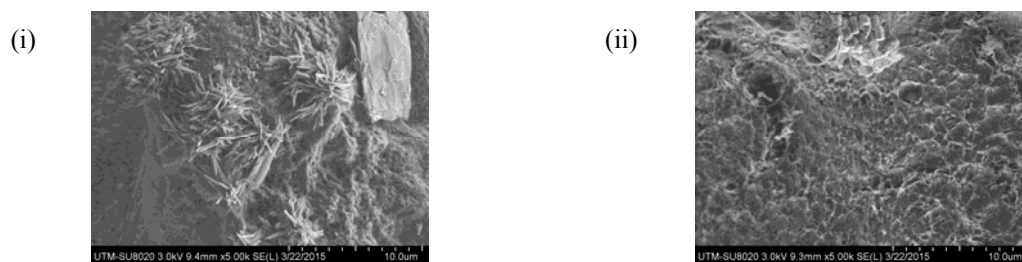
(i)   (ii)

Figure 1: Micrographs of(i) CS-MWCNTs beads and (ii) immobilized RML onto activated CS beads at 5,000 magnifications.

Fourier Transform Infrared Spectroscopy - Attenuated Total Reflectance (ATR)

The spectrum of RML-CS-MWCNTs in **Figure 2**showed numerous peaks in the range of 670-1575 cm^{-1} as a result of activation by NHS and EDAC. Peak presents at 1026.31 cm^{-1} belonged to the secondary amines which indicated the presence of unstable o-acylisourea intermediates formed as the by-product in the reaction of EDAC and –COOH groups (Raghavendra*et al.,* 2013). Emergence of multiple peaks at 1642.98, and 1420.33 cm^{-1}suggesting that immobilized RML retained its native structure (Collins *et. al,* 2011). Slight shifting to higher wavenumber of peaks and increasing of absorption bands indicate a possible covalent interaction between the support and enzyme (Diaconu*et al.,* 2010).
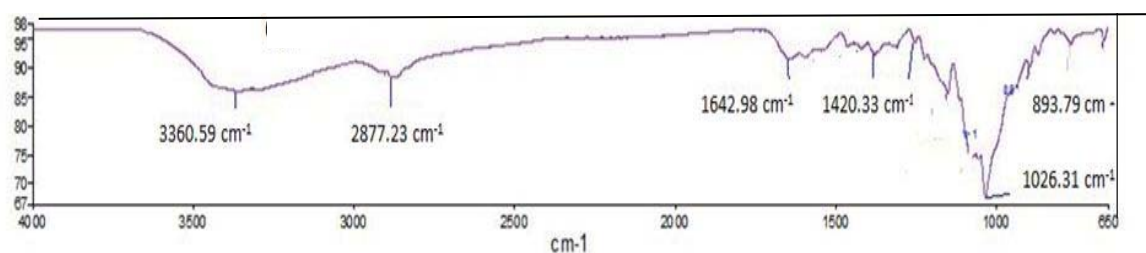
Figure 2: IR spectrum for RMLimmobilized onto activated CS beads.

Thermal Gravimetric Analysis (TGA)

Thermal properties RML/CS/MWCNTs beads were assessed by thermogravimetric analysis and depicted in Figure 3. The thermogram profile of RML/CS/MWCNTs beads revealed a relatively steep mass loss of nearly 30% that occurred at a lower temperature of approximately 250 °C. This observation is due to the enzyme molecules that are proteinaceous in nature that tended to prematurely decompose at lower temperatures as compared to other components in the RML/CS/MWCNTs composite. Based on the thermogram, the study found the covalent immobilization of RML to the surface of the CS/MWCNTs beads as calculated from the final weight percentage of the samples (Raghavendra*et al.,* 2013), was established to be 10.17%.

Figure 3: The thermogram for the thermal decomposition of RML/CS/MWCNTs beads

Model fitting and analysis of variance (ANOVA)

The CCD was the chosen design for the surface optimization of eugenol benzoate catalyzed by the RML-CS-MWCNTs biocatalysts since it is a wide accepted model for optimization studies. Themodel consisted of four factors: time (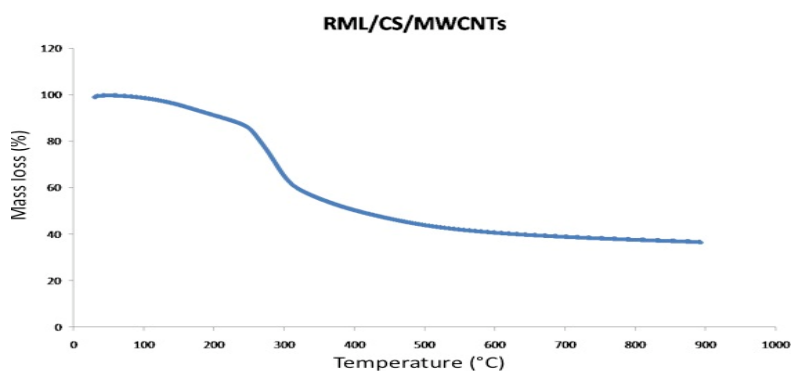A), temperature (B), enzyme loading (C) and molar ratio (D) and each factor was studied at five different levels (–2, –1, 0, +1, +2) and required 30 experiments.The experimental conditions design and their employed responses are depicted by the model. The predicted values were acquired with a model fitting technique by using the software Design Expert version 7.1.6 and were observed to be satisfactorily correlated with the observed values.Fitting of the data to various models (linear, two factorial, quadratic and cubic) and their following ANOVA, illustrated that the esterification of eugenol and benzoic acid was most suitably described with a quadratic polynomial model. The polynomial model was regressed for the conversion of benzoic acid and the **Eqn (2)** in terms of coded factors is shown as follows:

Conversion (%) =   + 36.65 -4.25A + 7.43B - 1.56C + 0.92D +6.44AB + 2.33AC – 4.91AD
– 3.73BC + 3.68BD + 1.63CD **(Eqn. 2)**

Where *A* is the time,*B*- the temperature,*C*- the solvent and *D*- the substrate molar ratio. The positive sign in front of term meant synergistic effect while the negative sign illustrates antagonistic effect, indicating the influence of independent variables on the esterification reaction process. It is agreed that the large *F*-value and smaller the *P*-value, the more significant the corresponding coefficient (Y.C. Wong *et al.,* 2015), hence, the results in this study suggested that the variable with the largest effect was the reaction temperature (**Table 1**).

Table 1: Analysis of variance and model coefficients

Source	Sum of squares	Degree of Freedom	Mean square	*F*-value	*P*-value Prob> F	
Model	3455.26	10	345.53	29.48	< 0.0001	significant
A-time	432.71	1	432.74	36.92	< 0.0001	
B-temperature	1325.66	1	1325.66	113.11	< 0.0001	
C-enzyme loading	58.38	1	58.38	4.98	0.0379	
D-molar ratio	20.44	1	20.44	1.74	0.2023	
AB	664.48	1	664.48	56.69	< 0.0001	
AC	86.72	1	86.72	7.40	0.0136	
AD	385.24	1	385.24	32.87	< 0.0001	
BC	222.83	1	222.83	19.01	0.0003	
BD	216.16	1	216.16	18.44	0.0004	
CD	42.61	1	42.61	3.64	0.0718	
Residual	222.69	19	11.72			
Lack of Fit	171.28	14	12.23	1.19	0.4570	Not significant
Pure Error	51.41	5	10.28			
Cor Total	3677.95	29				

Interactive effects of factors on the RML-CS-MWCNTs catalyzed esterification of eugenol benzoate

Effect of time and temperature

The interactive effect of both variables (**Figure 4a)** were evaluated at hold values of other parameters at molar ratio eugenol: benzoic acid (3:1) and enzyme loading of 250 IU. According to the *F*-value, the effect of the temperature (78.42) is more significant than the incubation time (24.40). The interaction between both parameters was significant because of the very small *P*-value (< 0.0001). It was clearly visible from the figure that the percent conversion of eugenol benzoate increased as the reaction temperature was elevated up to 57-63°C. Yields of eugenol benzoate close to 42% percent can be obtained under short reaction time by setting the reaction temperature to maximum coded levels. Prolonging the reaction time was found to be counterproductive probably due to the build up of water produced by the esterification reaction, favoring the reverse reaction that hydrolyzes (Abdul Rahman*et al.,* 2008) eugenol benzoate. Higher reaction temperature also tended to induce enzyme inactivation due to thermal denaturation of lipase (Chaibakhsh*et al.,*2012) particularly under extensive reaction time.

Effect of time and substrate molar ratio

The effect of time and molar ratio (acid/alcohol) on percent conversion of eugenol benzoate at a constant temperature of 50°C is depicted in **Figure 4b.** Again the results clearly revealed that the effect of time was more significant than molar ratio. The F-value time (36.92) was higher than that of molar ratio (1.74), highly suggestive that reaction time was more impacting on the RML-CS-MWCNTs catalyzed production of eugenol benzoate (Table 4.2). The ANOVA of factors also indicated that the mutual interaction between both parameters was very significant due to a very small P-value (< 0.0001). It can be seen that the highest percentage conversion can be achieved at short incubation time and at high substrate molar ratio, as the yield of eugenol benzoate as high as 44% was attainable at short reaction time of ~7.0 h by utilizing the substrate molar ratio in the range of 3.5:1 and 4.0:1 (acid: alcohol).On the other hand, the improved yield of the ester when the molar ratio of substrates was set to maximum coded levels may be associated to increased availability of eugenol for the RML-CS-MWCNTs (Chaibaksh*et al.,* 2012). Similarly, the higher ester yield may be the result of better solubility of the solid benzoic acid in higher volumes of eugenol (Abdul Rahman*et al.,* 2008) which elevated the probability of effective substrate-enzyme collisions (Wahab*et al.,* 2014).
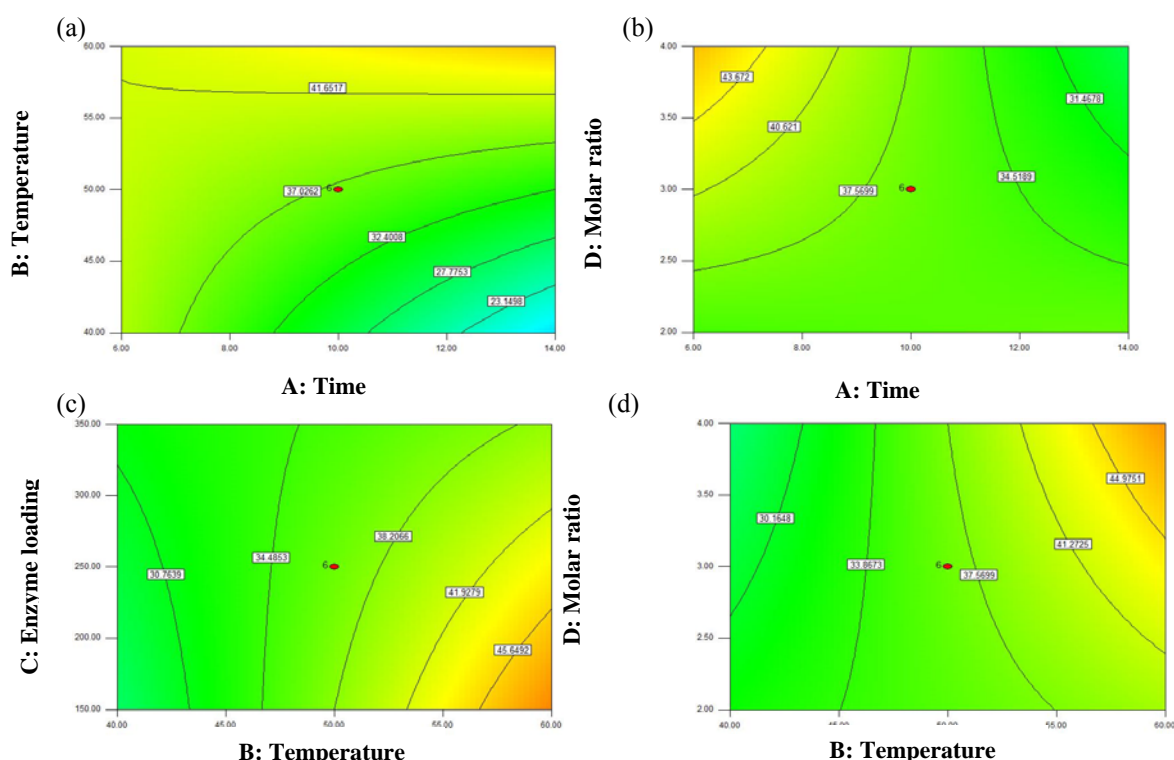

Figure 4: Contour plots between two parameters, (a) time and temperature, (b) time and molar ratio, (c) temperature and enzyme loading, (d) temperature and molar ratio,in the synthesis of eugenol benzoate. The numbers inside the contour plots indicate esterification yield (%) at given reaction conditions.

Effect of temperature and enzyme loading

Figure 3illustrates the contour plot for the interactive effects of temperature versus enzyme loading in the RML-CS-MWCNTs catalyzed synthesis of eugenol benzoate (**Figure 4c**). The interactive effect of both variables were evaluated at hold values of other parameters at molar ratio eugenol: benzoic acid (3:1) and incubation time for 10 h. As indicated by the linear coefficients and *F*-value, the effect of the temperature (1325.66) was substantially more significant than the enzyme loading (4.98). The interaction between both parameters was significant because of the very small *P*-value (0.0003). Generally, minimal use of enzyme for high conversion of product is favored due to the rather high cost of enzymes (Wahab*et al.,* 2014).It was clearly visible that the percent conversion of eugenol benzoate increased as the reaction temperature was elevated to 60°C. The yield of eugenol benzoate can be improved up to 46% percent when the reaction is performed at low enzyme loading at any values between 150-225 IU and temperature in the range of 54 to 60°C.As seen on the contour plot, immobilization of RML onto the CS-MWCNTs hybrid supports has probably improved operational stability of the lipase, reflected in the high yield of the ester when the reaction was increased to maximum coded levels. Such change can permit enzymes to work in a larger range of environments, in this

case, reaction temperature; hence, allowing enzymes to remain active at elevated temperature (Spahn and Minteer, 2008).

Effect of temperature and molar ratio

The interactive effect of temperature versus substrates molar ratio in the RML-CS-MWCNTs catalyzed synthesis of eugenol benzoate was evaluated at hold values of enzyme loading (250 IU) and incubation time of 10 h (**Figure 4d**). As indicated by the linear coefficients and F-value, the effect of the temperature (1325.66) was substantially more significant than the molar ratio (1.74). Their mutual interaction was found to be significant as represented by a very small P-value (0.0004).It was seen that the maximum yield of eugenol benzoate, as high as 45% could be achieved when both variables are set at maximum coded values. By simultaneously elevating the temperature to 55-60 °C and substrates molar ratio at any values between 3.5:1 to 4:1, the yield of eugenol benzoate could be positively enhanced.Apart from improved substrates integration and activation of enzyme activity that may occur at the proposed high reaction temperature, the higher concentrations of eugenol too, may favorably shift the esterification reaction from hydrolysis to ester biosynthesis. Such change can be associated with the re-direction of the reaction's equilibrium towards product formation when the concentration of nucleophile (eugenol) is elevated (Verissimo*et al.,* 2015) in the reaction mixture.

Attaining optimum condition and model validation

For developing efficient industrial processes for the esterification of eugenol that are of environmentally friendly, a statistically assistedoptimized process may provide a convenientsolution to this problem. (Wahab*et al.*, 2014).With regards to this, attaining a high degree of conversion was possible by solving the regression equation (**Eqn 1**) using Design Expert 7.1.6 and determines the optimum point on the response surface (Wahab*et al.,* 2014).The software proposed several experimental conditions in order to find the optimum point that maximizes percentage conversion of eugenol benzoate under a variety of preferred conditions. However, only one set of the predicted conditions suggested by the model were chosen. By evaluating several experimental conditions suggested by the software, a set of the most appropriate esterification condition with desirability value of 1 was chosen for this present study. Utilizing the chose set of conditions using fairly low enzyme loading and short reaction time, the highest percent conversion attained was 55.91% at 6 h of reaction time, 60 °C and substrate molar ratio of 1:4 of benzoic acid: eugenol. This is in comparison to the maximum conversion (56.13 %) for the synthesis of eugenol benzoate was predicted at the same conditions, where the predicted value was 57.34 % with 2.11 % deviation.Since the experimental values were found to be quite close to the predicted of the modelvalues, it was concluded that the proposed model was adequate and its validity confirmed.

CONCLUSION

The chitosan/multiwalled-MWCNTs beads were preparedsuccessfully as seen in the analyses of TGA, FESEM, and FTIR. The study also demonstrated that the RSM technique could be applied effectively to predict the optimized conditions for a reasonableRML/CS/MWCNTs-assistedproduction of eugenol benzoate. The findings showed the RML/CS/MWCNTs biocatalysts afforded a 56.13% yieldof the ester under the preferred optimized conditions of short incubation time and low enzyme loading; 60°C, incubation time of 6 h, enzyme loading of 15 mg and substrate molar ratio of eugenol/benzoic acid 4:1. Since the predicted yield (57.34%) closely agreed with the actual experimental value (56.13%), the suitability of the RSM prediction technique used in this study was justifiably proven. In view of minimizing the impact of conventional synthetic processes on the environment, the RML/CS/MWCNTs developed here as biocatalysts for the production of eugenol benzoate may prove valuable.

REFERENCES

Abdul Rahman, M.B., Chaibakhsh, N., Basri, M., Rahman, R.N.Z.A., Salleh, A.B., (2008).Modelling and optimization of lipase-catalyzed synthesis of dilauryladipate ester by response surface methodology. Journal of Chemical Technology and Biotechnology. 83, 1534-1540.

Al-Khatib, Ma AnFahmi Rashid Alam, Md. Zahangir and Mohammed, Rasha (2012). Statistical modellingoptimisation of cellulase enzyme immobilisation on functionalised multi-walled carbon nanotubes for empty fruit bunches degradation. Australian Journal of Basic and Applied Sciences, 6, 30-38.

Campos Carneiro, L.A.B., Costa-Silva, T.A., Fernandes Souza, C.R., Bachmann, L., Oliveira, W.P., and Said, S., (2014). Immobilization of lipases produced by the endophyticfungus Cercosporakikuchii on chitosan microparticles. Brazillian Archives of Biology and Technology. 57(4), 578-586.

Cesar, M, Jose, M.P., Gloria, F.L., Jose, M.G., and Roberto F.L., (2007).Improvement of enzyme activity, stability and selectivity *via* immobilization techniques.Enzyme and Microbial Technology. 40, 1451–1463.

Chaibakhsh, N., Basri, M., Hani, M.A., Abdul Rahman, M.B., and Rezayee, M., (2012).Optimization of enzymatic synthesis of eugenol ester using statistical approaches.Biocatalysis and Agricultural Biotechnology. 1, 226-231.

Chaibakhsh, N., Basri, M., Hani, M.A., Abdul Rahman, M.B., and Rezayee, M., (2012).Optimization of enzymatic synthesis of eugenol ester using statistical approaches.Biocatalysis and Agricultural Biotechnology. 1, 226-231.

Charpe, T.W and Rathod, V.K., (2011). Biodiesel production using waste frying oil.Waste Management. 31, 85–90.

Collins, S.E., Lassalle, V., and Ferreira, M.L., (2011).FTIR-ATR characterization of free *Rhizomucormeihei* lipase (RML), Lipozyme RM IM and chitosan-immobilized RML. Journal of Molecular Catalysis B: Enzymatic. 72(3–4), 220–228.

Diaconu, M., Litescu, S.C., and Radu, G.L., (2010).Laccase–MWCNT–chitosan biosensor—A new tool for total polyphenolic content evaluation from in vitro cultivated plants. Sensors and Actuators B. 145, 800–806.

Hedge, K. and Veeranki, V. D., (2014). Studies on immobilization of cutinases from Thermobifidafusca on gluteraldehyde activated chitosan beads. British Biotechnology Journal. 4(10), 1049-1063.

Horchani, H., Ben Salem, N., Zarai, Z., Sayari, A., Gargouri, Y., and Chaâbouni, M., (2010). Enzymatic synthesis of eugenol benzoate by immobilized Staphylococcus aureus lipase: Optimization using response surface methodology and determination of antioxidant activity. Bioresource Technology. 101, 2809-2817.

Kroustalli, A., Zisimopoulou, A.E., Koch, S., Rongen, L., Deligianni, D., Diamantouros, S., Athanassiou, G., Kokozidou, M., Mavrilas, D., and Jockenhoevel, S., (2013). Carbon nanotubes reinforced chitosan films: mechanical properties and cell response of a novel biomaterial for cardiovascular tissue engineering. Journal of Materials Science Materials in Medicine. 24(12), 2889-2896.

Lau, S.C., Lim, H.N., Basri, M., FardMasoumi, H.R., Ahmad Tajudin, A., Huang, N.M., Andou, Y. (2014).Enhanced Biocatalytic Esterification with Lipase-Immobilized Chitosan/Graphene Oxide Beads.PLoS ONE, 9(8), e104695. doi:10.1371/journal.pone.0104695.

Mohamad, N.R., Buang, N.A., Mahat, N.A., Lok, Y.Y., Huyop, F., Aboul-Enein, H.Y., and Abdul Wahab, R., (2015). A facile enzymatic synthesis of geranyl propionate by physically adsorbed Candida rugosa lipase onto multi-walled carbon nanotubes. Enzyme and Microbial Technology. 72, 49–55.

Mubarak, N.M., Wonga, J.R., Tana, K.W., Sahuc, J.N., Abdullah, E.C., Jayakumar, N.S., and Ganesan, P., (2014). Immobilization of cellulase enzyme on functionalized multiwall carbon nanotubes. Journal of Molecular Catalysis B: Enzymatic. 107, 124-131.

Radzi, S.M., Mustafa, W.A.F., Othman, S.S., and Noor, H.M., (2011). Green synthesis of butyl acetate: A pineapple flavor via lipase catalyzed reaction. World Academy of Science, English, and Technology. 59, 677-680.

Raghavendra, T., Basak, A., Manocha, L.M., Shah, A.R., and Madamwara, D., (2013). Robust nanobioconjugates of Candida antarctica lipase B – Multiwalled carbon nanotubes: Characterization and application for multiple usages in non-aqueous biocatalysis. Bioresource Technology. 140, 103–110.

Skoronski, E., Padoin, N., Soares, C., and Furigo, Jr.A., (2014). Stability of immobillizedRhizomucormiehei lipase for the synthesis of pentyloctanoate in a continuous packed bed bioreactor.Brazilian Journal of Chemical Engineering. 31(3), 633-641.

Solanki, P.R., Kaushik, A., Ansari, A.A., Tiwari, A., and Malhotra, B.D., (2009). Multi-walled carbon nanotubes/sol–gel-derived silica/chitosan nanobiocomposite for total cholesterol sensor. Sensors and Actuators B: Chemical. 137, 727-735.

Spahn, C. and Minteer, S.D., (2008).Enzyme Immobilization in Biotechnology.Recent Patents on Engineering. 2, 195-200.

Verissimo, L.A.A., Soares, W.C.L., Mol, P.C.G., Minim, V.P.R., da Silva, M.C.H., and Minim, L.A., (2015). Optimization of flavor ester synthesis catalysed by Aspergillusniger lipase. African Journal of Microbiology Research. 9(13), 922-928.

Wahab, R., Abdul Rahman, M.B., Chaibakhsh, N., Leow, T.C., Basri, M., Abdul Rahman, R.N.Z., and Salleh, A.B., (2014).Enzymatic production of a solvent-free menthyl butyrate via response surface methodology catalyzed by a novel thermostable lipase from Geobacilluszalihae.Biotechnology & Biotechnological Equipment. http://dx.doi.org/10.1080/13102818.2014.978220.

Yudianti, R., Onggo, H., Sudirman, Saito, Y., Iwata, T., and Azuma, J., (2011). Analysis of functional group sited on multi-wall carbon nanotube surface. The Open Materials Science Journal. 5, 242-247.

Zou, B, Hu, Y, Yu, D., (2010). Immobilization of porcine pancreatic lipase onto ionic liquid modified mesoporous silica SBA-15.Biochemical Engineering Journal. 53(1), 150–153.

GENERATION OF PROTONIC ACID SITES FROM ALKANES OVER WO₃-ZrO₂ EVIDENCED BY FTIR AND ESR SPECTROSCOPY

Asmida Kamarudin[1], Aishah Abdul Jalil[2] and Sugeng Triwahyono[1]*
[1]Department of Chemistry, Faculty of Science, Universiti Teknologi Malaysia, 81310 Johor Bahru
[2]Department of Chemical Eng., Faculty of Chemical and Energy Eng., Universiti Teknologi Malaysia, 81310 Johor Bahru

Abstract

The interaction of molecular hydrogen with the surface of WO₃-ZrO₂ to generate protonic acid sites was observed using ESR Spectroscopy and lutidine pre-adsorbed FTIR Spectroscopy. The WO₃-ZrO₂ sample was characterized by BET and XRD technique. The surface area of WO₃-ZrO₂ was 49 m^2/g, with pore distribution of mesoporous solid and the content of WO₃ on ZrO₂ was 15 wt %. Lutidine pre-adsorbed FTIR showed the presence of protonic acid sites 1644cm^{-1} and 1632cm^{-1}. For ESR spectroscopy, a decrease in the ESR signals at g=1.98 upon heating with alkane and in the UV irradiation suggested the formation of electrons that have been trapped by the electron deficient metal cationand radicals.

Keywords: Protonic acid sites,WO₃-ZrO₂, Alkanes, ESR, Lutidine pre-adsorbed FTIR

INTRODUCTION

Solid acid catalysts are known to be less corrosive and harmful. Most of important industrial reactions are catalyzed by solid acids. Solid acid catalyst plays an important role on providing surface sites for adsorption and conversion of hydrocarbon which leads to produce petrol with high quality. Tungsten Oxide Zirconia (WO₃-ZrO₂) will be used to generate the protonic acid site from hydrocarbon molecules (alkanes) thus provides the active sites for conversion of hydrocarbon. Different alkanes which are *n*-pentane, *n*-hexane, and *n*-heptane will be used to observe their ability to form the protonic acid site.

WO₃-ZrO₂is the solid acid catalysts that supported by zirconia. Zirconia (ZrO₂) is one among the other support that received considerable interest because of its potential as a catalyst support. ZrO₂ presents special characteristic such as high thermal stability, extreme hardness, stability under reducing condition, and both acid and base functions [1]. Zirconia supported metal oxide catalyst have received big attention due to their potential catalytic application in alkane conversion reactions in the petrochemical industry. They become an efficient catalyst for isomerization of saturated straight alkane.

EXPERIMENTAL

Preparation of WO₃-ZrO₂

Zirconium hydroxide (Zr(OH)₄) was prepared from an aqueous solution of zirconium oxychloride,(ZrOCl₂.8H₂O) by hydrolysis with an aqueous solution of ammonia, followed by washing with deionized water and drying at 373K at air. The WO₃-ZrO₂ sample was prepared by impregnation of Zr(OH)₄ with aqueous solution of ammonium metatungstate (NH₄)₆[H₂W₂O₄₀] followed by calcinations at 1093K in air. This series of catalysts are denoted by their weight percentage of WO₃ and calcinations temperature. The content of WO₃ in this sample catalyst was 15wt. %.

Characterization of WO₃-ZrO₂

Characterization of prepared catalyst was performed by using Brunauer, Emmet and Teller (BET) and X-Ray Diffraction (XRD). BET is used to measure the specific surface of finely divided and porous solid. XRD is used to find the crystal structure of unknown material and measure the size, shape and internal stress of small crystalline regions.

Generation of Protonic Acid Sites

To generate the protonic acid sites, two techniques were used which is by ESR spectroscopy (JEOL-FA100 ESR Spectrometer) and lutidine pre-adsorbed FTIR spectroscopy. WO₃-ZrO₂ was run by ESR at room temperature before evacuate and then evacuate at room temperature for 10 minutes. The WO₃-ZrO₂ then was

outgassed at 400K for 30 minutes followed by the introduction of 10Torr of *n*-pentane (C5) at room temperature. Then the catalyst was heated to room temperature, 323K, 348K, 373K, 398K, 423K and 448K.The procedure was repeated, replacing*n*- pentane with other alkane (*n*-hexane and *n*-heptane).

The IR Spectra were recorded using Perkin Elmer GX FTIR Spectrometer in the region (500-4000 cm^{-1}). 0.06 g of WO_3-ZrO_2 was ground by using the mortar. The sample must be ground until it fine and not coarse to form a thin and flat pellet. The pellet than was pressed under the hydraulic pressure. The CaF2 windows in the cell reactor must be tight to prevent leak that will affect the data. The background of FTIR was scanned followed by blank cell. The pellet then was put in the sample holder and its spectra were determined at room temperature. The pellet was put in the cell reactor then was evacuated at 673 K under vacuum for 30 minutes and then was exposed to 5 Torr of lutidine and hold for 10 minutes at room temperature. The pellet is outgassing at room temperature, 323 K, 373 K and 423 K. and it was cooled before scanned in FTIR. As for the formation of protonic acid sites from hydrocarbon molecules, the pellet was exposed to 10 Torr of alkane at room temperature and was heated up from 323 K to 423 K. After that, the pellet was cooled to 318 K and scanned.

Formation of Radical

In this experiment, the formation of radical is observed by using Electron Spin Resonance with injection of ultraviolet (UV) rays USHIO Optical Modulex. WO_3-ZrO_2 was run by ESR at room temperature before evacuate and then evacuate at room temperature for 10 minutes. The WO_3-ZrO_2 then was outgassed at 400K for 30 minutes followed by the introduction of 10Torr of pentane (C5) at room temperature. Then the sample was put in ESR and injected with UV rays and scan as a function of time (1, 5, 10, 15, 20, 25, 30 minutes).The data were observed and recorded. The procedure was repeated, replacing *n*-pentane with other alkane (*n-hexane* and *n*-heptane).

RESULT AND DISCUSSION

XRD pattern for WO_3-ZrO_2

Figure 1.0 depicts the XRD diffractogram for WO_3-ZrO_2. The XRD pattern showed monoclinic and tetragonal phases of WO_3-ZrO_2 solid acid catalyst. In this study, only two phases were observed in the sample. The stable tetragonal phase was observed at the peaks 2θ= 30.4° which is correspond to specific peak of zirconia.The presence of WO_3 on ZrO_2 disappeared the predominant monoclinic phase of zirconia and develop the tetragonal phase markedly as depicted in figure 4.1. The peaks at about 28.28° and 31.44° are assigned as monoclinic ZrO_2. Hence, doping with certain amount of WO_3 is essential to obtain the active metastable tetragonal phase in the catalysis.
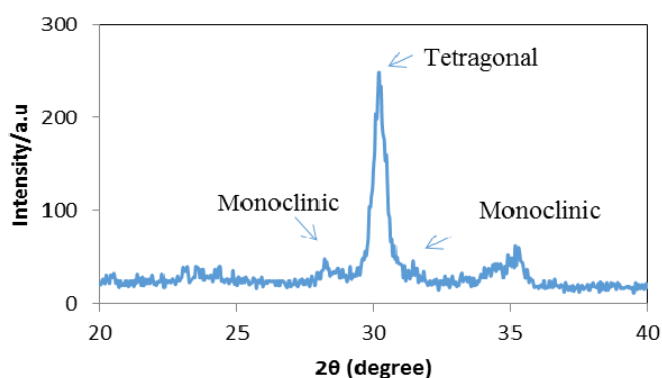

Figure 1.0: XRD Pattern of WO_3-ZrO_2

BET Surface Analysis

Figure 2.0 presents the pore size distribution curves of WO_3-ZrO_2. From the graph, the pore size distribution size for WO_3-ZrO_2 catalyst was presence in the range of 6-8 nm. Hence, WO_3-ZrO_2 could be classified as mesoporous solid due to maximum peaks of pore diameter.That pore structure provides an extremely larger surface area within a relatively small volume of material and it makes the sample suitable for catalysis

application.The WO_3-ZrO_2 catalyst calcined at 1093 K has 49 m^2/g of surface area where the weight content of WO_3 is 15wt%.

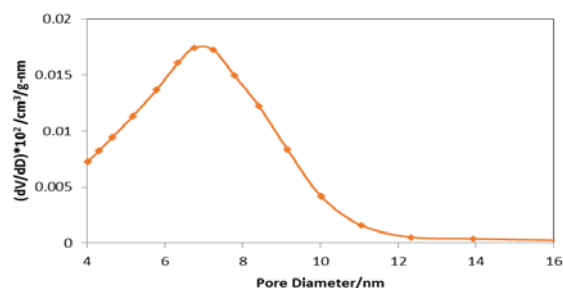**Figure 2.0**: Pore distribution size for WO_3-ZrO_2

Lutidine Pre-Adsorbed FTIR Spectroscopy

Figure 3.0 shows the IR spectra of WO_3-ZrO_2 whichwas treated in vacuum for 30 minutes at 400 K and after the lutidine was adsorbed to the sample WO_3ZrO_2 at room temperature. When lutidine was adsorbed on WO_3-ZrO_2 sample, one peak doublets arose, one of them centred as 164cm^{-1} and 1632cm^{-1} .The other doublets peak centred at 1556cm^{-1} and 1544cm^{-1} is due to interaction of lutidine with the Lewis sites. The presence of Lewis acid sites is indicated by a small band and these bands are characteristic of lutidine coordinated to Lewis acid centres.
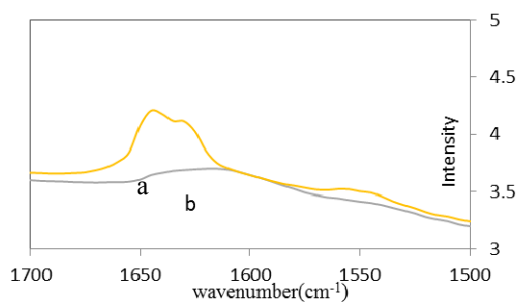

Figure 3.0: IR spectra for (a) lutidine adsorbed on WO_3-ZrO_2(b) treatment of WO_3-ZrO_2 invacuo at 400 K

FTIR spectroscopy was used to observe the formation of protonic acid sites from alkanes on the lutidine pre-adsorbed WO_3-ZrO_2. The intensities of peak of Bronsted acid sites increased at 1600-1500cm^{-1} when the temperature was increased up to 423 K. The intensities of peak of Lewis acid sites decreased at 1600-1500cm^{-1} when the temperature was raised. It shows that the protonic acid site was generated. Figure 4.0 shows the IR spectra of lutidine pre-adsorbed WO_3-ZrO_2 in the presence of *n*-pentane. The adsorption of lutidine on WO_3ZrO_2 in the presence of*n*-pentane formed protonic acid sites at 1644cm^{-1} and 1632cm^{-1}. The fractions of Bronsted acid were plotted against the temperature of heating in *n*-pentane, *n*-hexane and *n*-heptane as shown in figure 5.0 below.
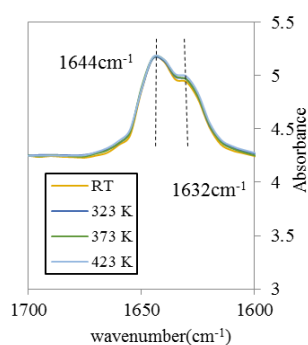

Figure 4.0: IR spectra of adsorption of *n*-pentane on WO_3ZrO_2 in the range 1700-1600cm^{-1}

As the hydrogen atom converted into protonic acid sites and a hydride, the Lewis acid sites loses its function.The doublets peak appeared at 1556cm^{-1} and 1544cm^{-1} when the sample lutidine pre-adsorbed WO3-ZrO2 was heated in the presence of alkane. These result indicated that lewis acid site converted into protonic acid sites when the sample was heated with *n*-pentane, *n*-hexane and *n*-heptane. Figure 6.0 shows the IR spectra at 1600-1500cm^{-1} when lutidine pre-adsorbed WO_3-ZrO_2 was heated from room temperature until 423 K in the presence of 10 Torr of *n*-pentane. The spectral changes would be more clearly shown in the fraction of lewis acid sites. Figures 7.0 showed the fraction of Lewis acid sites which are plotted against the temperature of heating in *n*-pentane.
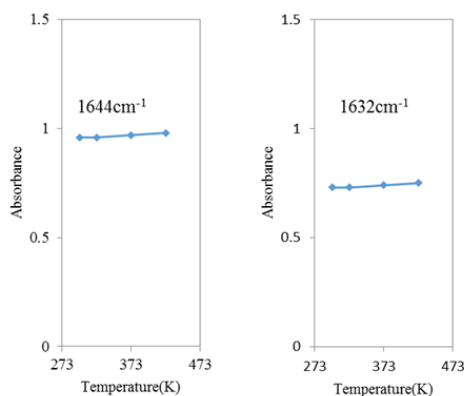

Figure 5.0: The fraction of Bronsted acid sites of WO_3ZrO_2 on heating in the presence of *n*-pentane
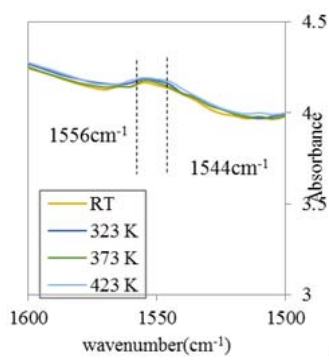

Figure 6.0: IR spectra of adsorption of *n*-pentane on WO_3ZrO_2 in the range 1600cm^{-1}-1500cm^{-1}
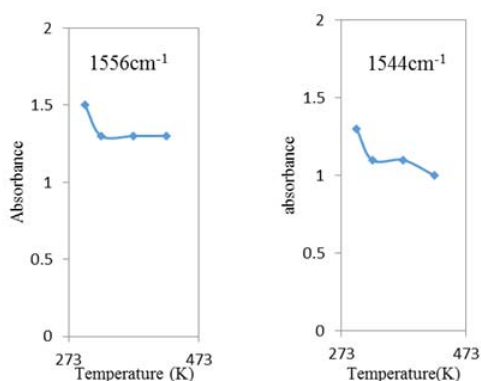

Figure 7.0: The fraction of Lewis acid sites of WO_3ZrO_2 on heating in the presence of *n*-pentane.

ESR Spectroscopy

The generation of protonic acid sites

The ESR signal decreased as the temperature increased. The ESR signal shows the electron and proton were formed on the surface of WO_3-ZrO_2. When the sample was heated at 323 K, the intensity of the ESR signal increased at g=1.98 which correspond to the trapped electrons that have localized on metal cation. A signal of g=1.98 and g=1.97 was observed at 323 K in the presence of *n*-alkane. Exposure of WO_3-ZrO_2 catalysts to *n*-pentane lead to the formation of W^{5+} species and organic radical on the surface [2]. The introduction of gaseous alkane, followed by heating at 323, 348, 373, 423 and 448 K resulted in the formation of electrons and protonic acid sites that decreased the signal at g=1.98 because the electron will be trapped in the electron deficient metal cation. Figure 8.0 shows the variation of the intensity of ESR signal as a function of temperature.
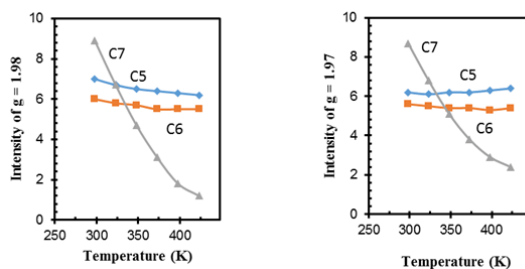

Figure 8.0: The variation of the intensity of ESR signal at g=1.98 and g=1.97 as a function of temperature.

Formation of radicals by injection of Ultraviolet (UV)

The chemical changes in sample WO_3-ZrO_2 in the presence of *n*-pentane, *n*-hexane and *n*-heptane, especially radical formation after ultraviolet (UV) irradiation was observed. The enhanced ESR signal decay showed the generation of free radical from sample WO_3-ZrO_2 in the presence of *n*-alkane. That is means when the UV was injected into the sample WO_3-ZrO_2 in the presence of n-alkane, the intensity of the signal is decreased and it shows the formation of free radicals. Figure 9.0 below shows the variation of intensity of the ESR signal at g=1.98 and g=1.97 as a function of UV injection time.
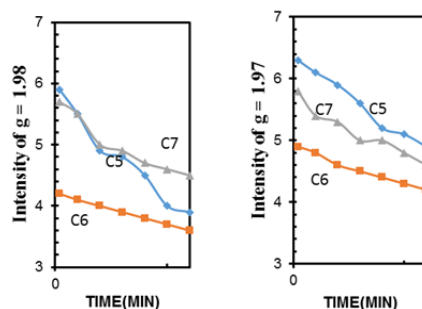
Figure 9.0: The variation of intensity of the ESR signal at g=1.98 and g=1.97 as a function of UV injection time.

For organic radicals, the g-value is in the range 1.99-2.01. Alkyl radicals (pentyl, *n*-hexane radical cation, and heptyl) are believed to be observed based on the different of g-value (1.98313, 1.98434 and 1.98381) which were formed on the surface of WO_3-ZrO_2 in the presence of *n*-alkane.

CONCLUSION

The protonic acid sites were generated from the WO_3-ZrO_2 in the presence of hydrocarbon molecule (*n*-pentane, *n*-hexane and *n*-heptane) evidenced by lutidine pre-adsorbed FTIR and ESR spectroscopy.

REFERENCE

1. M.G.Falco,S.A.Cavanese,N.S.Figoli.(2005) Preparation of Tungsten Oxide Promoted Zirconia by Different Method.*Catalysis Today*.**107**.778-78
2. S.Kuba, P.Lukinkas, R.K.Grasselli,B.C.Gates and K.Helmut(2003).Structure and Properties of Tungstated Zirconia Catalysts for Alkane Conversion.*Journal of Catalysis.***216**.353-361
3. C.X.Ying, C.Guillaume, T.Karine and M.Houalla(2010).Correlation Between Structure, Acidity and Catalytic Performance of WOx/Al$_2$O$_3$.*Journal of Catalysis.***273**.236-244

DECOLORIZATON OF METHYLENE BLUE DYE USING MAGNETIC *ANANAS COMOSUS* LEAF

Siti Fairuz Ab Rashid, Zaiton Abdul Majid, and Nursyafreena Attan
Department of Chemistry, Faculty of Science, Universiti Teknologi Malaysia, 81310 Johor Bahru.

Abstract

The study was conducted to investigate the feasibility of using magnetic *Ananas comosus* leaf (MACL) as adsorbent for the removal of Methylene Blue (MB) dye. *Ananas comosus* leaf (ACL) was chosen due the availability of this waste material.The ACL was first pretreated with different concentration of nitric acid, HNO$_3$ to compare its surface area before modification process. Following that, ACL with the highest surface area was selected to produce MACL by precipitation of iron oxide on the surface of ACL. Both adsorbents, ACL and MACL were characterized using Fourier Transform Infrared Spectroscopy (FTIR), Brunauer-Emmett-Teller (BET), Scanning Electron microscopy (SEM) and Energy Dispersive X-Ray (EDX). The BET surface area of ACL and MACL recorded are 35.20 m^2/g and 81.42 m^2/g respectively. Equilibrium and kinetic studies were carried out under different pH of MB solution, adsorbent dosage, contact time and initial MB concentration. The equilibrium data were fitted to Langmuir and Freundlich isotherms. The equilibrium adsorption for both ACL and MACL were best described by the Langmuir isotherm, with MACL exhibiting a larger adsorption capacity compared to ACL. The sorption data was also analysed using pseudo-first-order and pseudo-second-order kinetic model. The experimental data obtained was found to follow pseudo-second-order with correlation coefficient R^2 of 0.9889 and 0.9998 for ACL and MACL respectively.

Keywords: Ananas comosus leaf, methylene blue, kinetic model, equilibrium study

INTRODUCTION

Discharge of untreated or partially treated dye from industrial wastewater into the environment poses a serious threat and danger to life, not only by retarding the physicochemical and biological properties of environmental components but also from the toxicological point of view.Hence, the removal of synthetic dyes such as methylene blue is of great concern since some dyes and their degradation products may be carcinogens and toxic [1]. Methylene blue (MB), is a heterocyclic aromatic chemical compound, also known as Swiss blue [2]. Among the available technologies for dye removal from aqueous media, adsorption is widely studied because it is efficient, easy to operate, environment-friendly, and easy to disseminate. Adsorption technique is preferredcompared to othertechniques such as biodegradation, electrochemical degradation, photochemical degradation, coagulation/flocculation, sonicated degradation, membrane filtration, among others because adsorption has been found to be an efficient and economical process for the removal of pigments and other colorants and also to control the bio-chemical oxygen demand. However, of late, attention has been geared towards the application of magnetic particle technology to overcome environmental problems. The magnetic particles can be used to adsorb contaminants from aqueous or gaseous effluents and can be easily separated from the medium by a simple magnetic process after adsorption [4].

Adsorbent for the removal of MB from aqueous media was prepared from *Ananas comosus* leaf (ACL) or pineapple.The pineapple leaf is used in this study due to its availability in the pineapple industry. The production of magnetic *Ananas comosus* leaf (MACL) was carried out by precipitating iron oxide onto pretreated ACL. The characteristic of MB removal by ACL and MACL was analyzed by Langmuir and Freundlich adsorption isotherm through batch sorption experiment.

MATERIALS AND METHODS

Materials

The materials used for the study is ACL obtained from Pekan Nenas, Johor.Analytical grade sodium hydroxide pellet from Merck (99.5% purity), analytical grade Ferric chlorideferrous sulphate from Merck), nitric acid (Merck), ethanol and Methylene Blue from Sigma-Aldrich (M). The general chemical structure of Methyene Blue is illustrated in Figure 1.

Preparation and Characterization of ACL and MACL

The ACL were pre-treated by drying in an oven (80^{0}C), ground and sieved (<75 µm) until fine powder was obtained. The ground ACL was treated using different concentration of nitric acid (HNO$_3$) i.e. 0.1 M, 0.5 M and

1.0 M for 24 hours. The magnetic ACL (MACL) was prepared by suspending 1.0 g ACL in 20 mL distilled water. A ferric chloride solution ($FeCl_3$) of 0.09 M was freshly prepared by adding 0.72 g of $FeCl_3$ into 52 mL distilled water. A ferrous sulphate solution, ($FeSO_4$) of 0.88 M was also prepared by adding 0.8 g $FeSO_4$ into 6 mL distilled water. Both solution were combined and vigorously stirred at 60-70^{0}C. The suspension formed was added into an aqueous solution of ACL at room temperature and stirred slowly for 30 min. After mixing, 10 M NaOH was added dropwise into the suspension until the pH raised to 10-11. After mixing for 60 min, the suspension was aged at room temperature for 24 hours and then repeatedly washed with distilled water followed by ethanol. The MACL was vacuum filtered and dried overnight at 50^{0}C in a hot air oven.The prepared ACL and MACL were characterized using BET Single Point Surface Analyzer, FTIR, XRD, XRF, FESEM-EDX, and SEM-EDX.
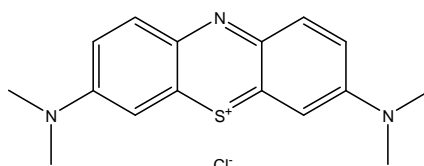
Figure 1: Chemical structure of MB dye

Batch Equilibrium Adsorption Study

Stock solution of MB was prepared by dissolving 0.1 g of MB into 1 L volumetric flask. The test solutions were prepared by diluting 1 mL, 1.5 mL, 2.0 mL, 2.5 mL and 3.0 mL are transferred into 100 mL volumetric flasks and diluted to series of 10 mg/L, 15 mg/L, 20 mg/L, 25 mg/L and 30 mg/L. A calibration curve was plotted using absorbance versus concentration of the solution to identify the concentration of MB solution after adsorption process.

The effect of ACL and MACL dose on the amount of MB adsorbed was obtained by contacting 100 mL of 50 mg/L MB solution with different amount of adsorbent. The amount of ACL and MACL used are in range of 0.1 to 1.0 g to see the effect of adsorbent dosage toward removal of MB.

The effect of pH on the removal of MB was analyzed under pH range 3-11. Experiments were conducted at 50 mg/L initial MB concentration for both 0.50 g ACL and MACL at 30 ºC to observe whether pH is significant to the adsorption process.

A series of an appropriate concentration of 50 mg/L, 100 mg/L, 150 mg/L, 200 mg/L and 250 mg/L MB were prepared for quantifying the effect of initial MB concentration on adsorption rate with known amount of 0.50 g ACL and at a temperature of 30 ºC.

RESULTS AND DISCUSSION

Characterization ACL and MACL

The FTIR spectra obtained revealed various functional groups on the surface of ACL and MACL. Based on the Table 1, some peaks were shifted or disappeared and new peaks were also detected. Iron oxide appeared at 473.17 cm^{-1} and 590.56 cm^{-1}at MACL indicates thepresence of iron oxide onto ACL.

Table 1: FTIR data of ACL and MACL

Functional group	ACL	MACL
O-H (stretching)	3367.10	3402.67
C-H (stretching)	2918.43	2920.05
C=O	1737.83	-
C=C (aromatic)	1638.76, 1459.34	1633.17, 1419.95
N=O	1516.61, 1383.81	-
C-N	1338.22	1341.01
Iron oxide	-	473.17, 590.56

Absorbance in cm^{-1}

Surface area analysis (BET)

The surface areas of ACL and MACL treated with different concentration of nitric acid are shown in Table 2.The surface area analysis of ACL (35.20 m^2/g) and MACL (81.42 m^2/g) pretreated with 0.5 M HNO$_3$ shows the highest surface area .

Table 2: BET analysis of ACL and MACL

Sample	Surface area (m^2/g)
Raw ACL	7.69
ACL 0.1M HNO$_3$	31.70
ACL 0.5M HNO$_3$	35.20
ACL 1.0M HNO$_3$	32.02
MACL 0.1M HNO$_3$	69.80
MACL 0.5M HNO$_3$	81.42
MACL 1.0M HNO$_3$	65.52

Surface Morphology Analysis

Figure 1 (A-D) and Figure 1 (E-H) show the SEM micrograph of ACL and MACL at different magnification respectively. The ACL appears fibrouswith the presence of agglomerates. The MACL surface shows the presence of pores..Precipitation of of iron oxide onto surface of ACL plump out the agglomerated surface into a porous texture with iron oxide particles covering the pores. The distribution of pores are uniform. Pore development during iron oxide formation process enhanced the surface area of MACL compared to ACL.

Elemental Analysis

The elemental analysis of ACL and MACL are shown in Table 3. Elemental analysis of MACL shows the presence of iron attributed to the precipitationof iron oxide, confirming the precipitation of iron oxide on the ACL.

Table 3: Elemental analysis of ACL and MACL

Sample	Weight (%)				
	Carbon(C)	Oxygen(O)	Aluminium(Al)	Phosporus (P)	Iron (Fe)
ACL	59.78	40.22	-	-	-
MACL	34.44	38.76	1.04	1.07	29.66

Adsorption Isotherm Study

Effect of dosage

The effect of adsorbent dosage on adsorption of MB onto ACL and MACL is illustrated in Figure 2. From the graph of ACL, the percent removal of MB increased from 48.63% to 85.07% from an increased in ACL dosage from 0.10 to 0.80 g. It was observed that the percent removal MB increased with increasing adsorbent dosage until to 0.80g ACL and gradually remains unchanged. The highest percentage removal of MB achieved using ACL was 85.07% and the optimum dose was found to be 0.80g for 100 mL of MB solution.

MACL displayed highest percent removal of MB up to 95.92%. The percent removal of MB using MACL increased rapidly using varies amount of MACL of 0.10 to 0.50 g which showed the percent removal of 90.56% to 95.92%. The graphs concluded that MACL promoted higher MB removal compared to ACL. These may be associated to the presence of iron oxide. For MACL, the optimum dose was 0.50 g with percentage removal of 95.92%.

Effect of solution pH

The effect of pH on the adsorption capacity of MB on ACL and MACL was studied by performing equilibrium adsorption experiments at different pH. Based onFigure 3, ACL shows the highest adsorption capacity at higher pH and achieve equilibrium at minimum pH 7. The adsorption capacity of MB increased up to pH 8 and remained nearly constant at pH 9 and above. Lower adsorption capacity of MB at acidic pH is due to the presence of excess H$^+$ ions in the adsorbate which competes with cation groups on MB for adsorption site. A similar result was reported for adsorption of MB onto ACL and rejected tea [2][5].

Similarly, MACL also shows equilibrium adsorption capacity at a minimum pH 7. However, MACL displayed higher adsorption capacity compared to ACL. Both graphs exhibited increase in adsorption capacity at increase pH.
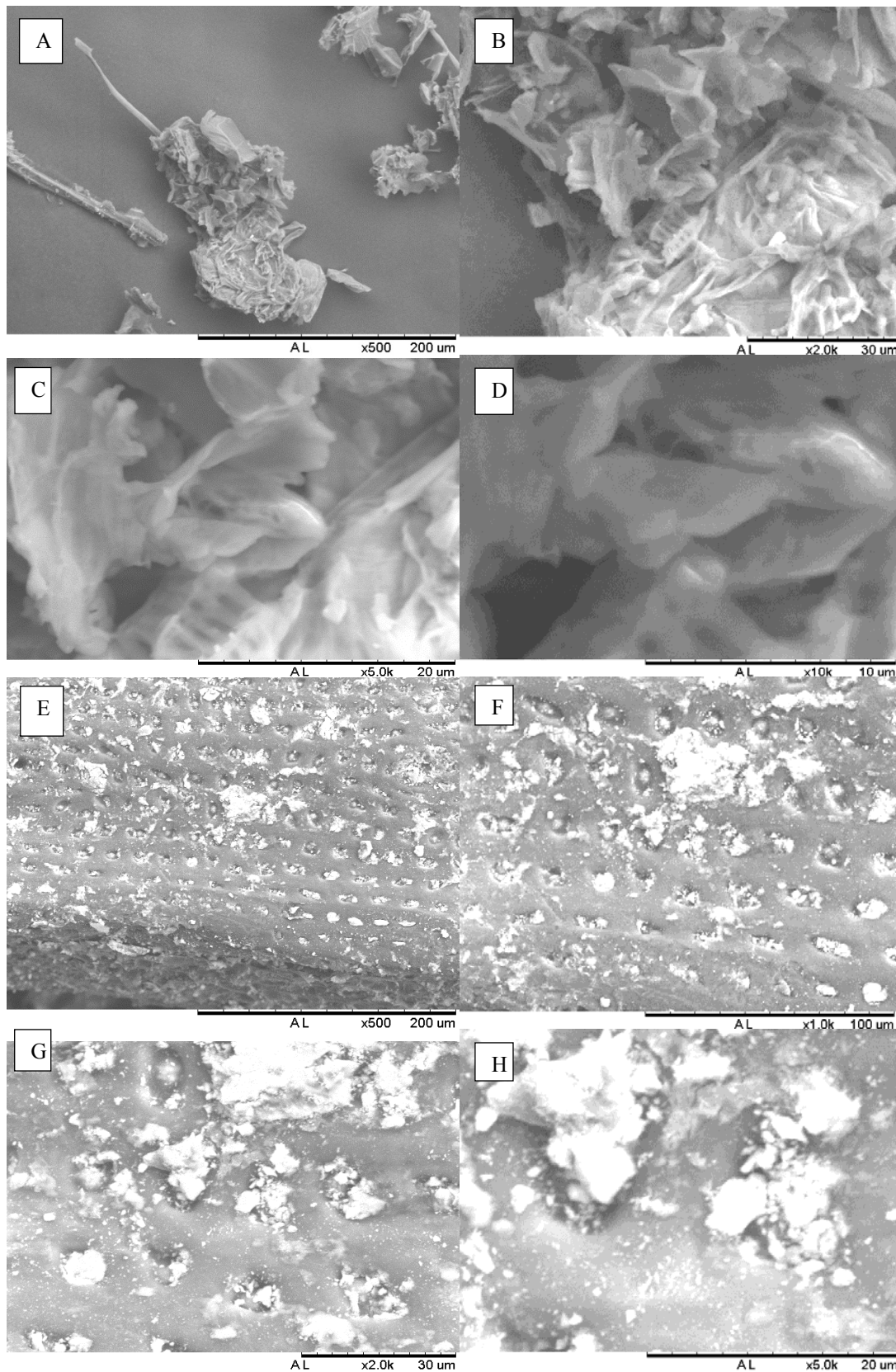

Figure 1 : SEM of ACL (A) x 500, (B) x 2.0k, (C) x 5.0k, (D) x 10.0k and MACL (E) x 500, (F) x 1.0k, (G) x 2.0k, (H) x 5.0k
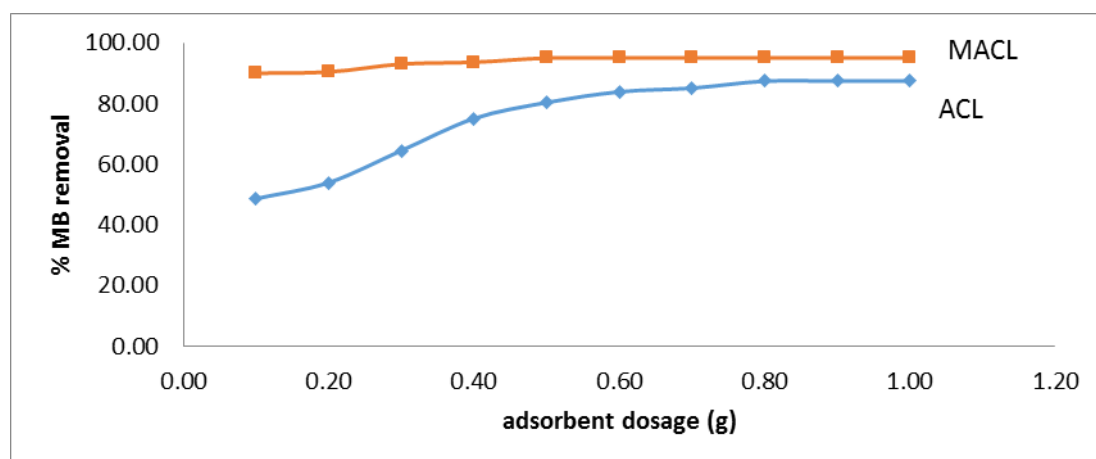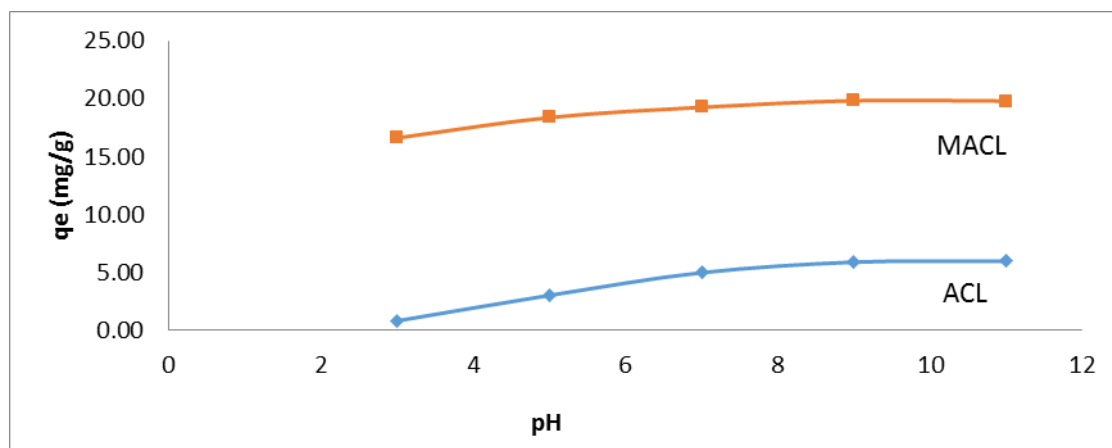
Figure 2: Effect of adsorbent dosage

Figure 3: Effect of solution pH on adsorption of MB

Effect of initial concentration and contact time

Figure 4shows the effect of initial dye concentration (50-250 mg/L) on the adsorption of MB. For ACL, it was observed that amount of MB adsorbed was rapid for the first 40 minutes and proceeded gradually at slower rate and finally reached saturation at 90 minutes for 50 mg/L. The equilibrium adsorption increases from 5.90 to 21.3 mg/g with concentration of 50 to 250 mg/L. It was found out that equilibrium removal of MB decreased from 88.0% to 68.4% as concentration increased from 50 to 250 mg/L. MACL shows rapid adsorption for the first 25 minutes and reached equilibrium at 30 minutes for 100 mg/L.

Equilibrium Study

Based on the Table 4, value of q_{max} for ACL is lower compared to MACL. MACL shows higher maximum adsorption capacity of 70.92 mg/g. This results fromthe higher surface area of MACL compared to ACL. Moreover, iron oxide also plays an important part as active site in MB removal. R^2 value is an indication to determine the favourability of adsorption. From the value of coefficient correlation R^2, both ACL and MACL exhibit $R^2 > 0.99$. This means that Langmuir isotherm is more favourable.

Table 4: Langmuir isotherm parameter

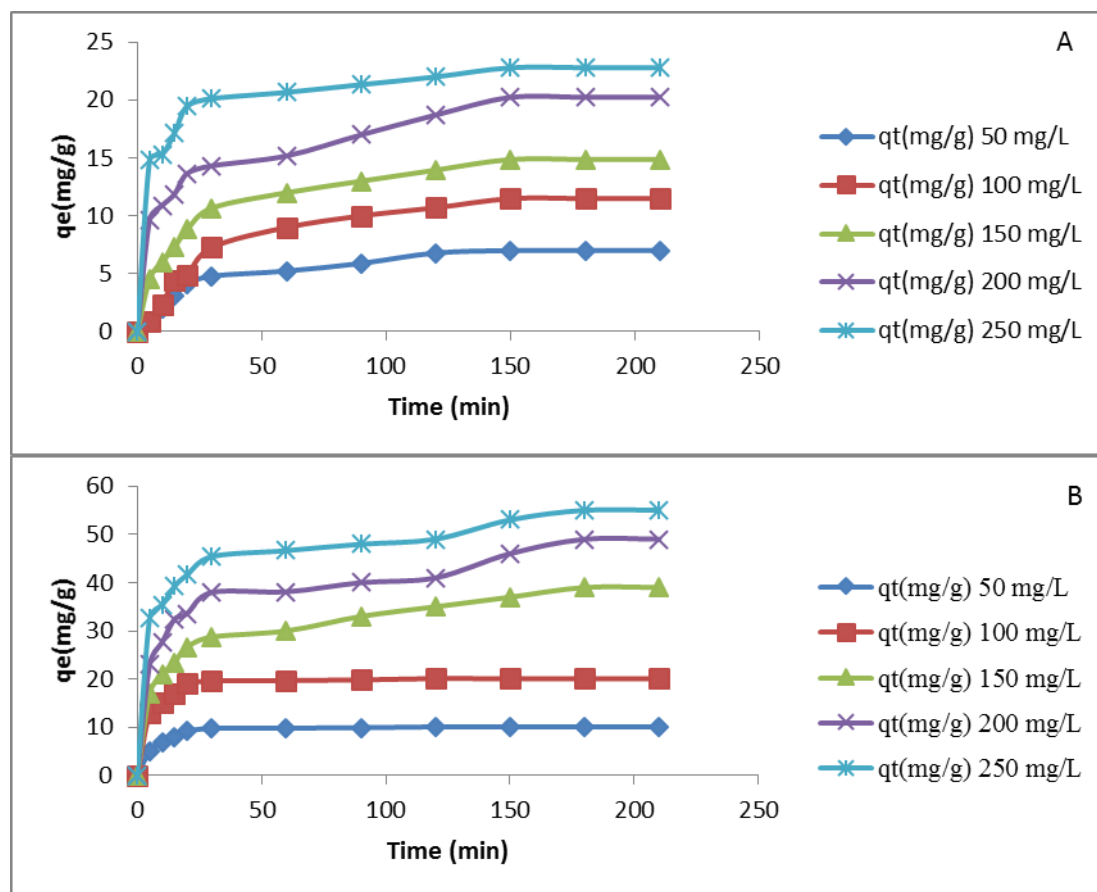| Sample	q_{max} (mg/g)	K_a (dm^3/mg)	R^2
ACL	30.769	0.034	0.9937
MACL	70.92	0.091	0.9942

109

Figure 4: Effect of contact time and initial concentration on the adsorption of MB on (A) ACL and (B) MACL

Table 5: Freundlich isotherm parameter

Sample	K_F	$1/n$	R^2
ACL	1.090	0.8614	0.8957
MACL	4.500	1.0471	0.9566

Multilayer adsorption is best described by Freundlich isotherms where only employed onto heterogeneous surface. The Freundlich isotherm for ACL and MACL parameters were tabulated in Table 5. There are two Freundlich constants which are K_F and n. K_F is known as adsorption or distribution coefficient that show the quantity of dye adsorbed for a unit equilibrium concentration. $1/n$ indicates the surface heterogeneity. The adsorption is said heterogeneous when value of n closer to zero [6]. From the $1/n$ values above, the adsorption of ACL and MACL are homogeneous as the $1/n$ values are further than zero. R^2 value for both ACL and MACL are 0.8957 and 0.9566.

Thus, in brief the adsorption follows Langmuir isotherms as R^2 value higher than Freundlich. It can be concluding that the adsorption involved only monolayer coverage which focusing on chemical adsorption.

Kinetic study

Table 6 indicated that the kinetic data did not fit well with pseudo-first-order. The R^2 results from pseudo-first-order are rather low which are 0.6353 and 0.9156 for ACL and MACL. The q_e experimental and q_e calculated gave a big different hence the adsorption of MB onto ACL and MACL does not follow pseudo-first-order kinetic.

The plot of t/q_t against t as in Figure 6 shows that the intercept are very close to zero. This means that the pseudo-second-order is more applicable and favourable. The coefficient correlation, R^2 for pseudo-second-order is $R^2 > 0.98$ for both ACL and MACL. Since the q_e calculated and q_e experimental of pseudo-second-order displayed the almost same value, the kinetic studied is more suitable and applicable to pseudo-second-order.

Table 6: Kinetic parameters

Sample	Pseudo-first-order				Pseudo-second-order		
	q_e exp (mg/g)	q_e cal (mg/g)	k_1 (1/min)	R^2	q_e cal (mg/g)	k_2 (1/min)	R^2
ACL	30.76	14.64	0.030	0.6353	25.19	0.005	0.9889
MACL	70.92	24.15	0.023	0.9156	76.92	0.006	0.9998

CONCLUSION

Based on adsorption study, the adsorption capacity obtained for ACL and MACL are 30.77 mg/g and 70.92 mg/g respectively. Based on R^2values which are 0.9937 for ACL and 0.9942 for MACL, the adsorption could be fitted to the Langmuir isotherm. Kinetic studiesshows that the adsorption is pseudo-second-order with R^2 values for ACL is 0.9889 and MACL 0.9998.

REFERENCES

1. Weng C.H., Lin Y.T., Tzeng T.W. (2009). Removal of methylene blue from aqueous solution by adsorption onto pineapple leaf powder, *Journal of Hazardous Materials*, **170**, 417–424
2. Chen, M.C., Wu, J.Y., Huang, C.C., Liang, Y.M. and Hwang, S.C.J. (2003) Decolourization of azo dye using PVA-immobilized microorganisms, *J. Biotechnol*, **101**, 241–252.
3. Rakesh Kumar Ghosh, D. Damodar Reddy. (2013). Tobacco Stem Ash as an Adsorbent for Removal of Methylene Blue from Aqueous Solution: Equilibrium, Kinetics, and Mechanism of Adsorption, *Water Air Soil Pollut* 224:1582, 1-12
4. Luiz C.A. Oliveira et.al. (2002). Activated carbon/iron oxide magnetic composites for the adsorption of contaminants in water, *Carbon 40*, 2177-2183
5. Nasuha N, Hameed B.H., Azam T. Mohd Din. (2010). Rejected tea as a potential low-cost adsorbent for removal of methylene blue, *J. Hazard. Mater*, **175,** 126-132
6. Zhen, C., Wei, M. and Mei, H. (2008). Biosorption of Nickel and Copper onto treated alga (undaria pinnatifida): Application of isotherm and kinetic models. *Journal of Hazardous Materials*. **155**. 327-333

SYNTHESIS AND BIOASSAY STUDIES OF BENZOXAZIN-4-ONE AND QUINAZOLIN-4-IMINE DERIVATIVES

Ng Choon Meng and Joazaizulfazli Jamalis
Department of Chemistry, Faculty of Science, Universiti Teknologi Malaysia, 81310 Johor Bahru.

Abstract

The 4*H*-3,1-benzoxazin-4-one and quinazolin-4-imine derivatives have been synthesized in simple and one step reaction. The reaction of anthranilic acid and benzoyl chloride, terephtaloyl dichloride and 4-chlorobenzoyl chloride in pyridine yielded 2-phenyl-4*H*-3,1-benzoxazin-4-one (78.91%), 1,4-(di-4*H*-3,1-benzoxazin-4-one)benzene (55.23%) and 2-(*p*-chlorophenyl)-4*H*-3,1,-benzoxazine-4-one (33.20%) respectively. The benzoxazin-4-one derivatives were then treated with hydrazine hydrate in absolute ethanol to form 2-phenylquinazolin-4-imine (70.90%), 1,4-(diquinazolin-4-imine)benzene (43.70%) and 2-(*p*-chlorophenyl)quinazolin-4-imine (35.81%). The resulting compounds were characterized using ATR and ^{1}H NMR using CDCl$_3$ as solvent. From both spectra it showed that the synthesis of targeted compound, 4*H*-3,1-quinzolin-4-one was unsuccessful. The resulting compounds after treated with hydrazine hydrate were proposed to be quinazolin-4-imine compounds based on the data analyzed from ATR and ^{1}H NMR spectrum. Antioxidant test using DPPH free radical scavenging has been carried out on the six compounds synthesized. The results showed that 4*H*-3,1-benzoxazin-4-one derivatives did not show antioxidant activity while the compounds of quinazolin-4-imine derivatives showed good antioxidant activity as the IC$_{50}$ value obtained are lower than positive control of ascorbic acid except for 1,4-(diquinazolin-4-imine)benzene. Among the quinazolin-4-imine derivatives, 2-phenylquinazolin-4-imine showed the highest antioxidant activity at IC$_{50}$ value at 2.66ppm. The introducing of electron withdrawing group at phenyl substituent was found to reduce ability of compounds in antioxidant activity.

Keywords: Heterocycle, synthesis, 4*H*-3,1-benzoxazin-4-one, quinazolin-4-imine, antioxidant

INTRODUCTION

Benzoxazinone belongs to the group of heterocyclic compounds that consist of unsaturated six-membered rings with two heteroatoms of oxygen and nitrogen. While the quinazoline consist of unsaturated six-membered rings with two heteroatoms of nitrogen. Heterocyclic compounds are commonly become an interest in pharmaceuticals and agrochemical industries due to their natural occurrence [1]. Numerous additives and dyes used in industrial application such as cosmetic are heterocyclic in nature. The common biological activities possessed by synthetic heterocyclic compounds are antibacterial [2], antifungal [3], anti-inflammatory [4] and antioxidant [5].The wide range of biological activities possessed by heterocycles is mainly due to the extraordinary wide range of reaction of the compounds. Heterocyclic can behave as either acid or base to form anion or cation depending on the pH value of the medium. Besides, some heterocyclic easily interact with electrophilic reagent while some with nucleophiles, or both. Some can be easily oxidized but reduction resistant, or vice versa. Furthermore, there are heterocyclic compounds which simultaneously demonstrate all of the mentioned properties.

Benzoxazinone can exist in various types depends on the position of keto group. The keto group may occur ateither position two, four or both [6].The keto group also may occurat position three of the structure such as natural occurring of benzoxazinone in maize and wheat [7]. Among all the types of benzoxazinone and quinaozoline, 4(3*H*)-benzoxazinone and quinazolinone are more prevalent to be used as intermediates of drugs synthesis or as natural products in biosynthetic pathway. This is partly because of its structure possess wide range of reaction and being derived from anthranilates with various esters, isotoicanhydride and anthranilamide.In this paper, we report the synthesis and characterization of 4*H*-3,1-benzoxazin-4-one and quinazolin-4-imine compounds **(1-6)**. In addition, all the compounds were evaluated for their antioxidant activity using DPPH radical scavenging.

EXPERIMENTAL

Thin layer chromatography (TLC) analysis was conducted by using thin aluminium plate of Merck Silica gel 60F254 of 0.2 mm thickness. The spots on TLC were visualized using Ultraviolet at 254nm and 365nm. The purification of compound was carried out by column chromatography using Merck Silica gel and the eluent used was mixture of hexane acetone in the ratio of 40:60. The products were characterized by using ATR and ^{1}H NMR. Sample product was measured on Attenuated Total Reflectance (ATR) with 20 scans for each sample at a resolution of 4cm^{-1} per measure. The IR spectra was recorded on PerkinElmer FT-IR Spectrometer Frontier. The ^{1}H spectra were obtained using 300MHz spectrometer for benzoxazinone and 400MHz spectrometer for

quinazoline and the chemical shift were reported in ppm using CDCl$_3$ as solvent. The ^{1}H NMR spectra was recorded at 300 MHz and 400 MHz using Bruker Avance Spectrophotometer.
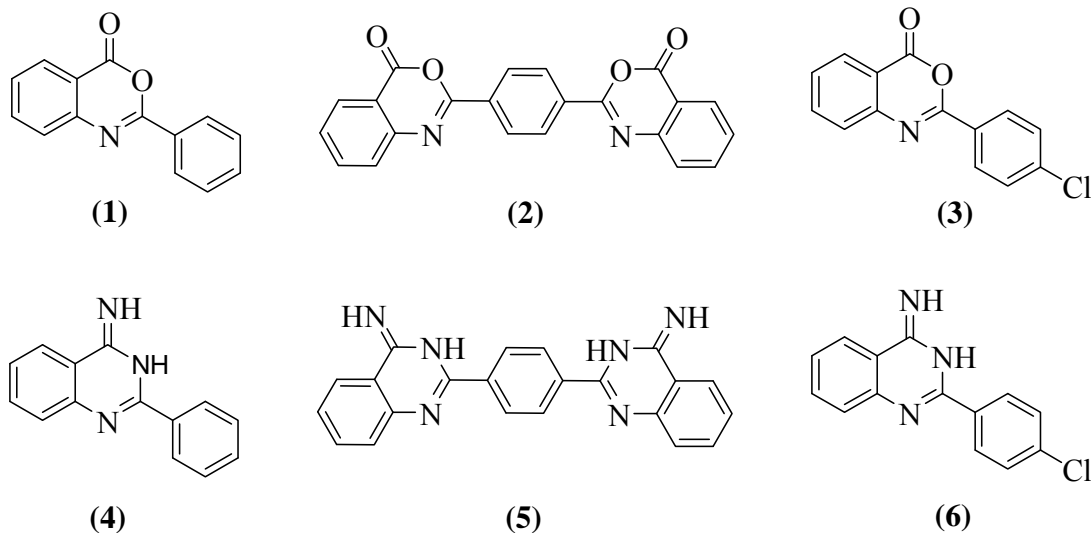
ORGANIC MATERIALS

Starting material used was anthranilic acid which was purchased from Sigma-Aldrich. The derivatives of acyl chloride of benzoyl chloride, terephtaloyl dichloride and 4-chlorobenzoyl chloride were purchased from Tokyo Chemical Industry CO., LTD in December 2014.

SYNTHESIS AND CHARACTERIZATION

Benzoyl chloride (10.00mmol) was added into anthrannilic acid (1.03g, 7.50 mmol) and pyridine (30 mL) separately. The mixture was then refluxed for 3 hours and the reaction was monitored under thin layer chromatography (TLC). The spots on TLC were visualized under UV light. Upon the reaction was completed, the reaction mixture was cooled and then poured into cooled diluted hydrochloric acid (15mL). The solid was filtered and recrystallized from ethanol. The synthesis method is repeated by replacing terephtaloyl dichloride (1.00g, 7.3mmol) and 4-chlorobenzoyl chloride (1.00g, 7.3mmol). The compound synthesized from terephtaloyl dichloride(**2**) is further purified by silica gel-60 column chromatography and mixture of hexane-acetone in 40:60 ratio.The compound (**1**) was obtained is a white solid (1.33 g, 78.91%). Compound (**2**) obtained as yellow solid (0.74 g, 55.23%), compound(**3**) appeared as white solid (0.62g, 33.20%). The 4*H*-3,1-benzoxazin-4-one derivatives synthesized were subjected to characterize by using ATR and ^{1}H NMR. The confirmed compounds were used for the synthesis of the corresponding quinazolin-4-imine derivatives.

A mixture of 2-phenyl-4*H*-3,1-benzoxazin-4-one (0.30g, 1.34mmol)(**1**) and hydrazine hydrate (64%, 2.00mmol) was refluxed in ethanol (30 mL) for 4 hours. The reaction was monitored under thin TLC. The spots on TLC were visualized under UV light. Upon the reaction was completed, the reaction mixture was cooled and poured into cooled distilled water (20 mL). The mixture was then concentrated and filtered off the solid. The separated solid was recrystallized from ethanol. The synthesis method was then repeated by replacing 2-phenyl-4*H*-3,1-benzoxazin-4-one with 1,4-(Di-4*H*-3,1-benzoxazin-4-one)benzene (0.10g, 0.39mmol)(**2**) and 2-(*p*-chlorophenyl)-phenyl-4*H*-3,1-benzoxazin-4-one (0.10g, 0.35mmol)(**3**).The compound (**4**) was obtained as a white solid (0.41 g, 70.90%). Compound (**5**) obtained as yellow solid (0.34 g, 43.70%), compound (**6**) appeared as white solid (0.03 g, 35.81%).

The six compounds synthesized were used to carry out antioxidant testing. The method in determination of antioxidant activity was referring to the method used by Fu. R. *et al* in their previous research [8]. Each sample was dissolved in methanol to prepare 1000 ppm of sample solution. The stock solution was then diluted to 800ppm, 600ppm, 400ppm, 200ppm, 100ppm, 80ppm, 60ppm, 40ppm, 20ppm, 10ppm, 5ppm and 1ppm. The purple solution of 2,2-diphenyl-1-picrylhydrazyl, DPPH was prepared by dissolve DPPH (3.94 mg) in methanol (100mL) in a dark container covered with aluminium foil. Ascorbic acid was used as the positive control. Each sample solution of different concentration (100μL) was added into the sample well together with the DPPH solution (100μL) and methanol (100μL) for blank sample separately. Triplicate samples were used for each

sample with different concentration. The mixtures were then incubated at 25°C for 30min, and the absorbance at 517nm was measured using microplate reader.The radical scavenging activity was calculated using equation as follow:

$$radical\,scavenging\,activity(\%) = \left[1 - \frac{(A_i - A_s)}{A_c}\right] x\,100$$

Where A_c is the absorption of the negative control, A_i is the absorbance of the experimental group and A_s represents the background absorption.

RESULTS AND DISCUSSION

Compound **(1)** was obtained from the recrystallization appeared as a white solid (1.33 g, 78.91%). The ATR spectrum of compound **(1)**is inagreement with the research conducted before [8].The ATR spectrumshowed a stretching peak for C-H bond of aromatic is observed above 3000cm^{-1} and was typically showed as a multiplicity of weak band due to the present of more than one benzene system in the structure. The stretching ofC=O bondwas observed as a strong band at 1762 cm^{-1} which is slightly higher than the theoretical value of normal ester compound.The increase in intensity and wavenumber were caused by the conjugation with the ester single bonded-oxygen. The lone pair electron on oxygen atom donated to form a temporary C=O bond causes the oxygen atom to be more positive. This causes the electron deficiency in oxygen atom and results in the pulling of electron from C=O ester by inductive effect.The C=N stretching mode is observed at wavenumber of 1610 cm^{-1} as studied by previous research [9]. The stretching of C=N bondat lower wavenumber is due to the conjugate effect of C=C from the phenyl group attached at position two of the benzoxazinone skeleton. The C=C aromatic absorption peaks are observed at 1572 cm^{-1} and 1474 cm^{-1}.Analysis of the ^{1}H NMR spectrum showed that all proton of benzoxazinone exhibited a low field signal started from 7.5ppm. The most low field signal δ 8.33(J=7.2Hz) belongs to hydrogen located at *ortho*-position of the phenyl substituent, H_O which was subjected to the electrostatic field effect from lone pair electron of nitrogen [10]. The proton in fifth position, H_5 showed signal at δ 8.26 (J=7.8Hz, 0.9Hz) which is low field than H_6 to H_8 due to the electron deshielded by an anisotropic effect of the *peri*-carbonyl at the fused ring.H_7 and H_8 were observed at δ 7.85 (J=7.8Hz, 0.9Hz) and δ 7.71 (J=7.8Hz). The remaining protons were observed at δ 7.49-7.61 (4H).

Compound **(2)** obtained was appeared as yellow solid (0.74g, 55.23%) after recrystallization and purification using silica gel column. The ATR spectrum showed absorption peak similar to compound **(1)** where3040 cm^{-1} belongs to C-H aromatic, 1763 cm^{-1} was C=O ester, 1694 cm^{-1} was C=N, 1612 and 1474 cm^{-1}for C=C aromatic. From the ^{1}H NMR spectrum, the low field peak was the peak of ortho-position proton, $H_O$at δ 8.50. This peak represented four protons from the phenyl substituent without splitting as the protons are identical to each other by symmetry [11]. These protons would give only a single NMR peak since they have the same chemical shift. The other protons at the fused ring exhibited similar chemical shift and splitting with the compounds**(1)**, which peaks at δ 8.31for H_5(J= 7.4Hz), H_7 atδ 7.90 (J = 7.4Hz), H_8 at δ 7.78 (J = 7.4Hz) and H_6 at δ 7.60 (J = 7.4Hz). Compound**(3)** obtained is a white solid (0.62 g, 33.20%). Both ATR and ^{1}H NMR spectrum showed similar peak as observed in compound **(1)**except for the absence of H_p in ^{1}H NMR since the $H_p$in **(3)**had been replaced by the chlorine atom. The ATR spectrum of **(3)** showed absorption peak at 1769 cm^{-1} for C=O ester, 1622 cm^{-1} for C=N, 1604 cm^{-1} and 1489 cm^{-1} for C=C aromatic. ^{1}H NMR spectrum showed peaks at δ 8.27 for both H_O and H_5, δ7.85 for H_7(J =7.8 Hz, 1.2 Hz), δ7.70 H_8(J =7.8 Hz) and δ7.54 for both H_m and H_6.

For the condensation process of 4*H*-3,1-benzoxazin-4-one with hydrazine hydrate, the targeted compound synthesis was the 3-amino-2-substituted-4*H*-3,1-quinazolin-4-one derivatives as reported previously [12]. However, from the ATR and ^{1}H NMR obtained, the proposed structure of compounds synthesized was quinazolin-4-imine derivatives. Compound **(4)** obtained as a white solid (0.21g, 70.90%).From the ATR, the C=O stretching did not observe in compound **(4)** and a peak was observed at 1649 cm^{-1} was believed to belongs to C=N. Besides, the N-H stretching peak at 3318 cm^{-1} also observed in the ATR.Other than that, two peaks which were 1603 cm^{-1} and 1449 cm^{-1} also observed for C=C aromatic. From the ^{1}H NMR, a N-H peak was observed at δ 11.88and it was believed to come from N-H at position 3 that resembled to the compound of 2-phenyl-4H-3,1-quinazolin-4-one as reported in other research [14]. Therefore it is further proven that the solid formed was a quinazolin-4-imine derivative. The proton at the fuse ring, H_5 was found to shift to lower field at δ 8.83 (J =7.7 Hz) as compare to the H_5 in **(1)**. The H_O was observed atδ 8.06 (J =6.8 Hz), H_6 at δ 7.12 (J =7.7 Hz) and the remaining six proton were observed in the δ 7.63 to 7.12.

Compound (5) was obtained as a yellow compound (0.24g, 43.70%). From the ATR, the N-H stretching was observed at 3351 cm^{-1}, followed by C=N stretching at 1666 cm^{-1}. The C=C aromatic stretching were observed at 1587 cm^{-1} and 1446 cm^{-1}. The ^{1}H NMR spectrum was similar to compound (1), where the N-H peak was observed at δ 12.44, followed by H$_5$ at δ 8.83 (J =7.6 Hz). The *ortho*position proton, H$_O$ was observed at δ 8.25 (J =7.0 Hz), H$_8$ at δ 7.92 (J=7.6 Hz), H$_7$ at δ 7.61 (J=7.6 Hz) and H$_6$ at δ 7.22 (J=7.6 Hz). The N-H from imine was observed at δ 8.16 (J=7.0 Hz).Compound (6) appearedas a white (0.23g, 35.81%). From the ATR, the N-H stretching was observed at 3319 cm^{-1}, followed by C=N stretching at 1668 cm^{-1}. The C=C aromatic stretching were observed at 1600 cm^{-1} and 1451 cm^{-1}. The ^{1}H NMR spectrum showed the peak of N-H at δ 11.97, followed by H$_5$ at δ 8.82 (J=7.7 Hz). The *ortho*position proton, H$_O$ was observed at δ 8.00 (J=8.4 Hz), H$_8$, H$_7$, H$_m$, and imine N-Hwere observed as multiplet peak at δ 7.46 - 7.61. The H$_6$ was observed at δ 7.15 (J =7.7 Hz).

The antioxidant activity of benzoxazzinone and quinaozolin-4-imine was tested using 2,2'-diphenyl-1-picrylhydrazyl (DPPH). From the results obtained, it clearly shows that the compounds of 4*H*-3,1-benzoxazin-4-one derivatives do not possess any antioxidants activities after incubation of 30 mins with DPPH. The negative results of the antioxidant activities from 4*H*-3,1-benzoxazin-4-one can be explained by the lack of free hydrogen atom to be donate and stabilize the free radical DPPH. The compounds of all quinazolin-4-imine synthesized possess good antioxidant activities even at low concentration of 100ppm. The capability in antioxidant is due to the active hydrogen at the nitrogen atom of the quinazolin-4-imine skeleton. The IC$_{50}$ of compound (4), (5) and (6) were 2.66ppm, 28.40ppm and 8.04 ppm respectively. From the IC$_{50}$ values, it was concluded that the introducing of chlorine atom at *p*-position of phenyl group slightly reduced the ability of the compound due to the inductive effect.

CONCLUSION

A series of 2-substituted-4*H*-3,1-benzoxazin-4-one and quinazolin-4-imine compounds had been synthesized with a simple and single step method by using anthranilic acid as starting material. The benzoxazin-4-one compound derivatives synthesized are 2-phenyl-4*H*-3,1-benzoxazin-4-one (1) (78.91%), 1,4-(di-4*H*-3,1-benzoxazin-4-one)benzene (2) (55.23%) and 2-(*p*-chlorophenyl)-4*H*-3,1,-benzoxazine-4-one (3) (33.20%). In the synthesis of the quinazolin-4-one derivatives, the desired product is not obtained. Instead of quinazolin-4-one is synthesized, the unexpected products synthesized were proposed to be the quinazolin-4-imine derivatives based on the data analysis from ATR and ^{1}H NMR spectrum obtained. Therefore in the study, the quinazolin-4-imine derivatives obtained are 2-phenylquinazolin-4-imine (4) (70.90%), 1,4-(diquinazolin-4-imine)benzene (5) (43.70%) and 2-(*p*-chlrophenyl)quinazolin-4-imine (6) (35.81%).

The compounds synthesized were characterized and the bioactivity of anti-oxidant of each compounds were tested by using DPPH radicals scavenging method. From the bioassay, all the 4*H*-3,1-benzoxazin-4-one derivatives compounds do not shows antioxidant as there is no free active hydrogen to stabilize the radical of DPPH. While all the quinazolin-4-imine derivative compounds synthesized shows good antioxidant ability as the IC$_{50}$ is lower compare to ascorbic acid except for compound (5). Among the quinazolin-4-imine derivatives, 2-phenylquinazolin-4-imine shows the lowest IC$_{50}$ value at 2.66ppm while the highest IC$_{50}$ value belongs to 1,4-(diquinazolin-4-imine)benzene (5), which is 25.40ppm. From the IC$_{50}$ values it can conclude that the present of electron withdrawing group at the phenyl substituent causes inductive effect to quinazolin-4-imine compounds and decreases its ability to donate hydrogen for antioxidant purpose.

REFERENCES

1. Saini, M. S., Kumar, A., Dwivedi, J., & Singh, R. (2013). A Review: Biological Significances of Heterocyclic Compounds. *International Journal of Pharma Science and Research,* **4**. 66-77.
2. Kumar, B. V., Vaidya, S. D., Kumar, R. V., Bhirud, S. B., & Mane, R. B. (2006). Synthesis and Anti-Bacterial Activity of Some Novel 2-(6-Fluorochroman-2-Yl)-1-Alkyl/Acyl/Aroyl-1h-Benzimidazoles. *Eur J Med Chem*, **41(5)**, 599-604.
3. Chen, C. J., Song, B. A., Yang, S., Xu, G. F., Bhadury, P. S., Jin, L. H., Hu, D. Y., Li, Q. Z., Liu, F., Xue, W., Lu, P., & Chen, Z. (2007). Synthesis and Antifungal Activities of 5-(3,4,5-Trimethoxyphenyl)-2-Sulfonyl-1,3,4-Thiadiazole and 5-(3,4,5-Trimethoxyphenyl)-2-Sulfonyl-1,3,4-Oxadiazole Derivatives. *Bioorg Med Chem,* **15(12)**, 3981-3989.
4. Palaska, E., Sahin, G., Kelicen, P., Durlu, N. T., &Altinok, G. (2002). Synthesis and Anti-Inflammatory Activity of 1-Acylthiosemicarbazides, 1,3,4-Oxadiazoles, 1,3,4-Thiadiazoles and 1,2,4-Triazole-3-Thiones. *IlFarmaco,* **57**, 101-107.
5. Cheng, J. H., Hung, C. F., Yang, S. C., Wang, J. P., Won, S. J., & Lin, C. N. (2008). Synthesis and Cytotoxic, Anti-Inflammatory, and Anti-Oxidant Activities of 2',5'-Dialkoxylchalcones as Cancer Chemopreventive Agents. *Bioorg Med Chem,* **16(15)***,* 7270-7276.

6. Rajput, R., & Mishra, A. P. (2012). A Review on Biological Activity of Quinazolinones. *International Journal of Pharmacy and Pharmaceutical Science,* **4(2)**. 66-70.

7. Fomsgaard, I. S., Mortensen, A. G., &Carlsen, S. C. (2004). Microbial Transformation Products of Benzoxazolinone and BenzoxazinoneAllelochemicals--a Review. *Chemosphere,* **54(8)**, 1025-1038.

8. Ambujakshan, K. R., Varghese, H. T., Mathew, S., Ganguli, S., Nanda, A. K., &Panicker, C. Y. (2008). Vibrational Spectroscopic Studies and Theoretical Calculations of 2-Phenyl-4*H*-3,1-Benzoxazin-4-One. *Oriental Journal of Chemistry,* **24(3)**, 865-874.

9. Vince, R., & Hua, M. (1990). Synthesis and Anti-Hiv Activity of Carbocyclic 2',3'-Didehydro-2',3'-Dideoxy-2,6-Disubstituted Purine Nucleosides. *Journal of Medicinal Chemistry,* **33**, 17-21.

10. Osbone, A. G., &Goolamali, Z. (2000). ^{1}H and ^{13}C NMR Spectral Studies of Some 4*H*-3,1-Benzoxazin-4-Ones and Their 2-Acylaminobenzoic Acid Precursors. *Specrochimica Act Part A,* **56**, 1079-1100.

11. D., P., Lampman, G., Kriz, G., & Vyvyan, J. (2008). Introduction to Spectroscopy. 4th. Ed. Canada:Cengage Learning. 135.

12. Alagarsamy, V., Salomon, V. R., Vanikavitha, G., Paluchamy, V., Chandran, M. R., Sujin, A. A., Thangathirupathy, A., Amuthalakshmi, S., &Revathi, R. (2002). Synthesis, Analgesic, Anti-Inflammatory and Antibacterial Activities of Some Novel 2-Phenyl-3-Substituted Quinazolin-4(3*H*) Ones. *Biological & Pharmaceutical Bulletin,* **25(11)**, 1432-1435.

DEMETALLIZATION OF TOXIC AND HEAVY METALS IN CLAM, *PAPHIA TEXTILE* UTILIZING CATALYTIC CHELATION TECHNIQUE

Nur Syafiqah Mohamad Sa'adan , Wan Azelee Wan Abu Bakar, Wan Nur Aini Wan Mokhtar
Department of Chemistry, Faculty of Science, Universiti Teknologi Malaysia, 81310 Johor Bahru

Abstract

This research was carried out to study the toxic and heavy metals removal like lead (Pb), cadmium (Cd) and nickel (Ni) from *Paphia textile*. Three types of chelating agents, namely trisodium citrate, sodium acetate and disodium oxalate and three types catalysts supported on Al_2O_3 namely MgO, CaO and BaO were used. The demetallization treatment screening carried out at a 400 mg/L, one hour treatment time and treatment temperature of 32.5 ± 0.5°C on *Paphia textile*, revealed trisodium citrate was the most potential chelating agent. Metals concentration were analysed using Flame atomic absorption spectroscopy (FAAS). The initial concentration of Pb, Ni and Cd in *Paphia textile* were found to be 1.05±0.18 μg/g, 0.83±0.21 μg/g and 0.56±0.02 μg/g respectively. The results on the optimization chelation technique showed that 400 mg/L of trisodium citrate gave the highest percentage removal of toxic and heavy metals with Pb 84.69% (0.16±0.05 μg/g), Ni with 78.60% (0.18±0.08 μg/g) and Cd with 41.96% (0.33±0.01 μg/g). Among the three catalysts studied, CaO/Al_2O_3 catalysts at an optimum calcination temperature of 1000°C, in the presence of trisodium citrate, gave the highest percentage removal with 87.79% (0.13±0.15 μg/g) of Pb, 83.56% (0.14±0.11 μg/g) of Ni and 76.43% (0.13±0.01 μg/g) of Cd. This study showed that catalytic chelation technique at optimum conditions able to remove further the toxic and heavy metals compared to chelation technique from *P. textile* to achieve permissible limits set by Malaysian Food Regulation (Cd and Ni: 1.00 μg/g; Pb: 2.00 μg/g) and EU Regulation (Cd and Ni: 1.00 μg/g; Pb: 1.50 μg/g).

Keywords: Toxic and heavy metal, Paphia textile, Chelating agent, Catalyst, Flame Atomic Absorption Spectroscopy (FAAS)

INTRODUCTION

Paphia textile (Family: Veneridae) is known as Lala in Malaysia. *P. textile* is an infaunal filter-feeding which feed on phytoplankton, small zooplankton and other organic materials. This bivalve commonly found in the sandy-muddy bottoms of the internal and sublittoral zones of the coastal environment [1]. Basically, *P. textile* was found in Pantai Bagan Panchor until Pantai Remis, Perak of Peninsular Malaysia.

Heavy metals such as cadmium and mercury and toxic metals such as arsenic, lead, magnesium, manganese, selenium, vanadium, and essential metals such as copper and zinc could be classified as potentially dangerous heavy metals [2]. These heavy metals contribute to degradation of marine ecosystems by reducing species diversity and abundance and through accumulation of metals in living organisms and food chains [3]. The factors which influence metal concentration and accumulation are bioavailability of metals, season, size, sex, hydrodynamics of the environment, changes in tissue composition and reproductive cycle [4]. Basically, clams focused on the use of total soft tissues of clams rather than the clams shell as a quantitative indicator to reflect the heavy metal contamination in the coastal area. Basically, types of toxic and heavy metals found in clams are Cd, Cr, Cu, Fe, Pd, Ni, Hg and Zn and Fe is the highest concentration accumulated in the soft tissue of clams [5]. Concentration of heavy metals in clams revealed that Fe gives the high concentration by having 289 ppm [6]. One of the effective ways to treat heavy metals poisoning is through chelating technique [7]. Chelation technique is recommended for heavy metal poisoning and these metals exert their toxic substances by combining with one or more reactive groups essential for normal physiological functions. The chelating agent is the formation of ring-like structure that called as 'chelate' and the chelating agent will be bind to the metal ion and form a complexes before excrete out from the flesh. The used of catalysts is needed in order to enhance the chelation technique. The purpose of the study is to remove toxic and heavy metals (Pb, Ni and Cd) from contaminated *P. textile* using several types of chelating agents with addition of catalysts. The result should compliment with the permissible limit set by the Malaysian Food Regulations (1985) and Commission Regulation of EU (2006).

MATERIALS AND METHODS

Pb, Ni and Cd metals were analyzed through Flame atomic absorption spectroscopy, FAAS (Perkin Elmer Pin AAcle). All reagents used in the study were analytical grade and were used without any purification. All the solutions were prepared using distilled water. Samples were digested using HNO_3 (QRёC™, 65%). All the plastic and glassware were cleaned by soaking in diluted HNO_3 and rinsed with distilled water. The element standard solutions used for calibration were produced by diluting a stock solution. The chelating agents used were sodium citrate dehydrate, $C_6H_5Na_3O_7.2H_2O$ (QRёC™), disodium oxalate, $Na_2C_2O_4$ (Bendosen) and

sodium acetate trihydrate, $CH_3COONa. 3H_2O$ (QRëC™). Meanwhile for the catalyst, the chemicals were magnesium acetate tetrahydrate, $C_4H_6O_2Mg.4H_2O$ (Rinting Scientific), barium nitrate, $Ba(NO_3)_2$ (Sigma Aldrich) and calcium nitrate tetrahydrate, $Ca(NO_3)_2.4H_2O$ (Sigma Aldrich). For standard solution for calibration, Pb, Ni and Cd pure single-element standards (Perkin Elmer) were used.

Catalyst Preparation

The catalyst was prepared by dissolving 6.25 gram of magnesium acetate tetrahydrate salt powder into 5 mL of distilled water and stir until the powder was dissolved. Alumina pallets were immersed into the solution. Later, it was aged at 80°C for 24 hours before further calcined at 1000°C for another 5 hours. Similar procedure was repeated to prepare 5 mol calcium nitrate tetrahydrate powder (5 gram in 5 mL distilled water) and 0.5 mol of barium nitrate powder (5 gram in 50 mL distilled water). All analysis was conducted in three series of replicates.

Sampling

Paphia textile was purchased from the wet market in Pasar Taman Universiti, Skudai. These clam samples were then brought back to laboratory and were stored in refrigerator until treatment.

Toxic and Heavy Metals Removal

Treatment for toxic and heavy metals removal in *P. textile* was conducted using three types of chelating agents. *P. textile*s were put in sack and were soaked in the beaker that contains the chelating agents with stirring for 1 hour. *P. textile* was rinsed with distilled water and digested before analyzed using FAAS. Chelation process was optimized using chelating agent (300 to 600 µL/L), for 1, 3 and 5 hours of treatment time and at different treatment temperature (29.5±0.5°C, 32.5±0.5°C and 37.5±0.5°C). For catalytic chelation treatment, samples were soaked in chelating solutions by immersing 0.25 g of prepared catalysts which put in sack in the solution and left it at the bottom of the solution.

Toxic and Heavy Metal Analysis

All prepared samples were digested using 65% of HNO_3. The digestion was done until clear solutions were obtained. After the digestion process, the samples were allowed to cool and filtered using Whatman No 42 filter paper and then diluted to 10 mL with distilled water. The prepared samples were then analysed for Pb, Ni and Cd using FAAS. The concentrations are presented in µg/g. The standard solution and blank were also run for calibration.

RESULTS AND DISCUSSION

Toxic and Heavy Metal Concentration in *Paphia textile*

The initial concentrations of toxic and heavy metals in *P. textile* are presented in **Table 1.** The trisodium citrate was varied from 300 to 600 mg/L to get the optimum concentration of chelating agent. The obtained results from FAAS showed that the initial *P. textile* samples contain Pb a bit higher than permissible limit stated by European Union (EU) meanwhile, Cd and Ni concentration below the permissible limit stated by Malaysian Food Regulation (MFR) and European Union (EU) as stated in **Table 1**.

Table 1: Initial concentration of toxic and heavy metals in *P. textile* and the permissible limit of MFR and EU

	Cd (µg/g)	Ni (µg/g)	Pb (µg/g)
Initial Concentration	0.85±0.002	0.82±0.07	1.77±0.09
Permissible Limit:			
Malaysia	1.00	1.00	2.00
EU	1.00	1.00	1.50

The results of the three different chelating agents are presented in **Fig. 1.** The results indicated that trisodium citrate was the most effective chelating agents with the percentage removal of toxic and heavy metals (Pb: 84.69%, Ni: 78.60%, Cd: 41.96%) were obtained. The trisodium citrate gave the highest percentage removal of heavy metals in *P. textile* followed by sodium acetate and disodium oxalate. This trend showed that the high stability of the ring structured metal-citrate complex produced from chelation, thus increase the removal percentage of heavy metal ions [9].
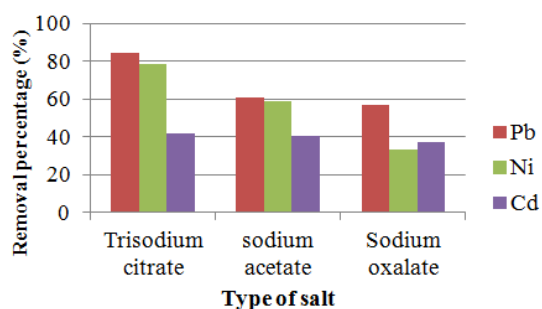

Fig. 1: Effect of chelating agent on toxic and heavy metals removal in *P. textile* at 400 mg/L trisodium citrate at 32.5±0.50°C for 1 hour.
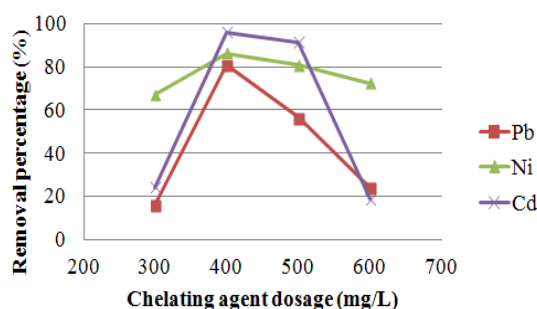
Fig. 2: Efficiency of trisodium citrate at different concentrations towards removal of toxic and heavy metals form *P. textile* at ambient temperature for 1 hour.

Optimization of Chelating Agents

The optimization treatment condition of chelation treatment by using trisodium citrate were at 400 mg/L concentration dosing, 32.50±0.50°C of treatment temperature and 5 hours treatment were initially selected as it gave the highest percentage removal of toxic and heavy metals in *P. textile*. Since one hour treatment was more practically used in laboratory and consumer's application thus, 1 hour of treatment time was applied for *P. textile* treatment with other chelating agents which are sodium acetate and disodium oxalate.

The efficiency of trisodium citrate at different concentrations in the removal of toxic and heavy metals concentration in *P textile* is presented in **Fig. 2**. From the results it is revealed that the levels of toxic and heavy metals studied were successfully reduced by trisodium citrate treatment (Pb; 80.96%, Ni: 86.99% and Cd: 96.20%) and the concentration of 400 mg/L was found to be the most effective with highest percentage removal of toxic and heavy metals. The analysis suggests that there is a trend on toxic and heavy metals removal by trisodium citrate as the increased in dosing of chelating agents. The removal of the toxic and heavy metals increased and reached optimum at concentration of 400 mg/L. Exceeding this concentration, the percentage removal of toxic and heavy metals decreased accordingly. This pattern could be explained by Le Chartelier's principle [8] whereby the increased in concentration of trisodium citrate will enhance the reversible reaction towards the formation of starting material, thus decrease the citrate ion production to chelate the toxic and heavy metals.
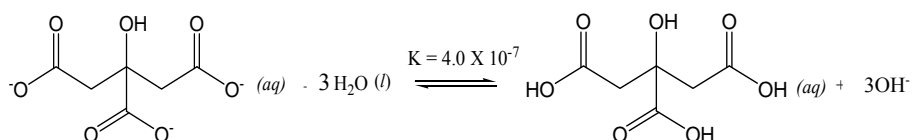
Further investigating was done in the treatment time with varied to one, three and five hours. Results showed that the percentage removal of toxic and heavy metals removal increased as the time increased (**Fig. 3**). Five hours treatment showed the highest percentage removal of toxic and heavy metals (Pb: 71.65%, Ni: 57.36%, Cd: 50.70%). It is most probably the longer period of treatment time allowing the trisodium citrate to remove the toxic and heavy metals from *P. textile*.

Effect of temperature on the efficiency of trisodium citrate was studied and results are presented in **Fig. 4.** From the results, the percentage removal of toxic and heavy metals increased from 29.50±0.50°C to 32.50±0.50°C and decreased at 37.50±0.50°C. Highest percentage removal of toxic and heavy metals (Pb: 84.69%, Ni: 78.60%, Cd: 41.96%) was observed at 32.50±0.50°C. The increased with temperature up to

119

32.50±0.50°C may due to habitat of clams which can survive at 31.11°C thus, increase the mucus gland in clam and the percentage removal of toxic and heavy metals increased. On the other hand, toxic and heavy metals removal decreased at 37.50±0.50°C due to the high mucus gland from *P. textile* which covered the flesh surface and prevent the chelating agent to remove toxic and heavy metals.
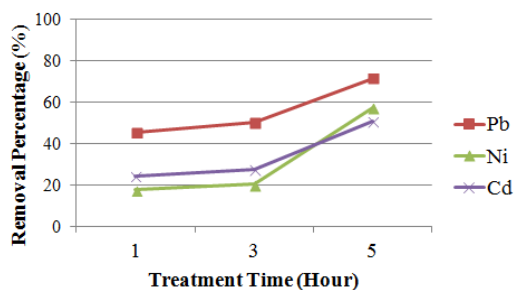

Fig. 3: Effect of treatment time on toxic and heavy metals removal in *P. textile* using 400 mg/L trisodium citrate at ambient temperature.
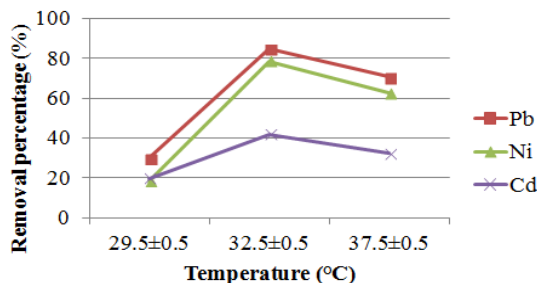
Fig. 4: Effect of reaction temperature on toxic and heavy metals removal in *P. textile* using 400 mg/L trisodium citrate for 1 hour.

Catalytic Activity

The study on the catalytic treatments was done to identify the effect of CaO, BaO and MgO supported with Al_2O_3 catalyst with 1000°C calcination temperature towards metals chelation of trisodium citrate. The heavy metals concentration with and without the presence of catalyst was determined. The results are presented in **Table 2**. The result showed that CaO/Al_2O_3 gave the highest percentage removal of toxic and heavy metals in *P. textile*. It indicates, with the presence of CaO/Al_2O_3 catalyst, the percentage removal of toxic and heavy metals increased compared without catalyst. Hence, the catalyst was optimized to get the optimum catalytic treatment. The increase in removal percentage of toxic and heavy metals probably due to the enhancement the formation of irreversible reaction by catalyst to produce the anion (citrate) which then reacts with the toxic and heavy metals in the contaminated *P. textile* [10].

The optimization for the treatment of catalyst, one hour treatment gives the highest percentage removal of toxic and heavy metals in *P. textile.* The results are presented in **Table 3.** The longer treatment duration with catalysts increased the frequency of catalytic chelation cycle and the possibility of the chelate ions to reach out the metal ions for complexation [10]. The removal percentages of heavy metals were not much different between 30 minutes and 45 minutes. Thus, from the results, it can shown that chelation technique and catalytic chelation technique can remove toxic and heavy metals in *P. textile* especially the catalytic chelation technique which can removed further towards heavy metals by having the highest percentage removal of toxic and heavy metals.

Table 2: Percentage removal of toxic and heavy metals in *P.textile* at 1000°C calcination temperature in trisodium citrate (400 mg/L) for 1 hour.

Chelating agents		Pb (µg/g)	Ni (µg/g)	Cd (µg/g)
Initial Concentration		1.05±0.18	0.83±0.21	0.56±0.02
Without catalyst		0.16±0.05	0.18±0.08	0.33±0.01
		84.69%	78.60%	41.96%
Calcined at 1000°C	CaO/Al_2O_3	0.13±0.15	0.14±0.11	0.13±0.01
		87.79%	83.56%	76.43%
	MgO/Al_2O_3	0.29±0.08	0.26±0.05	0.32±0.02
		72.17%	68.65%	43.09%
	BaO/Al_2O_3	0.54±0.01	0.25±0.19	0.33±0.03
		48.58%	69.59%	41.09%

Table 3: Percentage removal of toxic and heavy metals in *P. textile* at 1000°C calcination temperature in trisodium citrate (400 mg/L) at different treatment times.

Chelating agents	Pb (µg/g)	Ni (µg/g)	Cd (µg/g)
Initial Concentration	1.05±0.18	0.83±0.21	0.56±0.02
Treated for 1 hour	0.13±0.15	0.13±0.11	0.13±0.01
	87.79%	83.56%	76.43%
Treated for 45 min	0.47±0.11	0.14±0.06	0.30±0.00
	55.15%	82.80%	46.39%
Treated for 30 min	0.46±0.08	0.15±0.01	0.31±0.02
	56.34%	82.05%	44.90%
Treated for 15 min	0.52±0.010	0.53±0.12	0.27±0.04
	50.95%	36.05%	52.03%

CONCLUSIONS

The chelation method is found to be a potential technique for the removal of toxic and heavy metals in *P. textile.* The optimization treatment conditions were obtained by having 400 mg/L trisodium citrate, one hour of treatment time and 32.50±0.50°C of treatment temperature. Present investigation illustrates the efficiency of the studied chelation agents in the order of trisodium citrate > sodium acetate > sodium oxalate. The trisodium citrate gave the highest percentage removal of toxic and heavy metals, whereby 84.69% (0.16±0.05 µg/g) of Pb, 78.60% (0.18±0.08 µg/g) of Ni and 41.96% (0.33±0.01 µg/g).of Cd. The highest percentage removal of toxic and heavy metals for catalytic chelation technique were achieved in the presence of CaO/Al_2O_3 catalysts, namely 87.79% (0.13±0.15 µg/g) of Pb, 83.56% (0.14±0.11 µg/g) of Ni and 76.43% (0.13±0.01 µg/g) of Cd at calcinations temperature 1000°C. In conclusion, both chelation and catalytic chelation technique can remove toxic and heavy metals. However, the catalytic chelation technique offers better removal of toxic and heavy metals from *P. textile* to achieve permissible limits set by Malaysian Food Regulation and EU Regulation.

REFERENCES

1. Argente, F. A., Estacion, J. S., (2014). Effect of different harvesting practices on the dynamics of *Paphia textile* (Gmelin 1792) (Bivalvia: Veneridae) populations at two sites in Zamboanga del Norte, Southern Philippines. *Environmental and Experimental Biology* **(12),** 113-120.
2. Al-Mohanna, S. Y., Subrahmanyam, M. N. V. (2001). Flux of heavy metal accumulation in various organs of the intertidal marine blue crab, *Portunus pelagicus* (L.) from the Kuwait coast after the Gulf War. *Environment International,* **27(4)**, 321-326.
3. Hosono, T., Su, C., Delinom, R., Umezawa, Y., Toyota, T., Kaneko, S., Taniguchi, M., (2011). Decline in heavy metal contamination in marine sediments in Jakarta Bay, Indonesia due to increasing environmental regulations. Estuar. Coast. Shelf Sci. (92), 297–306.
4. Krishna, Kumari, L., Kaisary, S., and Rodrigues, V. (2006). Bio-accumulation of some trace metals in the short-neck clam *Paphia malabarica* from Mandovi estuary, Goa. *Environment International,* **32(2)**, 229-234.
5. Baby, J., Raj., J. S., Biby. (2010). Toxic effect of heavy metals on aquatic environment. Int. J. Biol. Chem. Sci. **4(4),** 939-952.
6. Juncharoenwongsa, N., Siriprom, W., Kaekhao, J., Chaeysuppaker, A., Limsuwan, P., Phachana, K., (2011). A Biomarkers Study: Trace Metal Elements in *Paphia Undulate* Shell for Assessing Pollution of Coastal Area. *Procedia Engineering* **(8)**, 80-84.
7. Sivakumar, S., Khatiwada, C. P., & Sivasubramanian, J. (2012). Bioaccumulations of aluminum and the effects of chelating agents on different organs of Cirrhinus mrigala. Environmental Toxicology and Pharmacology, **34(3)**, 791-800.
8. Ihsan, W.A. (2013). *Catalytic Chelation Technique for the Removal of Toxic and Heavy Metals from Green Mussel, Perna viridis*. Master's thesis, Universiti Teknologi Malaysia, Skudai.
9. Nurul Hazirah, M. (2013). *Removal of Toxic and Heavy Metals from Anadara granosa Using Chelating Agent.* Master's thesis, Universiti Teknologi Malaysia, Skudai.
10. Hui, K.P. (2015). *Detoxification of Heavy Metals in Freshwater Catfish, Clarias spp. Utilizing Chelation and Catalytic Chelation Techniques*. Master's thesis, Universiti Teknologi Malaysia, Skudai.

DETERMINATION OF CHEMICAL COMPONENTS IN THE RHIZOMES OF
Hedychium coronarium

Siti Nazeerah Binti Kamarruddin and Hasnah Binti MohdSirat

Department of Chemistry, Faculty of Science, UniversitiTeknologi Malaysia, 81310 Johor Bahru.

Abstract

*Hedychiumcoronarium*or locally known as white ginger lily belongs to Zingiberaceae family. Hydrodistillation of the fresh rhizomes yielded 0.02% of the essential oil. The composition of the essential oil was analyzed both by gas chromatography and gas chromatography-mass spectroscopy. Eleven compounds were identified representing 79.78% of the whole compositions. 1,8-Cineole (39.03%) is the major component in the essential oil. Soxhlet extraction of the dried rhizomes of H. coronarium with chloroform as solvent yielded a crude extract 4.42%. Purification of the extract took place using column chromatography and preparative thin layer chromatography had afforded two diterpenes. Their structures have been identified using spectroscopic methods as two isomers of coronarin D (1.02%) and 14,15-dihydroxylabda-8(17),12-diene-15,16-olide (coronarin G) (0.1%). Antioxidant property was screened using DPPH radical scavenging assay and has been carried out on the chloroform crude extract, essential oil and two pure compounds. The results revealed that the crude extract gave moderate antioxidant property with IC_{50} 275.05 µg/mL. The antibacterial assay was conducted on chloroform crude extract, essential oil and coronarin D. Coronarin D was found to show moderate antibacterial property towards Gram positive bacteria *Bacillus subtilis* (BS) ATCC 6633 at a concentration of 450 ppm.

Keywords: *Hedychium coronarium,* labdane, coronarin, essential oil, bioassay.

INTRODUCTION

H. coronarium which has many common names including butterfly ginger, butterfly lily, cinnamon jasmine, garland flower, and ginger lily, is widely cultivated in India, Southeast Asian countries, South China, Taiwan, Japan, and Brazil. The rhizomes of *H. coronarium* is used in Chinese natural medicine, which has been prescribed for the treatment of headache, lancinating pain, contusion inflammatory, and sharp pain due to rheumatism in Chinese traditional preparations, while it is used as a febrifuge, tonic, excitant, and anti-rheumatic in the Ayurvedic system of traditional Indian medicine [1].

The chemical composition of the essential oils of ginger lily have been identified in the early studies such as α-muurolol (16.8%), α-terpineol (15.9%), 1,8-cineole (11.2%), α-fenchyl acetate (5.6%), citronellal (5.5%) and (*E*)-methyl cinnamate (5.1%). Some of the compounds that are present in the rhizomes of *H. coronarium* are the labdane diterpenes, (*E*)-labda-8(17),12-diene-15,16-dial, coronarin B, coronarin D, isocoronarin D, labda-8(17),11,13-trien-15,16-olide, an ester of labda-8(17),11,13-trien-15-al-16-oic acid and isoconarin D, and 7β-hydroxycoronarin B [2]. This research focused on the study of the rhizomes of *H. coronarium* and the objectives of this study are to extract the essential oil, phytochemical and to evaluate the bioactivity of *H. coronarium*. Purification of the chemical constituents present in the crude extracts of the rhizomes of *H. coronarium* and also to elucidate the structure of the compound using spectroscopic methods.

EXPERIMENTAL

Chemical composition analysis of the essential oil was carried out using a Gas Chromatography (GC) Hewlett Packard 5890 series II. A GC equipped with an Ultra 1 column (25 m long, 0.32 µm thickness and 0.17 mm internal diameter). The chromatogram of gas chromatography-mass spectrometry (GC-MS) was recorded using a Perkin Elmer Gas Chromatograph Clarus 680 equipped with mass Spectrometer Clarus SQ 8 S. All chemicals involved in this experiment are analytical grade. Soxhlet extraction, fractionation and purification were carried out using several types of organic solvents which are *n*-hexane, petroleum ether, diethyl ether, chloroform, methanol and ethyl acetate. Petroleum ether refers to PE with a boiling point 60-80°C and was redistilled before used. Thin layer chromatography (TLC) was carried out on 0.20 mm Merck silica gel plates (60 F254). Samples were spotted on the baseline (0.5 cm) drawn on the TLC. The compounds were visualized under a UV lamp (254 nm) and vanillin sulphuric acid spray. Fractionation and purification of the crude extracts were conducted using gravity column chromatography (CC) and preparative thin layer chromatography (prep TLC) with Merck silica gel 70-230 mesh and silica gel 60 PF254 (10–40 µ) containing gypsum, respectively. Infrared (IR) spectra were recorded on Perkin Elmer 1650 FTIR spectrophotometer using the attenuated total reflection (ATR) for the gummy samples. The 1H and 13C nuclear magnetic resonance spectra (NMR) were recorded on Bruker Avance 400 Spectrometer (400 MHz and 100 MHz respectively). Deuterated chloroform was used as solvent.

Intensity of the colour change of DPPH for antioxidant assay were recorded on Biotek Epoch Microplate Spectrophotometer. The wavelength was set to 517nm.

(1)   **(2)**   **(3)**   **(4)**
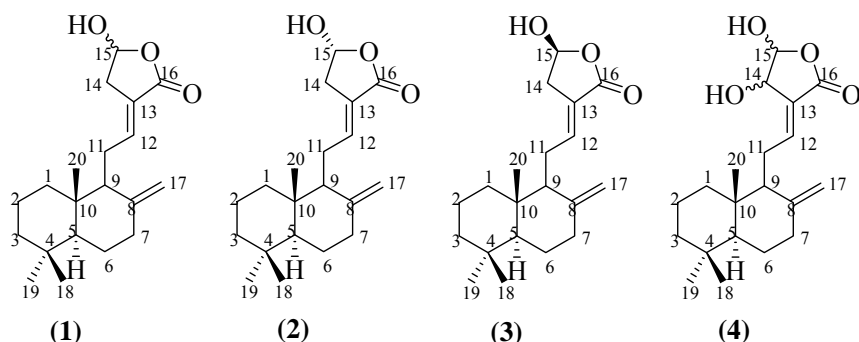
Plant Material

The sample of *H. coronarium* or also known as ginger lily was obtained from Skudai, Johor in 2014.

Extraction and Isolation

The fresh chopped rhizomes (205.0 g) were extracted using hydrodistillation technique in a Dean- Stark apparatus for 8 hours. The essential oil collected was extracted with ether (3×10 mL), dried over anhydrous magnesium sulphate and filtered. The ether was then evaporated at room temperature overnight to give the essential oil (0.039 g, 0.02%) as pale yellow oil with a fragrant scent.

The rhizomes of *H. coronarium* (74.0 g) were air dried, powdered and extracted with chloroform in a soxhlet apparatus for 20 h. The resulting chloroform extract was evaporated to dryness under reduced pressure using rotary evaporator to afford a thick dark yellowish browngum crude extract labeled as HC (3.3 g, 4.5%). The crude extract HC (2.0 g) obtained was purified using column chromatography (CC) (100×3.5 cm length) packed with Merck silica gel 70-230 mesh (60 g). The column was eluted using n-hexane and Et$_2$O as solvent with increasing polarity gives eight major compounds. Fraction HC 5 was evaporated under reduced pressure to give a mixture of epimers of coronarin D **(1)** (0.0203 g, 1.02%) as a dark yellowish brown gum. Further purification of fraction HC 4 using prep TLC afforded another four compounds using triple development with *n*-hexane and Et$_2$O (2:1). Fraction HC 4-4 was concentrated to give a compound that was tentatively predicted as 14,15-dihydroxylabda-8(17),12-diene-15,16-olide (Coronarin G) **(4)**.

RESULTS AND DISCUSSION

The essential oil of *H. coronarium* was analysed by GC and GC-MS. The mass spectrum of each peak was compared with mass spectrum from the National Institute of Standards and Technology (NIST). The high percentage matching (more than 80%) was selected as the constituents. The identified constituents of the essential oil of *H. coronarium* are listed in **Table 1**. A total of eleven components were successfully identified from the GC and GC-MS comprising 79.78% of the total. The essential oil consisted of only monoterpenes with 1,8-cineole (39.03%) as the main constituent. The other major components found in the rhizome oil were α-terpineol (21.67%) and β-pinene (8.05%). Previous study showed that the major essential oil components of *H. coronarium* from Mauritius is α-muurolol (16.8%), α-terpineol (15.9%), 1,8-cineole (11.2%), α-fenchyl acetate (5.6%), citronellal (5.5%) and (*E*)-methyl cinnamate (5.1%) [3]. Meanwhile another research from India reported that the major constituents of fresh rhizome oil were 1,8-cineole (41.42%), β-pinene (10.39%), α-terpineol (8.80%) and α-pinene (4.06%) [4]. The chemical composition of rhizome oil of H. Coronarium collected in Johor, Malaysia was closely resemble to the essential oil composition reported by Beena Joy [4], in which 1,8-Cineole is the major component.

Coronarin D epimers **(1)** were obtained as dark yellowish brown gum (0.02 g, 1.02 %) with a R$_f$ 0.38 (*n*-hexane:Et$_2$O, 1:2). The IR spectrum showed that there is weak hydroxyl bend at the position of 3373 cm^{-1}. The spectrum also showed a sharp bend at 1737 cm^{-1} for carbonyl C=O ester in the furan ring. It could be observed that the bend is shifted to a lower value due to the conjugation of double bond outside the ring causing it to weakened the strain of C=O bond. The ^{1}H NMR spectrum of compound **(1)** revealed the presence of a mixture of coronarin D epimers **(2)** and**(3).** The proton NMR spectrum showed three singlet integrating for three proton

each at δ 0.72, δ 0.82 and δ 0.89 which were attributed to three methyl groups. Two broad singlet proton resonated at δ 4.40 and δ 4.82 was assigned to exomethylene protons at C-17. These suggested that compound (**1**) has a labdane type skeleton. The epimers are assigned as coronarin D (A) (**2**) and coronarin D (B) (**3**). The position of the first set exomethylene could be given to compound (**2**), meanwhile for compound (**3**) two weak doublet protons resonated at δ 4.35 and δ 4.82 with a value of proton coupling $J = 0.8$ Hz. As for the ^{1}H-^{1}H COSY spectrum for compound (**1**) showed the correlation between H-11, H-14 and H-17. The ^{13}C NMR supported the presences of 23 peaks with three extra peaks due to the epimeric mixture that contains in compound (**1**). The duplicate peaks were at the position of C-8, C-12 and C-17 which can be assigned to one set to compound (**2**) while the other set belongs to compound (**3**). Analysis of DEPT spectrum showed the existing of three methyl group at δ 33.58 (C-18), δ 21.73 (C-19) and δ 14.35 (C-20); one exomethylene at δ 107.36 (C-17) for compound (**2**) while the other at δ 107.65 (C-17) for compound (**3**) and seven methylene at δ 39.21 (C-1), δ19.32 (C-2), δ 41.99 (C-3), δ 24.09 (C-6), δ 37.78 (C-7), δ 25.51 (C-11) and δ 124.48 (C-14); and four methine groups at δ 55.33 (C-5), δ 56.12 (C-9), δ 96.46 (C-15) and δ 143.55 (C-12) for compound (**2**) while the other at δ 143.64 (C-12) for compound (**3**). The complete assignments of the carbons were accomplished by the HMQC spectrum. The complete ^{1}H NMR and ^{13}C NMR parameters for coronarin D (**1**) epimers are listed in **Table 2.**

Table 1: Chemical composition of the essential oil of *H. coronarium*

No.	Compounds	Kovats Index	Percentage of Composition (%)
1	α-Pinene	928	1.81
2	β-Pinene	964	8.05
3	Myrcene	980	2.77
4	α-Phellandrene	997	0.47
5	1,8-Cineole	1017	39.03
6	*E*-Sabinene hydrate	1055	0.89
7	Linalool	1094	1.49
8	Camphor	1117	0.31
9	Pinocarvone	1132	0.90
10	Terpinen-4-ol	1160	2.39
11	α-Terpineol	1171	21.67
Total amount identified (%)			79.78

Table 2: ^{1}H and ^{13}C NMR data of compound (**1**)

Carbon	[1]H (δ ppm)	[13]C (δ ppm)
1	1.00-2.10	39.21
2	1.00-2.10	19.32
3	1.00-2.10	41.99
4	-	33.58
5	1.00-2.10	55.33
6	1.00-2.10	24.09
7	2.30-2.40 m	37.78
8	-	147.91/148.12
9	1.00-2.10	56.12
10	-	39.44
11	2.20/2.35	25.51
12	6.73 m	143.55/143.64
13	-	124.48
14	2.73 dd $J = 2$, 15.2/ 3.00-3.06 m	33.56
15	5.95 m	96.46
16	-	170.66
17	4.35/4.82 d $J = 0.8$ Hz 4.40/4.82 s	107.36/107.65
18	0.89 s	33.58
19	0.82 s	21.73
20	0.72 s	14.35

Preparative TLC of HC4 using *n*-hexane:Et_2O (1:1) afforded a minor constituent HC4-4 as a pale yellow oil (2.0×10^{-3} g, 0.1 %) with R_f0.5 (*n*-hexane:Et_2O, 1:1). The ^1H NMRspectrum HC4-4 revealed the presence of three singlet each integrating for three proton at δ 0.71, δ 0.82 and δ 0.89 and exomethylene proton at δ 4.57 and δ 4.89 suggested that HC4-4 has the labdane skeleton. Two deshielded protons were observed at δ 6.82 and δ 6.11 which were assign to be β-olefinic proton at C-12 and methine proton at C-14 respectively. Another broad singlet at δ 3.67 was an oxymethine proton at C-14. Due to insufficient amount of sample the compound (4), the ^{13}C NMR was not obtained to support the structure of compound. Therefore tentatively the compound was assigned as 14,15-dihydroxylabda- 8(17),12-diene-15,16-olide (Coronarin G) **(4)**.

Antioxidant activity was screened using DPPH radical scavenging assay and has been carried out on the chloroform crude extract, essential oil and two pure compounds. The results revealed that the crude extract gave moderate antioxidant property with IC_{50} 275.05 µg/mL. The antibacterial assay was conducted on chloroform crude extract, essential oil and coronarin D. Coronarin D was found to show moderate antibacterial properties towards Gram positive bacteria *Bacillus subtilis* (BS) ATCC 6633 at a concentration of 450 ppm.

CONCLUSION

The extraction of the fresh rhizomes by hydrodistillation afforded essential oil in 0.02% yielded. By GC and GC-MS analyzed revealed eleven compounds which contributed 79.78% of the total oil.Meanwhile, Soxhlet extraction of *H. coronarium* yielded chloroform extract (4.42%). Purification of chloroform extract have resulted in the isolation of two labdane diterpene compounds. The compounds were identified by using spectroscopic techniques and also by comparison with the literature value and the first compound has be proposed as epimers of coronarin D **(34)**. As for the second compound, it was tentatively identified as 14,15-dihydroxylabda-8(17),12-diene-15,16-olide (coronarin G) **(51)**. The DPPH free radical scavenging activity screening showed that the crude chloroform extract gave positive antioxidant, whereas epimer of coronarin D was active towards *Bacillus subtilis* (Gram positive bacteria).

REFERENCES

1. Matsuda, H., Morikawa, T., Sakamoto, Y., Toguchida, I., and Yoshikawa, M. (2002). Labdane-type Diterpenes with Inhibitory Effects on Increase in Vascular Permeability and Nitric Oxide Production from *Hedychium coronarium*. *Bioorganic & Medicinal Chemistry,* **10(8)**, 2527-2534.
2. Nakatani, N., Kikuzaki, H., Yamaji, H., Yoshio, K., Kitora, C., Okada, K., and G. Padolina, W. (1994). Labdanediterpenes from rhizomes of *Hedychium coronarium*. *Phytochemistry,* **37(5)**, 1383-1388.
3. Gurib-Fakim, A., Maudarbaccus, N., Leach, D., Doimo, L., and Wohlmuth, H. (2002). Essential Oil Composition of Zingiberaceae Species from Mauritius. *Journal of Essential Oil Research,* **14(4)**, 271-273.
4. Joy, B., Rajan, A., and Abraham, E. (2007). Antimicrobial activity and chemical composition of essential oil from *Hedychium coronarium*. *Phytotheraphy Research,* **21(5)**, 439-443.

FERRITE-CALCIUM ALGINATE AS MAGNETIC SOLID PHASE EXTRACTION ADSORBENT OF COPPER(II) IONS IN WATER PRIOR TO FLAME ATOMIC ABSORPTION SPECTROSCOPY

Nur Syafika Shah Bani[a], Wan Aini Wan Ibrahim[a]* and Hamid Rashidi Nodeh[a]
[a] Department of Chemistry, Faculty of Science, Universiti Teknologi Malaysia, 81310 UTM Johor Bahru, Johor, Malaysia

Abstract

A magnetic solid phase extraction (MSPE) procedure using ferrite-calcium alginate (Fe_3O_4-CaAlg) as adsorbent for Cu(II) ions prior to flame atomic absorption spectroscopy (FAAS) was developed. The extraction of Cu(II) ions using Fe_3O_4-CaAlg MSPE is simpler and faster than the conventional method such as solid phase extraction and traditional method such as liquid-liquid extraction. The simple extraction is based on the use of magnetisable adsorbent to extract Cu(II) ions, which can be readily isolated from water samples as a matrix with an external magnet. The adsorbent was prepared by mixing sodium alginate solution with Fe_3O_4 magnetic particles and calcium chloride solution to form magnetic alginate beads. Important parameters influencing the extraction and desorption process including type and volume of desorption solvent, agitation time, extraction time, weight of adsorbent and ample volume were optimized. Under the optimized conditions, calibration graph (external standard method) with coefficient of determination (R^2) of 0.974 in the linearity range 20-100 µg/L was observed. Good limit of detection (1.70 µg/L), and limit of quantification (5.6 µg/L) was obtained. Acceptable repeatability ($n = 3$) with RSDs 2.37% while reproducibility ($n = 9$) with RSD 5.15% were obtained for Cu(II) ions using the developed MSPE method. Finally, the proposed method was successfully applied for the determination of Cu(II) ion in tap water sample with relative recovery of 78.9% and 4.72% RSD. However, the proposed method was found to be less suitable for the determination of Cu(II) ion in river water sample with lower relative recovery (45.7% , 1.76% RSD) indicating that the method is sensitive to the matrix.

Keywords: Fe_3O_4-Calcium alginate, Magnetic solid phase extraction, Copper(II) ions, Water samples, flame atomic absorption spectrophotometry

INTRODUCTION

Copper (Cu) are extensively used in industry field such as electroplating, manufacture of electrical wire and industrial machinery since it has good resistance to corrosion, low thermal expansion and tensile strength. As well as for industry uses, Cu also has been recognized as an essential trace metal for living organisms and important for human`s growth and development. However, the amount of consumption has to be limit to 1–3 mg per day as an adequate and safe level of intake (Ndlovu et al., 2012) since it will affect human`s health and causing several disease if excessive. According to Guidelines for Drinking-water quality of the World Health Organisation, the limit for copper content in drinking water is 2.0 mg/L (Jana et al., 2011). Above this healthy limit, copper will accumulates in the liver and become toxic to human which causing diarrhoea, vomiting and neurological illness such as schizophrenia, depression, autism and epilepsy (Shrivas & Kumar, 2013). Since Cu has been widely used in industry and household plumbing, it will easily enter the environmental and water systems in a form of ion causing high exposure of people to Cu(II) ion residue by drinking water. Thus, method to remove Cu(II) ion from water supplies need to be developed to ensure the concentration is below the safety limit.

A simple, efficient and green sample preparation technique is required to replace conventional extraction techniques. In recent years, an alternative solvent minimization sample preparation approach, magnetic solid phase extraction (MSPE), has gained considerable attention. The advantages of the MSPE method are that this procedure is simpler and faster than LLE and SPE by the use of only an external magnetic force to isolate the adsorbent and analyte/s from sample matrix. Besides that, MSPE technique only requires small amount of organic solvent. With the advantages of MSPE, the development of modified Fe_3O_4 MNPs has to be developed and progress rapidly in order to improve the adsorption quality of the adsorbent and obtain the most efficient extraction results.

Alginates are natural anionic polysaccharide of brown algae which is composed of linear binary copolymers of (1-4)-linked β-D-mannuronic acid (M) and α-L-guluronic acid (G) monomers (Figure 1) (Draget et al., 2005). Due to high stiffness of gelling properties (Fuhrer & McHugh, 2003), high porosity and small size providing larger surface area (Paques et al., 2014), alginate has been applied as the adsorbent which encapsulate the Fe_3O_4 MNPs during the extraction of analyte. The polymer also consist of many carboxyl and hydroxyl groups which acts as potential adsorption sites for metal ions to bind (Draget et al., 2005).

In this study, a green MSPE analytical method was introduced by utilizing ferrite-calcium alginate (Fe_3O_4-Ca Alg) as the adsorbent. Calcium alginate (CaAlg) has the potential to be an effective adsorbent while MSPE is a simple and fast technique that contributes to minimize the time consuming, and use of organic solvent.

Thus, we consider this Fe_3O_4-CaAlg MSPE approach as it is effective and gives higher relative recoveries of Cu(II) ion.
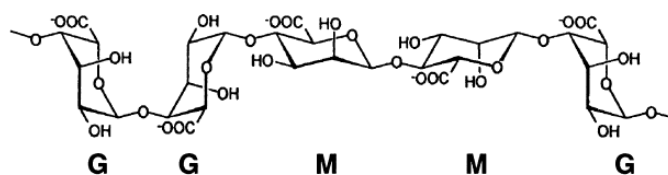

Figure 1: Chain conformation of (1-4)-linked β-D-mannuronic acid (M) and α-L-guluronic acid (G) polymer (Draget et al., 2005)

EXPERIMENTAL

Chemicals and Reagents

Water samples used were tap and river water from Sungai Skudai, Skudai, Johor. The glassware used in this project was washed with deionized water (DW) and have been sterilized. The Fe_3O_4-CaAlg adsorbent was obtained (previously synthesised) from the analytical laboratory in Universiti Teknologi Malaysia, Johor. Deionized water was used all the time when preparing stock and standard solution. Cu stock solution (1000 mg/L) was prepared from $CuSO_4$ obtained from analytical laboratory in Universiti Teknologi Malaysia, Johor. Then, Cu standard solution of 1, 2, 3, 4, and 5 mg/L were prepared from the stock solution. The desorption solvents used were nitric acid (HNO_3), hydrochloric acid (HCl) and sulphuric acid (H_2SO_4). Nitric acid, 65% was purchased from QRec (Asia) Sdn Bhd (Selangor, Malaysia), hydrochloric acid 36.5-38.0% was purchased from J.T. Baker (Philipsburg, USA) and sulphuric acid 95-97% was obtained from Merck (Darmstadt, Germany). All desorption solvents namely 0.1 M of each of HNO_3, HCl, H_2SO_4 and 1:1 mixture of HCl + HNO_3 were prepared by appropriate dilution of the concentrated solution.

Analytical Instrumentation

A PinA Acle 900T FAAS equipped with deuterium background correction and a copper hollow cathode lamp was used for absorbance measurements at 324.75 nm. All measurements were carried out in an air/acetylene flame. Instrumental parameters used were those recommended by the manufacturer.

Preparation of stock, standard solutions and real water samples

The Cu stock solution (1000 mg/L) was prepared by dissolving 0.25 g of copper sulphate ($CuSO_4$) in DW. The solution was made up to the 100 mL mark in a volumetric flask. Then, a series of standard solutions (1.0, 2.0, 3.0, 4.0, 5.0) mg/L were prepared by appropriate dilution of the stock solution. River water sample and fresh tap water sample were collected in bottles pre-cleaned with acetone. For the river water samples, the samples were filtered through a Whatman filter paper No. 1 (Maidstone, England) to remove any non-soluble particles. The samples were stored in freezer at 5ºC until analysis.

Preparation of Fe_3O_4-CaAlg Adsorbent

An amount of 4.5 g of sodium alginate was accurately weighed and dissolved in 200 mL deionized water with magnetic stirring. A calcium chloride solution was prepared by mixing 33 g of the salt with 1.5 L of DW, with magnetic stirring. For encapsulation process to form Fe_3O_4-CaAlg adsorbent, 4.0 g of the Fe_3O_4 MNPs were mixed with sodium alginate solution forming Fe_3O_4-NaAlg solution. Then the Fe_3O_4-NaAlg solution was slowly dropped into the calcium chloride solution. Fe_3O_4-CaAlg beads were formed immediately in the calcium chloride solution. Lastly, the Fe_3O_4-CaAlg beads were thoroughly rinsed with distilled and deionized water to eliminate any residues of calcium and chloride ions. Fe_3O_4-CaAlg beads were placed in the oven for 12 h to dry the water residue.

Fe_3O_4-CaAlg Magnetic Solid Phase Extraction Process and Optimization

The MSPE process is illustrated schematically in Figure 2. Briefly, 10 mL of water sample containing 1 mg/L of Cu(II) analyte from the prepared stock solution was added with 50 mg of Fe_3O_4-CaAlg adsorbent. Initially,

the mixture was shakened for 30 min to allow adsorption process of Cu(II) ion onto the Fe_3O_4-CaAlg adsorbent. The adsorbent was then collected easily and quickly by applying an external magnet on the beaker wall, and the supernatant was decanted directly. For desorption of Cu(II) ion from the Fe_3O_4-CaAlg adsorbent, 3 mL of approximately 0.1 M solution of the desorption solvent was added into the beaker containing the adsorbent, and agitated for about 5 min. The adsorbent was then collected with an external magnet outside and the eluent was collected eluent for analysis using FAAS.
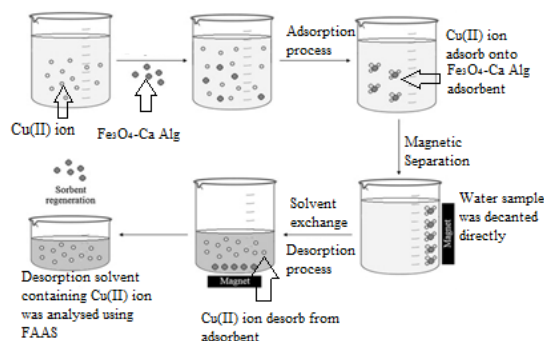
Figure 2: Schematic of Fe_3O_4-CaAlg MSPE process for Cu(II) ions from aqueous solution

In this study, three extraction and three desorption conditions were systematically optimized. Optimization of MSPE process was performed by varying one parameter at a time. The extraction parameters optimized were extraction time, weight of adsorbent and volume of sample while the desorption parameters optimized were types of desorption solvent, volume of desorption solvent and agitation time. Initally

RESULTS AND DISCUSSIONS

Effect of Desorption Solvent

In order to maximize the desorption of Cu(II) ion from Fe_3O_4-CaAlg adsorbent, a suitable solvent is required. Four different solvents namely 0.1 M HNO_3, 0.1 M HCl, 0.1 M H_2SO_4 and 0.1 M of a 1:1 mixture of HNO_3: HCl were used. During desorption of the Cu(II) ions, hydrogen ions were dissolved from the acid desorption solvent used and displaced the Cu(II) ions on the adsorbent. It was found that all the solvents examined showed almost equal desorption efficiency with recovery of Cu(II) ion in the range of 57.6%-61.6% but the highest percentage recovery was obtained with 1:1 mixture of HNO_3: HCl as the desorption solvent (Figure 3). Thus 1: 1 mixture of HNO_3: HCl was selected for further analysis.
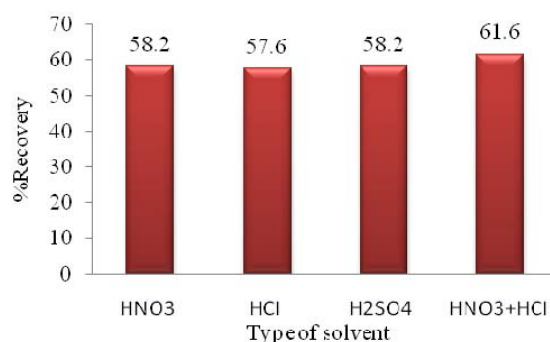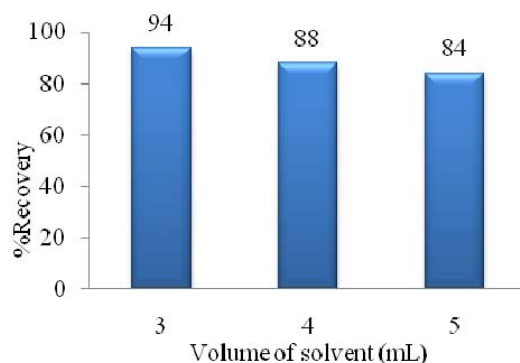

Figure 3: Effect of types of desorption solvent on Fe_3O_4-CaAlg MSPE of Cu(II) ion from water sample. Extraction conditions: 10 mL volume sample; 50 mg adsorbent weight; 30 min extraction time; Desorption conditions: 3 mL solvent volume with 5 min agitation time.

Effect of desorption solvent volume

In order to study the effect of desorption solvent on the recovery of Cu(II) ion, different volumes of the 1:1 HNO_3-HCl desorption solvent were optimized. This is to ensure quantitative recovery with minimum volume of

desorption solvent. Thus, the 0.1 M 1:1 mixture of HNO_3+HCl solvent was set (3, 4 and 5 mL). Figure 4 shows that the percentage recovery of Cu(II) decreases as the desorption solvent increases from 3 to 5 mL. Desorption of Cu(II) ion from the Fe_3O_4-CaAlg adsorbent was most effectively achieved using 3 mL of the optimized solvent. This indicates that 3 mL of the desorption solvent was sufficient to desorb adsorbed Cu(II) ions from the adsorbent. Thus, 3 mL of the 1:1 mixture of HNO_3+HCl solvent was selected for further analysis.

Figure 4: Effect of desorption solvent volume on Fe_3O_4-CaAlg MSPE of Cu(II) ion from water sample. Extraction conditions: 10 mL volume of sample; 50 mg mass of adsorbent; 30 min extraction time; Desorption conditions: 1:1 mixture of HNO_3+HCl desorption solvent with 5 min agitation time

Effect of extraction time

Generally, sufficient time is required to achieve adsorption equilibrium for the analyte on the adsorbent. In this study, the effect of extraction time on the extraction efficiency of Cu(II) ion on Fe_3O_4-Ca Alg adsorbent was investigated by changing the extraction time from 1 to 60 min under the optimum conditions. Five sample solutions were continuously shakened using an orbital shaker at room temperature at 250 rpm. From the results obtained (Figure 5), it can be seen that equilibrium was reached within 5 min extraction time by showing recovery 104.5%. Decrease of percentage recovery was observed starting from 10 to 60 min extraction time. This might due to back-extraction of Cu(II) ion from Fe_3O_4-CaAlg adsorbent into sample solution since ion exchange between cation group of adsorbent and Cu(II) ion in the water sample is reversible and the bond formed is just temporary (Wierucka & Biziuk, 2014). Thus, 5 min was selected for further analysis.
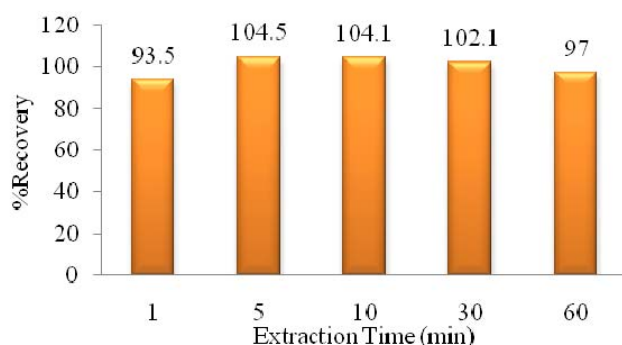

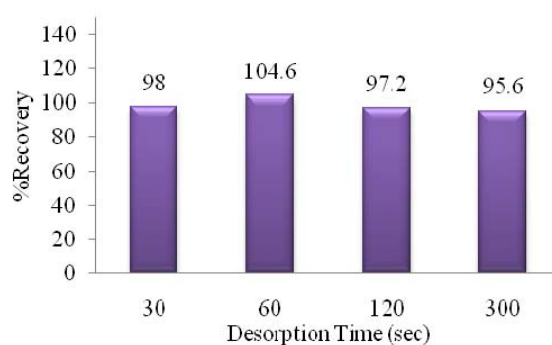**Figure 5:** Effect of extraction time on Fe_3O_4-CaAlg MSPE of Cu(II) ion from water sample. Extraction conditions: 10 mL volume of sample; 50 mg mass of adsorbent; Desorption conditions: 3 mL of 1:1 mixture of HNO_3+HCl desorption solvent with 5 min agitation time
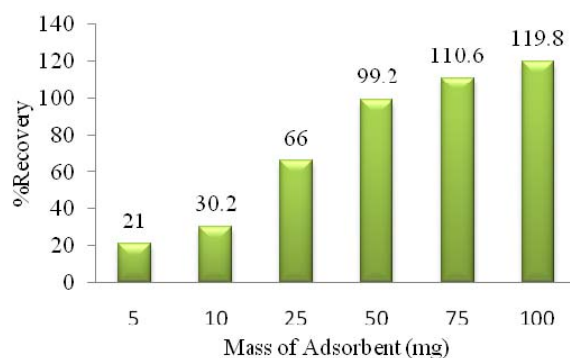
Effect of agitation time

In order to examine the influence of desorption time on the recovery of Cu(II) ions, different desorption time in the range of 30 to 300 s were optimized to ensure quantitative recovery of Cu(II) ions. The percentage recovery of Cu(II) ions increase as the desorption time increase from 30 s to 60 s but slightly decrease was observed at 120 s and 300 s. This might due to re-adsorbed of analyte by the adsorbent (Figure 6).Therefore, desorption time of 60 s was selected for further analysis for maximum desorption of analyte from adsorbent.

Effect of weight of adsorbent

Various weight (5 to 100 mg) of the Fe_3O_4-CaAlg adsorbent were used to study its effect on adsorption of Cu(II) ions. Based on the results obtained (Figure 7), increase in weight of adsorbent increase the extraction efficiency probably due to more adsorption sites or surface area available for Cu(II) ions to be adsorbed. However, a further increase in the weight of adsorbent higher than 50 mg did not cause significant improvement in the adsorption of Cu(II) ions. This might due to the adsorption of Cu(II) ions onto the adsorbent was completed (Paques et al., 2014). Thus, higher weight of adsorbent was not necessary to reduce analysis cost. Thus, 50 mg adsorbent was used for further analysis.

Figure 6: Effect of desorption time on Fe_3O_4-CaAlg MSPE of Cu(II) ion from water sample. Extraction conditions: 10 mL volume of sample; 50 mg mass of adsorbent; 5 min extraction time; Desorption conditions: 3 mL of 1:1 mixture of HNO_3+HCI desorption solvent

Figure 7: Effect of weight of Fe_3O_4-CaAlg adsorbent on MSPE of Cu(II) ions from water sample. Extraction conditions: 10 mL sample volume; 5 min extraction time; Desorption conditions: 3 mL of 1:1 mixture of HNO_3+HCI desorption solvent with 1 min agitation time

Effect of sample volume

In order to study the ability of the optimized weight of adsorbent in adsorbing Cu(II) ions different sample volumes were optimized. A series of 150 - 400 mL sample solutions containing 20 µg/L of Cu(II) ions were prepared. Based on the results obtained, 50 mg of adsorbent was found to sufficient to adsorb the highest Cu(II) ions from 150 mL sample (Figure 8). Increase in the sample volume was found to decrease the % recovery. This might due to breakthrough volume of adsorbent which have been exceeded. Thus, 150 mL sample volume was selected for further analysis.

Method Validation

The Fe_3O_4-CaAlg MSPE method was validated using the optimized conditions (50 mg adsorbent, 150 mL sample volume, 5 min extraction time, 3 mL of 1:1 mixture of HNO_3+HCI as desorption solvent with 1 min agitation time) for linearity, limit of detection (LOD), limit of quantification (LOQ), precision (repeatability and reproducibility) and accuracy (recovery). The results obtained are summarized in Table 1. Acceptable linearity from the linearity range of 20-100 µg/L was obtained with good coefficient of determination ($R^2 = 0.974$). LOD (3 S/N) and LOQ (10 S/N) obtained were 1.70 µg/L and 5.6 µg/L respectively. The precision studies were

performed for one day ($n = 3$) and for three consecutive days ($n = 9$). Concentration of Cu(II) ion used was 100 µg/L. Satisfactory RSDs were obtained; 2.37% for repeatability and 5.15% for reproducibility showing good precision of the Fe_3O_4-CaAlg MSPE method.
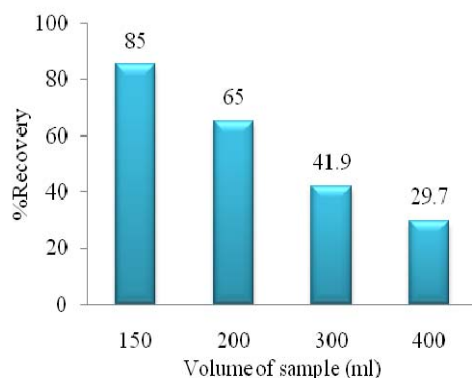

Figure 8: Effect of sample volume on % recovery of Cu(II) ions from water sample using Fe_3O_4-CaAlg MSPE. Extraction conditions: 50 mg adsorbent; 5 min extraction time; Desorption conditions: 3 mL of 1:1 mixture of HNO_3+HCl desorption solvent with 1 min agitation time

Table 1: Validation of Fe_3O_4-Ca Alg MSPE for Cu(II) ion

Linear range (µg/L)	R^2	LOD (µg/L)	LOQ (µg/L)	Repeatability (± %RSD, $n = 3$)	Reproducibility (± %RSD, $n = 9$)
20-100	0.974	1.70	5.6	2.37	5.15

Application of the developed Fe_3O_4-Ca Alg MSPE for Cu(II) ions from Tap and River Water Samples

In order to investigate the practicality of the proposed Fe_3O_4-CaAlg MSPE method, it was applied to the analysis of Cu(II) ions in tap and Sungai Skudai water samples. For tap water sample, the concentration of Cu(II) ion was found to be 11.84 µg/L while for river water sample, the concentration of Cu(II) ion found was 7.2 µg/L. Relative recovery studies were conducted by spiking tap water and river water samples to give a final concentration of 20 µg/L. Results showed that the relative recovery of tap water sample was 78.9% and for river water sample, 45.7% with RSDs < 4.72% ($n = 3$) for both (Table 2). The lower recovery of Cu(II) ions from the river water might be due to some external factor which affects the adsorption process such as the existence of cationic components in the river water sample as interferences. These components might compete with Cu(II) ions for the available adsorption sites thus decrease the extraction efficiency of Cu(II) ions (Paques et al., 2014). The alginate also may not be selective enough to adsorb Cu(II) ions in the complex sample. Besides, the pH of the river water sample should be taking into consideration as it may affect the extraction efficiency of metal ions. More acidic water sample contained more hydrogen ion which might also compete with the Cu(II) ion to adsorb onto the adsorbent.

Table 2: Relative recovery studies of Cu(II) ions from spiked tap and river water samples using the developed Fe_3O_4-CaAlg MSPE method

Sample	Spiked level (µg/L)	Concentration of Cu((II) ions found (µg/L)	% Relative Recovery (± % RSD, $n = 3$)
Tap Water	0	11.84	-
	20	15.78	78.9 (4.72)
River Water	0	7.20	-
	20	9.14	45.7 (1.76)

CONCLUSION

The synthesised Fe_3O_4-CaAlg was successfully used as an adsorbent for Cu(II) ions using the developed MSPE technique. Acceptable linearity from the linearity range of 20-100 µg/L was obtained with good coefficient of determination ($R^2 = 0.974$). LOD of 1.70 µg/L and LOQ of 5.76 µg/L was obtained for Cu(II) ions. Good precision was obtained for the developed method (2.37% RSD ($n = 3$) and 5.15% RSD ($n = 9$)) The developed Fe_3O_4-CaAlg MSPE method was successfully applied to the analysis of tap water sample with good relative recoveries (78.9%) and RSD (4.72%) but lower relative recovery (45.7%, RSD 1.76%) for Cu(II) ions from river water which might due to several external factors which affect the extraction efficiency. This shows that the developed MSPE method is sensitive to sample matrix. Further studies on parameters affecting recovery of Cu(II) ions such as pH of sample should be performed.

REFERENCES

Bruce Fuhrer, A., & Dennis McHugh, B. J. (2003). *Cover photograph: Durvillaea potatorum on wave-swept rocks food and agriculture organization of the united nations*.

Draget, K. I., Smidsrùd, P. O., & Skjåk-brñk, P. G. (2005). Alginates from Algae, 1–30.

Jana, Š., Andruch, V., Balogh, I. S., Kocúrová, L., Nagy, L., & Baze, Y. (2011). A novel , environmentally friendly dispersive liquid – liquid microextraction procedure for the determination of copper, *99*, 40–45.

Ndlovu, T., Arotiba, O. a., Sampath, S., Krause, R. W., & Mamba, B. B. (2012). Electroanalysis of copper as a heavy metal pollutant in water using cobalt oxide modified exfoliated graphite electrode. *Physics and Chemistry of the Earth, Parts A/B/C*, *50-52*, 127–131.

Paques, J. P., van der Linden, E., van Rijn, C. J. M., & Sagis, L. M. C. (2014). Preparation methods of alginate nanoparticles. *Advances in Colloid and Interface Science*, *209*, 163–71.

Shrivas, K., & Kumar, N. (2013). Dispersive liquid – liquid microextraction for the determination of copper in cereals and vegetable food samples using flame atomic absorption spectrometry. *Food Chemistry*, *141*(**3**), 2263–2268.

Wierucka, M., & Biziuk, M. (2014). Trends in Analytical Chemistry Application of magnetic nanoparticles for magnetic solid-phase extraction in preparing biological , environmental and food samples. *Trends in Analytical Chemistry*, *59*, 50–58.

KINETIC STUDY OF BIODIESEL USING EGG SHELL FOR BASE TRANSESTERIFICATION REACTION

Fatin Madihah binti Mamat and Abd Rahim Yacob

Department of Chemistry, Faculty of Science, Universiti Teknologi Malaysia, 81310 Johor Bahru

Abstract

The accumulative oil demands have produced a renewed interest in alternative fuels of biological origin. Alternative fuels, such as biodiesel has been focused unanimously because of current energy crisis. In this study, kinetics of heterogeneous transesterification of waste cooking oil (WCO) with prepared CaO-800 from the calcination of egg shell was discovered. Firstly, the egg shells were calcined at temperature of 800°C and 900°C. Then the catalysts were characterized using Thermal Gravimetry Analysis (TGA), Fourier Transformed Infrared (FTIR), Nitrogen Adsorption Analysis, Field Emission Scanning Electron Microscope (FESEM), and X-ray Powder Diffraction (XRD). The soluble basicity and the basic strength of the prepared catalysts were determined using back titration. The results showed that calcined egg shell at 800 °C was the most suitable catalyst to use in the biodiesel producton as it had high basicity and high surface area compared to calcined egg shell at 900 °C. The product biodiesel prepared was then analyzed using Gas Chromatography- Flame Ionization Detector (GC-FID). The kinetic studies for the reaction was carried out at reaction time of 30, 60, 90, 120, 150 and 180 mins at temperature 45°C, 55°C, 65°C, 75°C and 85°C temperature respectively. The results showed that the reaction follows the zero order reaction, has the rate constant of 0.13 s^{-1} and the activation energy is 23.2 kJ/mol.

Keywords:calcined egg shell, transesterification of waste cooking oil, biodiesel, kinetic study

INTRODUCTION

Biodiesel, long-chain fatty acid alkyl ester is one of the interesting alternative fuels which can be produced from renewable sources and provides complete combustion with less gaseous pollutant emission [1] The heterogeneous catalysts of alkaline earth metal oxides heteropolyacids and zeolites have been investigated for biodiesel production as they could be operated in continuous processes, could give high quality of products; they are reusable, environmentally and are more effective than acid catalysts and enzymes. Among these, alkaline earth metal oxides, and in particular CaO, have been shown to possess good performance of commercial significance for a wide spectrum of environmentally important reactions.

The biodiesel that were produced can be a renewable alternative to petroleum diesel and by using egg shell as catalyst we can reduce the production costs of biodiesel. Reuse of eggshell as catalyst for biodiesel production was investigated in the viewpoint of the recycle of eggshell waste, minimization of contaminants, reducing the production costs of biodiesel and making the process to produce biodiesel fully ecologically friendly.

Reaction kinetics is essential for reactor and process analysis, design, simulation and control. The previous research of the kinetic study for the transesterification of oil has been carried out for the alkali catalyzed reaction so this study will be carried out for based catalysed reaction.

EXPERIMENTAL

Materials

The chemical reagents used in this research were waste cooking oil, methanol, calcium oxide (CaO). The apparatus used are two-necked round bottom flask, measuring cylinder, hot plate stirrer, mortar and pastel, magnetic stirrer, thermometer, beaker, and retort stand.

Preparationof Egg Shell as Catalyst

The catalyst was prepared by the calcination of egg shell in electric furnace from temperature 800 °C to 900 °C. Firstly, the chicken egg shells were collected from cafeteria and washed with distilled water while the inner content of the egg shell were cleaned. The egg shells were washed again with distilled water, and dried using oven. The egg shells were crushed by using mortar and pastel until become powder and were calcined in an electric furnace from 800°C to 900 °C in 4 h.

Characterizations of Catalyst

The characterization of calcined egg shell has been carried out by using Thermogravimetric Analyzer (TGA), Fourier Transform Infrared (FTIR), X-Ray Diffraction (XRD), Field Emission Scanning Electron Microscopy (FESEM), Energy Dispersive X-Ray Spectroscopy (EDX), and N2 Adsorption)

Base Heterogeneous Transesterification and Characterization of Biodesel

A two-necked round bottom flask with a thermometer, a reflux condenser and magnetic stirrer were set up. A mixture containing of 0.1g prepared catalyst and 18.55g of purify methanol were heated 30 minutes with the temperature fixed at 65±5 °C and 20g of waste cooking oil was added into the round bottom flask. The biodiesel was distilled with temperature fixed at 65±5 °C to remove remaining impurities after cooled at room temperature. Then the mixture was centrifuged at 3000rpm for 10 minutes. The middle layer was extracted as biodiesel and was analyzed by using GC. The graphs of rate of reactions of biodiesel were plotted and the order of reaction was determined.

Characterization of biodiesel

The biodiesel that produced were characterized using Gas Chromatography - Flame Ionization Detector (GC-FID).The transesterification reaction for biodiesel production was recorded using a Hewlett Packed Gas Chromatography model 6890. The mobile phase used was helium gas and column DB-Wax with specification 0.25 μm thickness, 30 mm length and 0.20 mm internal diameter was used as stationary phase with Flame Ionization Detector (FID). Temperature conditions which applied in this research were oven temperature was set at initial value 40ºC and hold for 3 min, increase to 195ºC with the rate 25ºC/min , subsequently the temperature rise up to 205ºC with the rate 3ºC/min and finally the temperature goes to 230ºC with rate 8ºC/min. For each temperature points, 5 min holding times was selected in order to complete the separation for each temperature settings. 10 mg heptanes in hexane was prepared, and 1mL of this solution was added into 50 mg of sample. Then, 1 mL of this mixture was injected into GC.

The Kinetic Study

The kinetic study has been investigated to determine the order of reaction of the biodiesel by varied the temperature and time. The temperature and time were varied during the reflux process. The temperatures selected were at 45°C, 55°C, 65°C, 75 °C and 85°C while the time taken were 30 min, 60 min, 90 min, 120 min and 150 min.The graphs of rate of reactions of biodiesel were plotted using the percentage of conversion from the GC-FID results and the order of reaction was determined.

RESULTS AND DISCUSSION

In this study, biodiesel has successfully synthesized using the prepared calcined egg shell as catalyst and the order of reaction will be identified

Characterization of Catalyst

The characterization of calcined egg shell has been carried out by using Thermogravimetric Analyzer (TGA), Fourier Transform Infrared (FTIR), X-Ray Diffraction (XRD), Field Emission Scanning Electron Microscopy (FESEM), Energy Dispersive X-Ray Spectroscopy (EDX), and N2 Adsorption

Thermal Gravimetry Analysis (TGA)

Figure 3.1 and 3.2 show the thermogram of egg shell and the Percentage of weight lost with different temperature regions. A few minor increasing of percentage of weight loss at temperature range of 0 to 250 °C was due to the removal of adsorbed water at the surface of egg shell sample. The major weight loss occurred at temperature range of 500 to 750°C with value of 10.2% was due to the removal of organic from the egg shell sample. Other related report indicated that the suitable temperature for the transformation of egg shell was in the range of 800 to 1000 °C .Therefore, in this study, it is expected that the complete transformation of egg shell occurs at temperature above 750 °C.
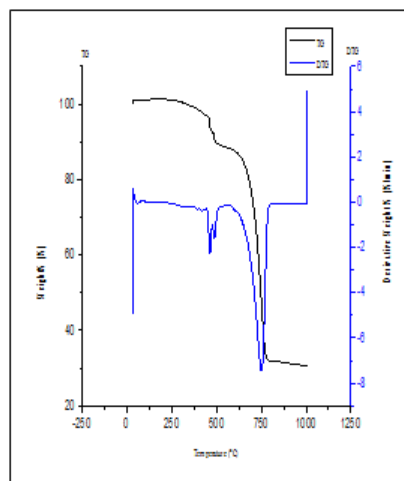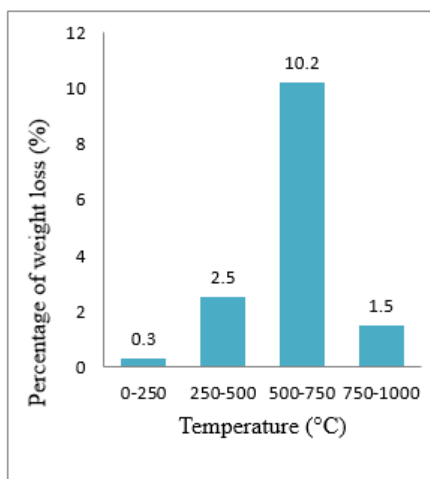
Figure 31: Thermogram of Egg Shell

Figure 3.2: Percentage of weight lost with different temperature regions

Fourier Transform Infrared (FTIR)

Figure 3.3 and Table 1 show FTIR spectra of prepared a) CaO-800 and b) CaO-900 and summarization of peak assignment for (a) Ca-800 and (b) CaO-900. The egg shell starts to lose carbonate and produce CaO and carbon dioxide gas during calcination. The intensities of the peaks decrease related to CO_3^{2-} molecules (613 cm^{-1}, 950 cm^{-1} and 1500 cm^{-1}) was observed expect for CaO-800. This phenomenon occurred due to the reduction of the reduced mass of related functional group of CO_3^{2-} molecules. For CaO-800, the intense peaks appear at the wavelength of 950 cm^{-1} and 1500 cm^{-1} (C–O vibration) indicates that the majority compound present in the sample is $CaCO_3$ which may due to incomplete removal of CO_3^{2-} molecules. For CaO-900, the weak peaks for vibration modes of mono and bidentate carbonate shows that the sample contains impurities $CaCO_3$ with the reason of incomplete transformation. On the other hand, CaO-900 may contain higher purity of CaO due to less intense peaks for C–O vibration than CaO-800.
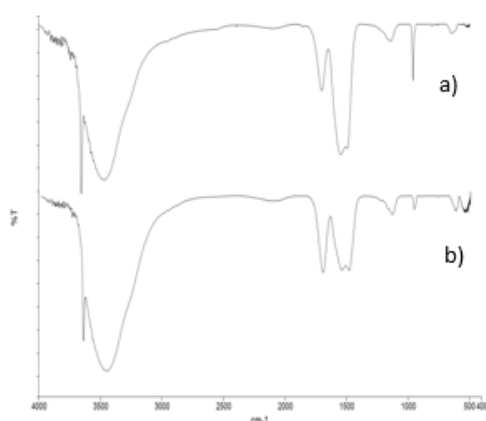

Figure 3.3: FTIR spectra of prepared a)CaO-800 and b) CaO-900

Wavelength (cm^{-1})	Peak Assignment
3640	O-H stretching vibration
3500	O-H stretching vibration
1650	O-H bending vibration
950 and 1500	C-O vibration modes
613	Lattice vibration $CaCO_3$
550	Ca-O symmetric vibration

Table1: Summarization of peak assignment for (a) Ca-800 and (b) CaO-900

X-Ray Diffraction (XRD) Analysis

Figure 3.4 shows that for CaO-900, diffraction reflections characteristics of calcite calcium carbonate, $CaCO_3$ was observed at 2θ= 32.25˚ while the peaks appear at 37.41˚, 53.91˚, 67.43˚ which displays diffraction reflections characteristics of portlandite calcium hydroxide, $Ca(OH)_2$. The prepared catalyst calcined at 800 °C,

135

contains $CaCO_3$ as major component and $Ca(OH)_2$ as minor component since the intensities of the peak of $CaCO_3$ at 32.21˚ is higher than the intensities of the peak of $Ca(OH)_2$ at 28.62˚. In contrast, the major component of prepared catalyst calcined at 800 °C, CaO-800 was $Ca(OH)_2$ while the minor component was $CaCO_3$.
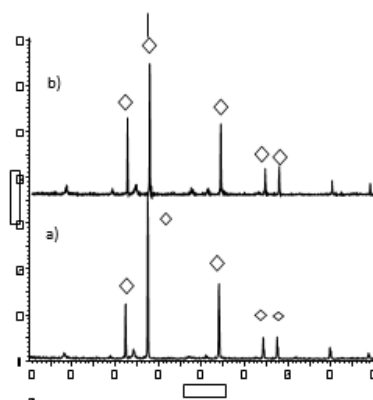

Figure 3.4: XRD Spectra of prepared a)CaO-800 and b)CaO-900

Nitrogen Gas Adsorption

As shown in Figure 3.5, an increase in specific BET surface area after calcination of egg shell (formation of CaO 800 and CaO-900) were observed where the BET surface area of CaO-800 was found to be 15.67 m2/g while the BET surface area of CaO-900 was found to be 14.96 m2/g. This phenomenon may cause the appearance of defect sites on the surface of CaO-900 due to the decomposition of egg shell to CaO at the temperature of 900 °C. This surface defects lead to an increase in catalytic activity of the reaction as the surface area of catalyst had been increased.

As CaO-800 with highest basicity and higher BET surface area had the most probably to exhibit higher catalytic activity for transesterification of waste cooking oil oil to produce biodiesel compared with CaO-900. This assumption is supported by basicity study and FESEM micrograph of the catalyst.
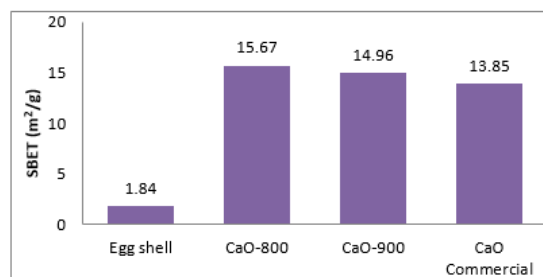

Figure 3.5: The specific SBET surface area of egg shell, CaO-800, CaO-900 and CaO commercial

Field Emission Scanning Electron Microscopy (FESEM)

Figure 3.7 and 3.8 demonstrate the surface morphology of CaO-800 and CaO-900 with magnification of 2.5 kX. From this study, CaO-800 comprises irregular shape of particles with various sizes due to the agglomeration of particles with each other. The surface of CaO-900 was not smooth. In addition, some wave-like surface and cracks on the surface which were not found over commercial CaO could possibly improve the surface area of CaO-900

Energy Dispersive X-Ray Spectroscopy (EDX)

From Figure 3.9, the prepared CaO-800 consists of major element which is calcium 72.67 % and oxygen which are 24.98 % respectively and some impurity elements were found such as Mg and C maybe because carbon

element had not completely removed from the sample by emission of carbon dioxide gas during calcination process while in figure 3.10 the prepared CaO-900 consists of major element which is calcium 54.74 % and oxygen which are 40.52 % respectively The percentage of major element, calcium in CaO-900 is less compared to percentage of calcium in CaO-800 that was 72.67 %. That was the reason why CaO-800 was chosen as the catalyst in the transesterification of waste cooking oil.
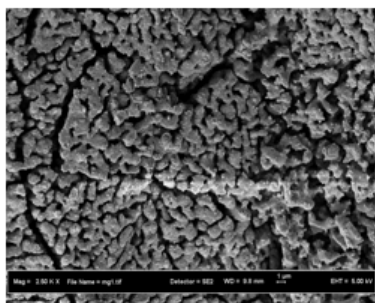

Figure 3.7: FESEM micrograph of CaO-800 with magnification of 2.5 kX
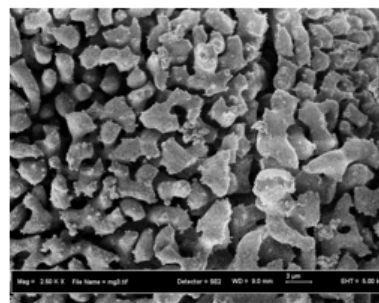
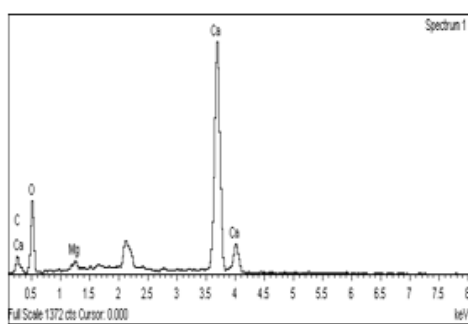**Figure 3.8**: FESEM micrograph of CaO-900 with magnification of 2.5 kX
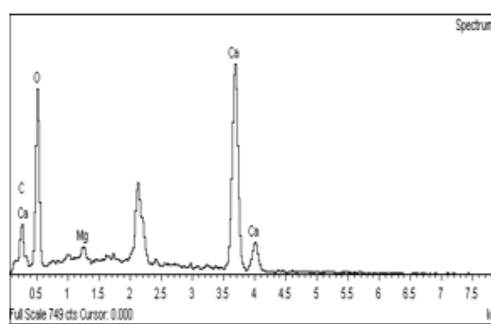

Figure 3.9: EDX Spectrum of CaO-800

Figure 3.10: EDX Spectrum of CaO-900

Characterization of Biodiesel

The biodiesel, which is fatty acid methyl esters (FAMEs), was analyzed by GC-FID in order to investigate the percentage conversion. Figure 3.11 shows an increase trend in percentage conversion of biodiesel as the reaction time increased. For 30, 60, 90, 120 and 150 minutes of reaction time, the percentage conversion of biodiesel were 67%, 75%, 78%, 82% and 83% respectively. It can be observed that as the reaction time increased, the percentage conversion or biodiesel yield also increased. It showed that the reaction time affect the yield of FAME while Figure 3.12 shows the increasing of percentage conversion of biodiesel when the temperature were increased. For temperature 45°C, 55°C, 65°C, 75 °C and 85°C, the percentage conversion were 36%, 47%, 81%, 83% and 85% correspondingly. When the reaction was carried out at 65°C, which is above the boiling point of methanol, the solvent vaporized and remained in the vapor phase in the reactor causing a reduction in the methanol in the reaction media.
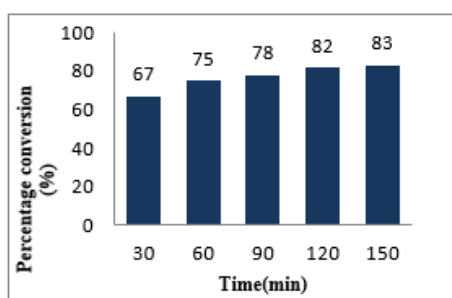

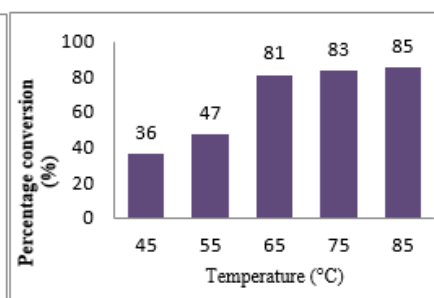**Figure 3.11**: Percentage conversion of palm oil to biodiesel vs reaction time

Figure 3.12: Percentage conversion of palm oil to biodiesel vs reaction temperature

The Rate of Reaction

Figure 3.13 shows the three graph of rate of reaction of (a) zero order (b) first order and (c) second order. R^2 obtained were 0.9163, 0.8946 and 0.7206 respectively. The R^2 of zero order was chosen as it was the highest R^2 and the rate constant was 0.13. The zero order signpost that rate of reaction apparently independent of the reactant concentration. The graph of ln K vs 1/T in Figure 3.14 below was plotted to determine the value of activation energy, Ea.
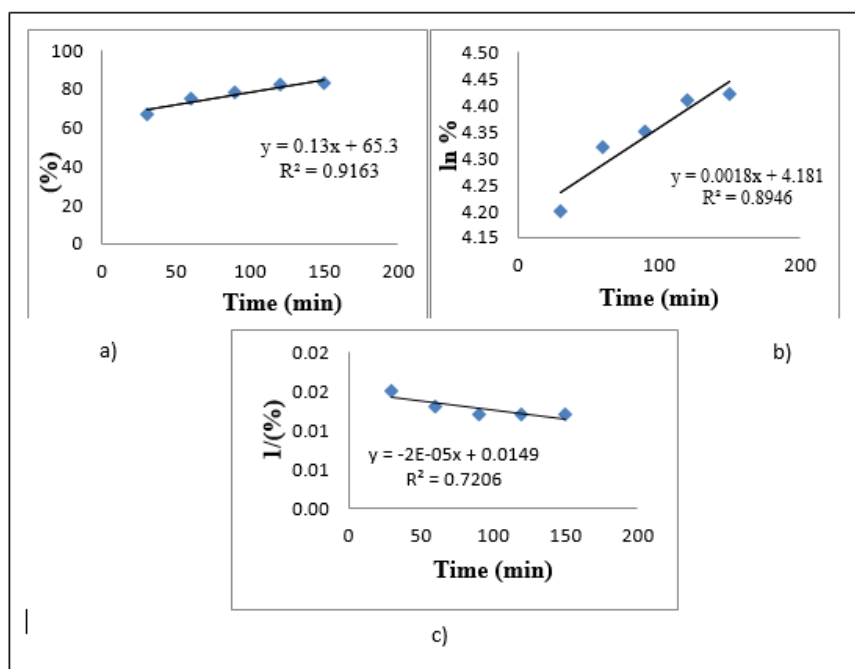

Figure 3.13: The rate of reaction of (a) Zero order (b) First order and (c) Second order

In Figure 3.14: Arrhenius plot for the calculated rate constants at thetemperature of 45°C, 55°C, 65°C, 75 °C and 85°C are presented. The slope define activation energy as a function of the reaction progress. The activation energy obtained was 23.2 kJ/mol. The activation energy which fall below the range of activation energy (26-82 kJ/mol) for heterogeneous transesterification reaction indicates that the reaction is not kinetic controlled
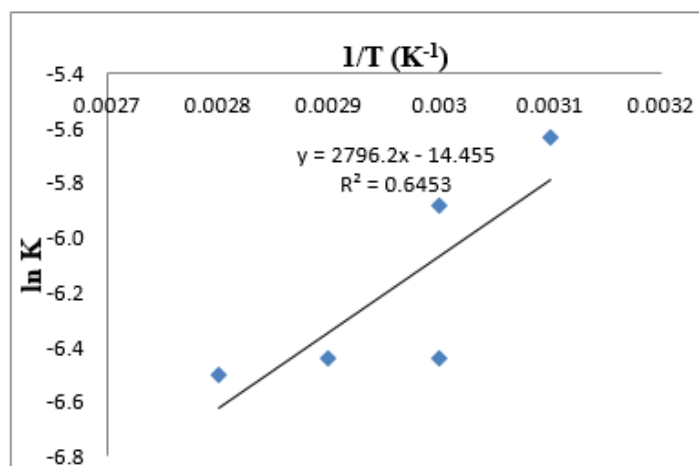

Figure 3.14 : Arrhenius law graph of zero order

CONCLUSION

In this study, calcium oxide that has been successfully prepared from the calcination process of egg shell at 800°C used to synthesize biodiesel. The kinetic reaction of transesterification reaction has been studied and the order of reaction has identified. The kinetic data used to optimize the process of biodiesel synthesis. From the high reaction rate obtained, the process proceeds via zero order and the activation energy obtained was 23.2 kJ/mol.

REFERENCES

1. N. Viriya-empikul a, P. Krasae b, W. Nualpaeng a, B. Yoosuk b, K. Faungnawakij. (2012). Biodiesel production over Ca-based solid catalysts derived from industrial wastes. *Fuel*, 239–244.
2. N. Viriya-empikul a, P. Krasae b, B. Puttasawat b, B. Yoosuk b, N. Chollacoop b, K. Faungnawakij a,*. (2009). Waste shells of mollusk and egg as biodiesel production catalysts. *Biosource Technology*, 3765-3768
3. Ziku Wei a,b, Chunli Xu a,b,*, Baoxin Li c. (2009). Application of waste eggshell as low-cost solid catalyst for biodiesel production. *Biosource Technology 100*, 2883–2885.
4. Kawashima, A. Matsubara, K. & Honda, K. (2008). Development of heterogeneous base catalysts for biodiesel production. Bioresource Technol**., 99**, 3439–3443.

ESSENTIAL OIL OF *PIPER BETLE* AND DERIVATIVES OF EUGENOL

Rafidah Binti Husain and Farediah Binti Ahmad
Department of Chemistry, Faculty of Science, Universiti Teknologi Malaysia, 81310 Johor Bahru.

Abstract

The essential oil of *Piper betl*e and the chemistry of its major compound have been investigated. The essential oil was obtained by hydrodistillation technique while the chemical compositions of the oil were determined by gas chromatography (GC), gas chromatography-mass spectrometry (GC-MS) and Kovats Indices. The yield of essential oil obtained from this plant was 0.64%. The compounds identified in the *P. betle* oil were six phenylpropanoids (40.38 %), three monoterpenes (0.15 %), and twenty one sesquiterpenes (38.95 %). Phenylpropanoids were the most dominant group in the oil of *P. betle* leaf with eugenol (32.64 %) being the main component. Eugenol was then seperated from the oil by column chromatography and analyzed spectroscopically. The synthetic eugenol was subjected to methylation and acetylation to form methyl eugenol and eugenol acetate, respectively. The oil, eugenol and its derivatives were screened for antibacterial and antioxidant activities. For the antibacterial activity, only essential oil showed positive result at concentration of 900 ppm. While for the antioxidant activity, essential oil at IC_{50} = 16.83 μg/mL and eugenol at IC_{50} = 3.03 μg/mL, proved that both samples showed positive results on antioxidant assay.

Key Words: *Piperaceae, Piper betle, eugenol, antioxidant, antibacterial*

INTRODUCTION

The Piperaceae or also known as the pepper family is a large family of flowering plants consisting of 1,920 currently accepted species in 13 genera. The vast majority of peppers can be found within the two main genera which are *Piper* and *Peperomia*. Piperaceae species have been placed among the basal angiosperm and are adapted to a variety of habitats including moist forests, secondary vegetation and dry high lands [1].This study was conducted on *P. betle* which is one of the members of Piperaceae family. *P. betle* is blessed as evergreen and perennial plant. Betle leaf has been described from ancient times as an aromatic, stimulo-carminative, astringent and aphrodisiac. The leaves are chewed with betel nut to improve the taste and to prevent halitosis [2]. The root have been used for treatment of cough, bronchial asthma, rheumatism, stomachalgia, edema of pregnancy and as contraceptive [3]. Consequently, the aim of this study was to evaluate the chemical compositions of the essential oil in the leaf and the chemistry of its major compound.

EXPERIMENTAL

Source of Sample

The sample of *P. betle* leaves were collected from Felcra Sungai Ara at Kota Tinggi. The leaves were washed and cut into small pieces.

Extraction and Analysis of Essential Oil

The fresh leaves (355 g) were placed in a round bottom flask (5 L) and covered with distilled water. The flask was equipped with a Dean Stark apparatus and water condenser and hydrodistilled for 10 hours. The mixture of oil and water in the Dean Stark was run off, extracted with Et_2O, dried over anhydrous $MgSO_4$ and filtered. The filtrate was left at room temperature for a few hours to evaporate the solvent. Evaporation of the solvent yielded *P. betle* oil (2.28 g, 0.64%) as a yellow liquid with pungent smell. The essential oil was analysed using GC chromatogram of the oil. Identification of the constituents was performed on the basis of their Kovats indices, which were calculated in relation to a standard hydrocarbon (C6-C26) and compared with those given in the literatures [4].

Isolation of Major Constituent

The essential oil (2.28 g, 0.64 %) was subjected to CC packed with SiO_2 (24.0 g). An eluent system consisted of a mixture of hexane and EtOAc of increasing polarity has afforded 135 fractions. Each fraction was monitored by TLC with hexane:EtOAc (90:10) as the developing solvent. Fractions with the same TLC

profiles were combined to give three new combined fractions. The fractions were labeled as F1 (0.047 g), F2 (0.196 g), and F3 (0.027 g). Fraction F3 was concentrated to yield eugenol **(1)** (0.027g, 1.20 %) as a yellow liquid; R_f 0.61 in (hexane:EtOAc/90:10).); IR (ATR) v_{max} cm^{-1}: 3516 (OH), 3077 (C-H sp^2), 2938 (C-H sp^3), 1638 (C=C olefinic), 1612 and 1431 (C=C aromatic), and 1264 (C-O); ^{1}H NMR δ (CDCl3): 3.39 (2H, d, *J=6.8 Hz*, H-1'), 3.91 (3H, s, OCH3), 5.18 (2H, m, H-3'), 5.85 (1H, s, OH), 6.04 (1H, m, H-2'), 6.76 (1H, dd, *J=8.4* Hz and *J=2.0* Hz, H-5), 6.94 (1H, d, *J=8.4* Hz, H-6), 6.95 (1H, d, *J=2.0* Hz, H-3); ^{13}C NMR δ (CDCl3): 39.9 (C-1'), 55.9 (OCH3), 111.1 (C-3), 114.3 (C-6), 115.6 (C-3'), 121.2 (C-5), 131.9 (C-4), 137.9 (C-2'), 143.9 (C-1) and 146.5 (C-2).

Chemical Modification of Eugenol (1)

Methylation

Eugenol **(1)** (0.10 g, 0.61 mmol) was mixed with CH3I (0.15 g, 24.1 mmol) and K2CO3 (2.0 g) in acetone (10 mL) and refluxed for 10 h. The reaction mixture was then filtered and concentrated. The concentrated product was extracted with EtOAc (3×10 mL). The combined EtOAc extracts was dried over anhydrous MgSO4, filtered and evaporated to dryness to give methyl eugenol as a yellow liquid (0.054 g, 53.8%) and R_f 0.60 (hexane:EtOAc/90:10). IR (ATR) v_{max} cm^{-1}: 3075 (C- H sp^2), 2936 (C-H sp^3), 1638 (C=C olefinic), 1511 and 1463 (C=C aromatic), 1260 (C-O); ^{1}H NMR δ (CDCl3): 3.36 (2H, d, *J=6.8* Hz, H-1'), 3.88 (3H, s, OCH3), 3.89 (3H, s, OCH3), 5.05 (2H, m, H-3'), 5.98 (1H, m, H-2'), 6.72 (1H, s, H-3), 6.83 (1H, d, *J=8.0* Hz, H-5), 6.87 (1H, d, *J=8.8* Hz, H-6). ^{13}C NMR δ (CDCl3): 39.9 (C-1'), 55.8 (OCH3), 55.9 (OCH3), 111.3 (C-3), 111.9 (C-6), 114.2 (C-3'), 121.2 (C-5), 132.6 (C-4), 137.8 (C-2'), 143.9 (C-1) and 146.4 (C-2).

Acetylation

Eugenol **(1)** (0.1042 g, 0.61 mmol), acetic anhydride (0.1299 g, 1.24 mmol) and pyridine (0.1356 g, 0.062 mmol) were stirred overnight. The organic layer was extracted with CH2Cl2 (3x5 mL) and dried over anhydrous MgSO4. The organic layer was then evaporated to dryness to give eugenol acetate **(3)** (0.0913 g, 87.6%) as a yellow liquid and R_f 0.62 (hexane:EtOAc/90:10). IR (ATR) v_{max} cm^{-1}: 3077 (C-H sp^2), 2939 (C-H sp^3), 1762 (C=O), 1638 (C=C olefinic), 1604 and 1508 (C=C aromatic), 1267 (C-O); 1H NMR δ (CDCl3): 2.32 (3H, s, CH3COO), 3.39 (2H, d, *J=6.3* Hz, H-1'), 3.83 (3H, s, OCH3), 5.14 (2H, m, H-3'), 5.97 (1H, m, H-2'), 6.79 (1H, dd, *J=8.4*, and *J=2.4*, H-5), 6.81 (1H, d, *J=2.4* Hz, H-3), 6.97 (1H, d, *J=8.4* Hz, H-6). ^{13}C NMR δ (CDCl3): 20.7 (CH3), 40.1 (C-1'), 55.8 (OCH3), 112.7 (C-3), 116.2 (C-3'), 120.7 (C-5), 122.5 (C-6), 137.0 (C-4), 137.9 (C-2'), 139.0 (C-1), 150.8 (C-2) and 169.3 (C=O).

Antibacterial Test

The tested microorganisms were Gram-positive and Gram-negative bacteria namely *Bacillus subtilis* ATCC 6633 and *Escherichia coli* ATCC 9027. The essential oil, eugenol **(1)**, methyl eugenol **(2)**, and eugenol acetate **(3)** were tested for antibacterial activity. Each sample was dissolved in DMSO to make 1.8 mg/mL stock sample. Disc of Streptomycin sulphate was used as the positive control while DMSO as the negative control. The McFarland reference was prepared by adding sulphuric acid (1% into broth nutrient) and hydrated barium chloride (1% into broth nutrient) (0.05 mL) in a covered vial and left at room temperature. The antibacterial tests were carried out through MIC (Minimum Inhibitory Concentration) and MBC (Minimum Bactericidal Concentration) method. The nutrient agar (20 g) and nutrient broth (8 g) were prepared by dissolved it with 1000 ml of distilled water. Then, the prepared solution were autoclaved for 2 hours 30 minutes at 50°C. The nutrient agar solution (5 mL) was pipetted into the agar plates. The agar plates were then kept in the refrigerator.

Antioxidant Activity

The essential oil, eugenol **(1)**, methyl eugenol **(2)** and eugenol acetate **(3)** were measured for antioxidant activity by observing the change of purple colour solution of DPPH (diphenylpicrylhydrazyl). The sample solution was prepared by dissolving each sample (1 mg) in methanol (1 mL) to produce a concentration of 1000

ppm. The dilution from the stock solution were prepared in concentration of 100 ppm, 80 ppm, 60 ppm, 40 ppm, 20 ppm and 10 ppm. The purple colour solution of DPPH was prepared by dissolving DPPH (4 mg) in methanol (100 mL). The sample solution (100 µL) was added to the DPPH solution (100 µL) in a sample well. Sample which bleached the purple colour to yellow was considered active as DPPH radical scavenging.

RESULTS AND DISCUSSION

The Chemical Composition of Piper betle Oil

The GC and GC-MS analysis of this oil have been yielded thirty constituents. The compounds identified in the *P. betle* oil were six phenylpropanoids (40.38 %), three monoterpenes (0.15 %), and twenty one sesquiterpenes (38.95 %). Phenylpropanoid was the most dominant group in the oil of *P. betle* leaf with eugenol (1) (32.64 %) being the main component. Sesquiterpenes such as elemol (24.92 %), α-cadinol (4.97 %), γ-elemene (1.60 %), and Germacene D (2.43 %) were the most abundant constituents in *P. betle* leaf oil. While for monoterpenes, the compounds present in the oil were camphene (0.04 %), *cis*-ocimene (0.03 %), and linalool (0.08 %).

Chemical Constituents of Piper betle Leaf Oil

Eugenol (1) was isolated as a yellow liquid with a strong smell of clove. The TLC analysis displayed a single yellow spot with R_f value 0.61 in hexane:EtOAc (90:10). The IR spectrum showed a strong broad band at 3516 cm^{-1}, indicating the presence of hydroxyl group which was confirmed by an absorption band at 1264 cm^{-1} attributed to C-O. The bands at 1612 cm^{-1} and 1431 cm^{-1} were assigned as C=C of aromatic stretching, while the C=C olefinic stretching was represented by a band at 1638 cm^{-1}.

The ^1H NMR spectrum displayed two singlets at δ 3.91 and δ 5.85 corresponding to methoxyl and hydroxyl groups, respectively. The presence of an allylic side chain was confirmed by the signal resonance at δ 3.39 (2H, d, *J=6.8 Hz*), 5.18 (2H, m) and 6.04 (1H, m) corresponding to H-1', H-3' and H-2', respectively. The ^1H NMR spectrum also showed a doublet at δ 6.96, *J=2.0* Hz attributed to aromatic proton H-3 while two mutual coupling aromatic proton of H-5 and H-6 were represented each by signal at δ 6.76 (dd, *J=8.4* Hz and *J=2.0* Hz), and δ 6.94 (d, *J=8.4* Hz). The ^{13}C NMR spectrum showed the presence of 10 carbons with a methoxyl carbon at δ 55.9, and the aromatic carbons (C-3, C-5 and C-6) resonated at δ 111.1, δ 114.3 and δ 121.2, respectively. The three allylic carbons resonated at δ 39.9 (C-1'), δ 137.9 (C-2') and δ 115.6 (C-3'). The quaternary carbons, C-1, C-2 and C-4 were observed at δ 143.9, δ 146.5 and δ 131.9, respectively.

Chemistry of Eugenol (1)

Eugenol (1) was subjected to methylation, and acetylation reaction which resulted in methyl eugenol (2), and eugenol acetate (3).
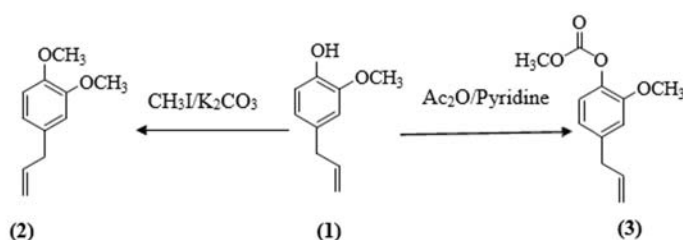
Methyl Eugenol (2)

Methylation of eugenol with CH_3I in the presence of K_2CO_3 as base yielded methyl eugenol as a yellow liquid (0.054 g, 53.8%) %) and R_f 0.60 (hexane:EtOAc/90:10). The mild base, K_2CO_3 abstracted the hydrogen of the hydroxyl group to form the phenoxide ion which undergo S_N2 reaction with methyl iodide to form (2). The IR spectrum of (2) exhibited the disappearance of OH absorption band at 3516 cm^{-1}. The ^1H NMR spectrum confirmed the formation of compound (2) by exhibiting two singlet signals at δ 3.88 and δ 3.89 corresponding to two methoxyl groups. In addition to this, the aromatic protons signals were observed at δ 6.72 (1H, s, H-3), 6.83 (1H, d, *J=8.0* Hz, H-5) and 6.87 (1H, d, *J=8.8* Hz, H-6). The ^{13}C NMR spectrum further

confirmed the success of methylation reaction by showing two signals at δ 55.8 and 55.9 attributed to two methoxyl groups.

Eugenol Acetate (3)

Treatment of eugenol (1) with acetic anhydride in pyridine has affored eugenol acetate as a yellow liquid (0.0913 g, 87.6%) and R_f 0.62 (hexane:EtOAc/90:10). The IR spectrum of (3) showed the presence of an absorption band at 1762 cm^{-1} corresponding to an acetyl function. The presence of the acetyl group was further supported by the ^{1}H NMR spectrum which showed a singlet at δ 2.32 attributed to three protons of an acetyl group. The dissappearance of hydroxyl signal at δ 5.85 for eugenol (1), have proved that the hydroxyl has been subtitude by the acetyl group. The rest of the signals for protons were similar to eugenol (1). The ^{13}C NMR spectrum displayed a signal at δ 169.3 corresponding to a carbonyl group. Based on these data, (3) was characterised as 4-allyl-2- methoxyphenyl acetate or eugenol acetate. The mechanism occurred when pyridine as a nucleophile attacked the carbonyl of acetic anhydride to form the acetate and pyridinium ions. The acetate ion which acted as a base, abstracted a proton from eugenol (1) to produce the phenoxide ion. The phenoxide ion attacked the pyridinium ion followed by elimination of pyridine to form eugenol acetate (3).

Bioactivity studies of Piper betle

Antibacterial Test

Essential oil, eugenol (1), methyl eugenol (2) and eugenol acetate (3) were examined for antibacterial activity using MIC (Minimum Inhibitory Concentration) and MBC (Minimum Bactericidal Concentration) as the quantitative assays. The essential oil was found to have weak antibacterial activity against *B.subtilis* and *E.coli* with a concentration of 900 ppm. On the other hand, eugenol (1) and its derivatives, methyl eugenol (2) and eugenol acetate (3) were inactive towards the tested bacteria. It might due to the synergistic effect of the components presence in the essential oil contributed to the activity.

Antioxidant Assay

The rapid screening for antioxidant activity was performed on the essential oil, eugenol and its derivatives. DPPH or 1,1-diphenyl-2-picrylhydrazyl radical solution which was purple in colour and have a strong absorption at 517 nm was used for this assay. Sample which able to change the purple to yellow colour of DPPH is claimed to have active radical scavenger of DPPH as the molar absorptivity of DPPH radical at 517 nm decreased due to the odd electron of DPPH radical becomes paired with hydroxylated benzene to form the reduced DPPH-H. As a result, essential oil and eugenol was proven to have an antioxidant activities which the changes of the purple solution were observed. From the **Table 1**, IC_{50} for the essential oil and eugenol were 16.83 μg/mL and 3.03 μg/mL respectively. Eugenol (1) had the lowest IC_{50} value which is 3.03 μg/mL compared to ascorbic acid with IC_{50} = 10.83 μg/mL. It showed that eugenol is a potent antioxidant compared to ascorbic acid and the *P.betle* oil.

Table 1 : IC_{50} values for the samples

Sample	IC_{50} (μg/mL)
Essential oil	16.83
Eugenol	3.03
Ascorbic acid	10.83

CONCLUSION

The hydrodistillation of fresh P. betle leaves afforded the essential oil (2.28 g, 0.64 %) as a yellow oil. The GC and GC-MS analysis of this oil have identified thirty constituents of six phenylpropanoids (40.38 %), three monoterpenes (0.15 %) and twenty one sesquiterpenes (38.95 %). A phenylpropanoid was found to be the main component in 32.64 % of eugenol (1). Camphene, cis-ocimene, and linalool were the compounds of

monoterpenes while elemol, α- cadinol, γ-elemene, and Germacene D represented the class of sesquiterpenes. Purification of the essential oil by column chromatography afforded the compound identified as eugenol (1). Methylation and acetylation of eugenol (1) produced methyl eugenol (2), and eugenol acetate (3) respectively. The essential oil, eugenol (1) and the derivatives were screened for antibacterial and antioxidant activity. For the antibacterial activity, only essential oil showed positive result at concentration of 900 ppm. While for the antioxidant activity, essential oil at IC50 = 16.83 µg/mL and eugenol at IC50 = 3.03 µg/mL, proved that both samples showed positive results on antioxidant assay.

REFERENCES

1. Nikhil Kumar. (2010). Piper betle Linn. a maligned Pan-Asiatic plant with an array of pharmacological activities and prospects for drug discovery. Current Science. Vol. 99, No.7, 922-932.
2. Lin, C.-F., Hwang, T.-L., Chien, C.-C., Tu, H.-Y., & Lay, H.-L. (2013). New Hydroxychavicol Dimer from the Roots of Piper betle. Molecules, 18, 2563-25570.
3. Huang, X. Z., Yin, Y., Dai, J. H., Liang, H., Dai, Y., & Bai, L. (2009). Two New Ceramides from the Stems of Piper Betle L. Chinese Chemical Letters, 21, 433–436.
4. Robert P. Adams. (2007). Identification of Essential Oil Components by Gas Chromatography/Mass Spectrometry, 4th Edition. pg 804.

THE EFFECT OF PH ON THE FORMATION OF NICKEL NANOSTRUCTURES BY CHEMICAL REDUCTION METHOD

Mohd Ridhwan bin Ramdzan and Che Rozid bin Mamat
Department of Chemistry, Faculty of Science, Universiti Teknologi Malaysia, 81310 Johor Bahru

Abstract

The synthesis of nickel (Ni) nanostructures through chemical reduction method using hydrazine ($N_2H_4.6H_2O$) as a reducing agent is reported. It was found the ratio of 6.65 of NaOH over $NiCl_2$ is necessary for the formation of pure nickel nanoparticles. NaOH was used to control the pH of solutions. Field Emission Scanning Electron Microscopy (FESEM) revealed that by varying $[OH-]/[Ni^{2+}]$ molar ratio, various types of Ni nanostructures with size between 20 to 800 nm are obtained. Changing the pH from 8.7 to 9.5 resulted in formation of Ni wool- like nanostructure composed from chain-like nanostructure particles. The presence of nickel nanoparticles was confirmed with phase analysis using X-ray diffraction (XRD). Results show that the formation of pure Ni metal nanoparticles of wool-like nanostructure only occur when $[OH-]/[Ni^{2+}]$ molar ratio was tailored to higher than four.

Keywords: chain-like, wool-like, nickel, nanostructures, nanoparticles

INTRODUCTION

Fascinating shapes and morphologies of nanoscale materials such as nanoparticles, nanorod, nanochain, nanocubes are among the most emerging classes of engineering materials due to its promising application in numerous technological and highly demanding fields such as sensing, biomedical, automotive, electronics, etc. [1-3]. Shape and size have been identified to have close relationship with chemical and physical properties of nanoscale materials. In some cases new properties are realized. The ability to produce nanoscale materials in various shapes and morphologies is becoming the key for further development of nanotechnology.

Pure bulk Ni is a lustrous white, hard and one of the four ferromagnetic elements at room temperature in transition metal group VIII of the Periodic Table. It has high ductility, good thermal conductivity, high strength and fair electrical conductivity. Ni nanoscale materials have received enormous attention due to their unique property in magnetic, thermal, electrical and chemical. It has been proven to have tremendous capability as catalyst, supercapacitor, additives in oil, magnetic carriers for biomedical and others [1,4-6]. Recently, synthesis of Ni in unique morphologies has becoming an interesting research because of the potential improvement of properties such as in chemical, electrical and magnetic. In some cases the new shape and morphologies create new properties which are differing when they are in spherical shape. Ni has been synthesized in various morphologies for instant, nanocubes, nanowires, flower-like, sea urchin-like and bowl-like [7-11].

In the synthesis of nanoscale materials, bottom-up approach is the most commonly used method. Bottom-up approach is a piecing together of system to a bigger system which usually involve chemical reaction such as wet chemical synthesis. Chemical reaction method has been extensively used as the synthetic method of producing nanomaterials with an advantage of more controllable of as-synthesized products. Utilizing this method, the preparation of nanoparticles can be achieved through various methods. Typical preparation chemical reaction method for Ni nanoscale materials includes polyol, microemulsion, microwave assisted and sol-gel [12-15]. Chemical reaction method requires consideration of several synthetic parameters for instant temperature, reaction time, reactants concentration etc. Wu et al. (2003) reported that Ni nanoparticles can only be obtained with appropriate amount of NaOH.

Ni nanostructure is structures that consist of Ni nanoparticles usually spherical in shape that self-assemble to form new structures. This unique phenomenon of self-assemblies, act differently depending on method of preparations. Under certain environment Ni nanoparticles tend to form secondary particles which are the results of van der Waals attractive forces and magnetic dipole interactions as well as thermodynamic driving force [17,18]. Different morphologies of nanoscale materials are normally associate with growth orientation direction. Chen et al. (2012) discovered that flower-like Ni structure is actually composed of sword-like petal particles that grows along (011) direction [19].

This work reports the effect of the pH to the shape and morphologies of as-synthesized particles by tailoring $[OH^-]/[Ni^{2+}]$ molar ratios using chemical reduction method. Investigation on the effect of pH on its shape and morphology will also be reported.

EXPERIMENTAL

Materials

All reagents are analytical grade and are used as received. Hydrazine hydrate 50% v/v, nickel chloride $NiCl_2.6H_2O$ and sodium hydroxide powder NaOH are bought from Sigma- Aldrich company.

Preparation of Ni nanoparticles

To prepare the Ni nanoparticles, chemical reduction method of nickel salt ($NiCl_2$) by strong reducing agent, hydrazine hydrate in the aqueous solution are used due to better structural control on the microscopic level and low reaction temperature. The molar ratio of N_2H_4/Ni^{2+} poured is 4.5 whereas that of $NaOH/Ni^{2+}$ is 2.66.
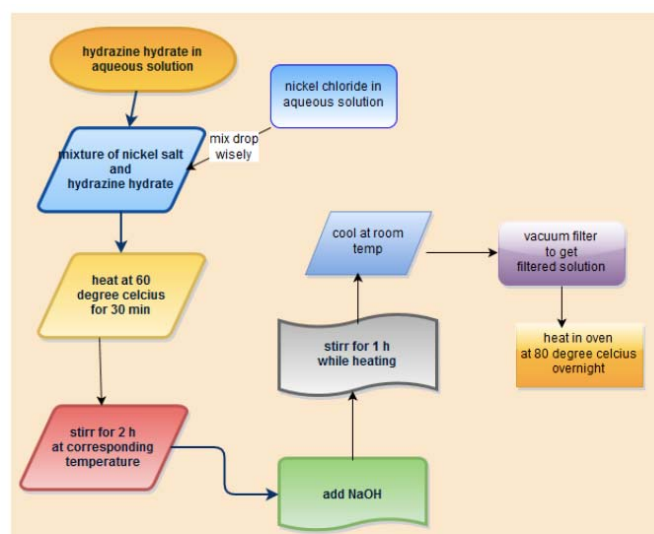
Figure 1: Process of synthesizing nickel nanoparticles product.

To be precise, 0.2 molar nickel chloride ($NiCl_2$) solutions are produced by diluting 0.5 g of nickel chloride solid salt with 10.517 mL of deionised water in a 25 mL beaker. 0.9 molar hydrazine hydrate (N_2H_4) are produced by diluting 2.12 mL N_2H_4 of 50% v/v concentration, 2.13 gcm^{-3} density, 40 $gmol^{-1}$ with deionised water to make it 25 mL of solution in 50 mL beaker. The determining factor in producing nickel nanoparticle size is the amount of basic sodium hydroxide (NaOH) to alter reaction pH. 0.532 molar NaOH solutions are prepared by diluting 0.4 g NaOH powder with deionised water and are made to have 18.8 mL of NaOH solution in a 25 mL beaker. Second NaOH solution is made to increase NaOH power by 0.2 g to increase pH properties. The addition of 0.2 g NaOH powder is repeated for third, fourth and fifth solution.

$NiCl_2$ salt is mixed with deionised water in 50 mL beaker and shaken well. The salt solution is then put into 50 mL burette. Salt solution is poured drop wise from the burette into an appropriate amount of hydrazine hydrate (N_2H_4) taken into a flask of 250 mL. The solution of nickel salt and hydrazine hydrate are heated at 60°C for 30 min. The violet solution thus obtained is stirred for 2 h by using magnetic stirrer. An appropriate amount of NaOH is poured at corresponding reaction temperature and stirred again for an hour. The reduction reaction that takes place may be expressed by the following equation (Eq. 1).

$$2Ni^{2+} + N_2H_4 + 4OH^- \rightarrow 2Ni + N_2 + 4H_2O \tag{Eq. 1}$$

The violet solution turned black in 10–15 min due to reduction reaction. The bluish- violet solution was obtained when the mixture of nickel chloride, $NiCl_2$ aqueous and hydrazine hydrate, N_2H_4 aqueous was heated for 30 min. The solution turns black when heated after the addition of sodium hydroxide, NaOH aqueous.

Figure 2: Bluish-violet solution

The resulting black coloured slurry is washed with deionised water repeatedly. The washing process is done in vacuum filtration filter filled with micron size filter paper before sucking process is done. The solid residue is vacuum filtered just after repeated washing with deionised water is done. Filtered nanopowder are placed in 1.5 L beaker and dried in the oven overnight at 80oC. Next day the dried powder is first crush into pieces using glass rod and taken into vial.

Characterization of Nickel nanoparticle

The particle sizes are determined by field emission scanning electron microscopy (FESEM) using a JEOL Model of JSM-6701F at 1nm (15kV) located at Institute of Ibnu Sina (IIS), Universiti Teknologi Malaysia Johor Bahru. FESEM is an ultra high resolution FESEM suitable for observation of fine structures of nickel nanoparticles.

XRD measurements are performed on a Bruker D8 Advance diffractometer which is licensed under Lembaga Perlesenan Tenaga Atom (LPTA) and is located in the Ibnu Sina Institute, Universiti Teknologi Malaysia Johor Bahru, using CuKα radiation (λ = 0.1542 nm). The samples for XRD analyse is obtained by recovering the nickel nanoparticles from solution using a permanent magnet, then ishing the precipitates using ethanol, and finally vacuum drying at room temperature.

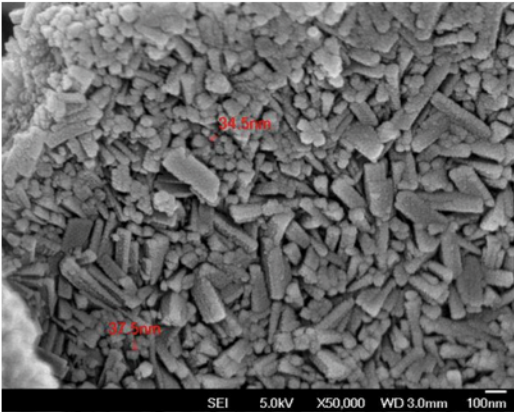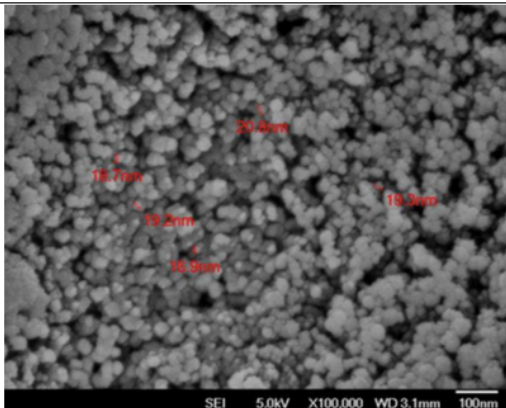**RESULTS AND DISCUSSION**

Formation of Ni nanoparticles

It is found that the addition of trace NaOH solution is necessary for the formation of pure nickel nanoparticles in an optimum reaction temperature of 60°C which is quite helpful in accelerating the reaction rate. It is found that the formation of nickel nanoparticles might be completed within 1 h at 60°C, but the reaction is not complete at 25 °C, even after 2 weeks. Therefore, the reaction temperature is set at 60-63°C in this work by using a digital hot plate to control the temperature.

The required molarity ratio of NaOH over $NiCl_2$ was raised from 2.66 to 6.65 by adding 1.0g of NaOH in the fourth trial as pH adjuster throughout the reduction reaction of nickel salt. The role of trace NaOH in the synthesis of Ni nanoparticles is quite interesting. The addition of trace NaOH led to the increase of solution pH from 8.7 to 9.5. It is suggested that the trace NaOH might act as a catalyst for the pure nanoparticle formation of nickel. Further investigation is necessary.

Particle size and structure   Field emission scanning electron microscopy analysis (FESEM)

A typical FESEM micrograph and the size distribution for the nickel nanoparticles are shown in Table 4.1. Sample one(1) and four(4) having pH value of 8.7 and 9.5 respectively were charazterized by FESEM at Institute of Ibnu Sina.

Table 1: FESEM structure and morphology sample 1 and 4.

Sample	Structure of nickel nanoparticle sample
1	

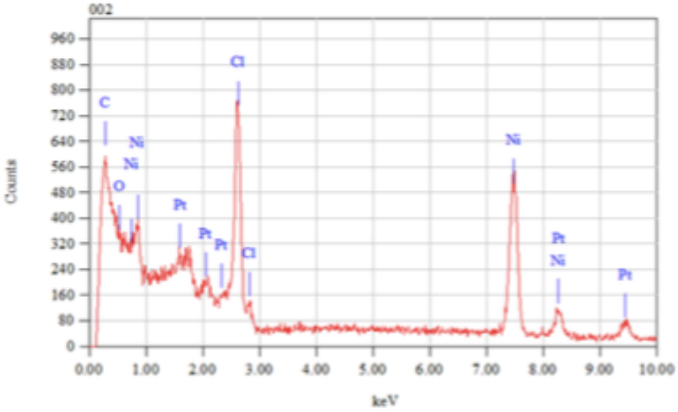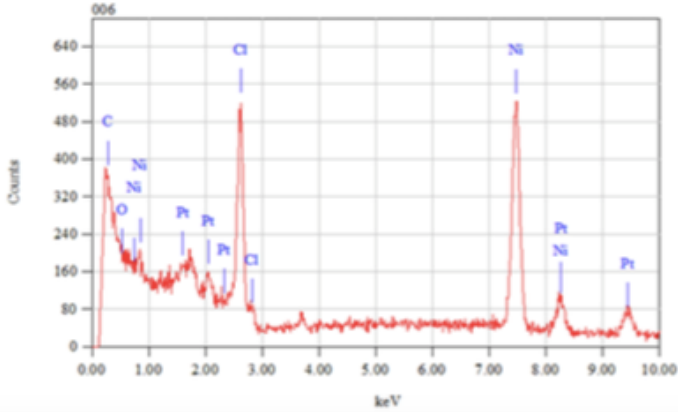| Sample	Structure of nickel nanoparticle sample
4	

The effect of OH^-/Ni^{2+} molar ratio on synthesized nanoparticles were investigated to study the effect on the reduction of Ni^{2+} ions, particles size distribution and morphology. FESEM micrographs of the particles obtained after reduction are shown in Table 1. The morphology of the starting $Ni(OH)_2$ precursor (a) corresponds to long needle-like particles at 8.7 pH value. Upon reduction at higher pH value which is 9.5, the particle shape changed (b). This result correlates well with the XRD data, a clear indication that sample one(1) contains $Ni(OH)_2$ precursor (i.e. elongated shape) while the Ni^0 nanoparticles is produced at higher pH value which is 9.5 for sample four(4) (i.e. round shape).

Besides, based on FESEM micrograph, higher molar ratio of OH^-/Ni^{2+} of sample four(4) resulted in the formation of Ni^0 precursor with smaller size. Sample four(4) has an average particle size of 19 nm which is smaller compared to sample one(1) which having particles of 36 nm averagely. Thus, it can be concluded that higher pH value of the reaction cause the formation of smaller particles during reduction reaction.

Energy Dispersive X-ray analysis (EDX)

EDX analysis was performed for sample one(1) and sample four(4) having pH value of 8.7 and 9.5 respectively to analyse elemental composition in both samples. Peaks of elements in both sample can be seen in Table 2.

Table 2: EDX analysis of sample one(1) and sample four(4).

Sample	Structure of nickel nanoparticle sample
1	
4	

Based on EDX analysis shown above, nickel element is exist in both samples. The presence of other metal such as platinum is due to the coating purpose when doing sample preparation for FESEM and EDX analysis. Nickel counts for both sample is also the same due to the same amount of nickel chloride concentration used for nickel nanoparticles synthesis process.

The presence of chloride ion Cl^- can be observed at both samples in EDX analysis. But rather, chloride ion counts of sample four(4) is lower than sample one(1) which indicates the more successful in reduction reaction while sodium chloride, NaCl solid is formed as a side product which then filter away by filter paper. Cl^- ion is still found in both sample is due to incomplete reduction reaction. This is believed due to the intensity of stirring process. The reduction reaction was performed with moderate stirring mechanism for all samples (intensity of 5 out of 10). Stronger stirring is needed to ensure complete reduction reaction. According to chemistry theory, more collision ensure better reaction which in this case is not that explain the existance of Cl^- ion in the sample.

X-ray diffraction analysis (XRD)

Sample one(1) of nickel nanopowder having 8.7 pH value is analysed by Bruker D8 Advance diffractometer using CuKα radiation (λ = 0.1542 nm) at 2θ in the range of 20º until 80º.
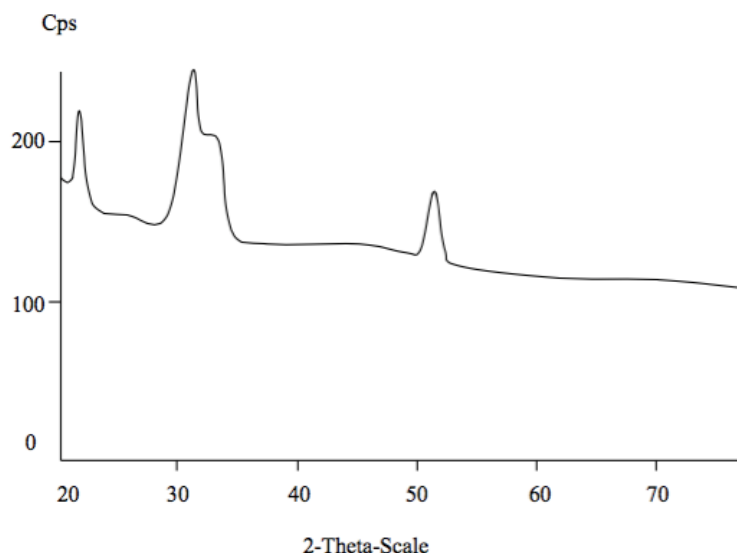
Figure 3: XRD peaks of sample one(1) at pH 8.7 (+0.0 g NaOH)

Based on the diffractogram shown above, major peaks are observed at around 21.948o and 31.337o which indicates the presence of $Ni(OH)_2$ precursor. Peak assigned to Ni^0 is seen only at 51.093° having 200 crystal lattice structure.
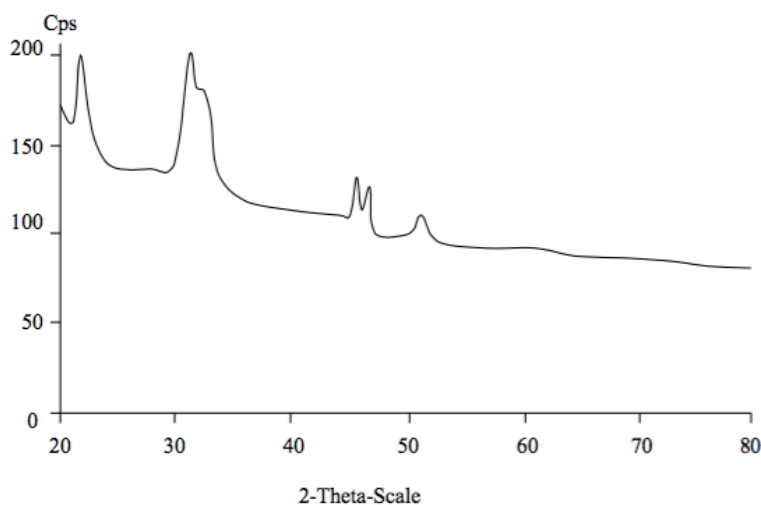

Figure 4: XRD peaks of sample four(4) at ph 9.5 (+0.6g NaOH)

Based on the spectrum above, major peaks are observed at around 21.943o, 31.235o, 32.510o, 45.445o and 51.275o. $Ni(OH)_2$ precursor are observed at 21.943o, 31.235o and 32.510o which are quite similar with peaks observed at sample one diffractogram. On the other hand, the peaks assigned to Ni^0 precursor are observed for sample four(4) at diffraction line of 45.445o, 51.275o. Pure Ni^0 was the only product observed for sample four(4), thus indicating that the reduction process leading to the formation of Ni^0 requires higher $NaOH/Ni^{2+}$ molar ratio.

Better Ni^0 precursor was found in sample 4 four(4) having 111 lattice structure. Ni^0 precursor having 200 lattice structure is also observed in sample four(4). As a conclusion, higher pH value in sample four(4) leads to the formation of Ni^0 precursor having 111 lattice structure. Ni^0 precursor at 45.445° is better than Ni^0

150

precursor at 51.275° due to the fast that 111 structure is higher in surface area. This criteria provide higher activity in term of catalysis in application scope.

Effects of sodium hydroxide on nickel nanoparticle crystal formation

Base on XRD spectra between sample one(1) and four(4), it is found that the addition of trace NaOH solution is necessary for the formation of pure nickel nanoparticles and an elevated reaction temperature of maximum 60oC is quite helpful in accelerating the reaction rate. It is found that the formation of nickel nanoparticles is completed within 1 h at 60oC, but the reaction is not complete at 25oC, even after 2 weeks. No nickel nanoparticle formation will happen even after one month of heating at 25oC.

Besides, adding extra NaOH molarity affect the formation of nickel nanoparticles precursor. This can be observed on the differences of sample four(4) and sample one(1) diffractograms. Sample four(4) contain diffraction lines of Ni^0 precursor while non is observed on sample one(1) diffractogram. It can be concluded that NaOH plays an important role in forming pure nickel nanoparticle formation and also as pH adjuster throughout the reaction.

CONCLUSION

Nickel nanoparticles have been synthesized by the hydrazine reduction of nickel chloride at 60°C without soluble polymer as a protective agent. It is found that the addition of trace NaOH is necessary to form pure nickel nanoparticles precursor. The resultant particles have been characterized to be nickel amorphous structure by XRD. Nickel nanoparticle size is observed by FESEM to be around 36nm in sample one while 20 nm in sample four. The determining factor is the molarity of NaOH which identify NaOH is crucial to enhance the reaction rate thus forming difference nanostructures at difference pH. At 9.5 pH value of higher $NaOH/Ni^{2+}$, FESEM reveals the existance of 111 Ni^0 precursor. Stirring intensity also affect the reduction reaction in producing nickel nanoparticles.

REFERENCES

1. Stixrude, Lars; Waserman, Evgeny; Cohen, Ronald (November 1997). "Composition and temperature of Earth's inner core". Journal of Geophysical Research (American Geophysical Union) 102 (B11): 24729–24740.
2. Derek G. E. Kerfoot (2005), "Nickel", Ullmann's Encyclopedia of Industrial Chemistry, Weinheim: Wiley-VCH, doi:10.1002/14356007.a17_157
3. Kittel, Charles. (1996). Introduction to Solid State Physics. Wiley. p. 449.
4. Keith Lascelles, Lindsay G. Morgan, David Nicholls, Detmar Beyersmann "Nickel Compounds" in Ullmann's Encyclopedia of Industrial Chemistry 2005, Wiley-VCH, Weinheim. doi:10.1002/14356007.a17_235.pub2
5. Greenwood, Norman N.; Earnshaw, Alan (1997). Chemistry of the Elements (2nd ed.). Butterworth-Heinemann. ISBN 0080379419.
6. Kuck, Peter H. "Mineral Commodity Summaries 2012: Nickel" (PDF). United States Geological Survey. Retrieved November 19, 2008.
7. Kuck, Peter H. "Mineral Yearbook 2006: Nickel" (PDF). United States Geological Survey. Retrieved November 19, 2008.
8. Davis, Joseph R (2000). "Uses of Nickel". ASM Specialty Handbook: Nickel, Cobalt, and Their Alloys. ASM International. p. 7–13.
9. Keith Lascelles, Lindsay G. Morgan, David Nicholls, Detmar Beyersmann "Nickel Compounds" in Ullmann's Encyclopedia of Industrial Chemistry 2005, Wiley-VCH, Weinheim.
10. Baucom, E. I.; Drago, R. S. (1971). "Nickel(II) and nickel(IV) complexes of 2,6- diacetylpyridine dioxime". Journal of the American Chemical Society 93 (24): 6469.
11. Mond, L.; Langer, K.; Quincke, F. (1890). "Action of carbon monoxide on nickel". Journal of the Chemical Society 57: 749–753.
12. Faraday, M. (1857) Philos. Trans. R. Soc. London , 147 , 145 – 181.
13. Turkevich, J., Stevenson, P.C., and Hillier, J. (1951) Discuss. Faraday Soc. 11, p. 55 – 75.
14. Rheenen, P.R.V., McKelvy, M.J., and Glaunsinger, W.S. (1987) J. Solid State Chem. 67, p. 151–169.
15. Henglein, A. (1989) Chem. Rev. , 89 , p. 1861 – 1873.
16. Burda, C., Chen, X., Narayanan, R., and El-Sayed, M.A. (2005) Chem. Rev. , 105 , p. 1025 – 1102.
17. Liz-Marzán, L.M. (2006) Langmuir , 22 , p. 32 – 41.
18. Sugimoto, T. (2000) Fine Particles: Synthesis, Characterization, and Mechanisms of Growth, Surfactant Sci. Series Vol. 92, Marcel Dekker Inc., New York.
19. Lea, M.C. (1889) Am. J. Sci., 37, p. 476 – 491.

20. Yamaguchi, Y. (2008) Kagakukougaku, 72, p. 344 – 348.
21. Stoeva, S., Klabunde, K.J., Sorensen, C.M., and Dragieva, I. (2002) J. Am. Chem. Soc., 124, p. 2305 – 2311.
22. Lee, S.C. (2005). Synthesis, Characterisation and Catalytic Properties of Titanium Containing Silica Aerogel. Universiti Teknologi Malaysia: Master thesis.
23. Zainal Arifin et. al. (2001). Workshop on qualitative XRD phase identification. School of Material & Mineral Resources Engineering, Engineering Campus, Universiti Sains Malaysia. p. 1-11.
24. Ekhsan, J. (2009). Effect of titanium loading on physical properties and catalytic performance of phosphate-vanadia impregnated silica. Universiti of Teknologi Malaysia: Bachelor Thesis.
25. Parida, K. M., Sahu, N., biswal, N. R., Naik, B., Prandhan, A. C. (2008). Preparation, characterisation and photocatalytic activity of sulphate-modified titania for degradation of methyl orange under visible light. Journal of Colloid and Interface Science. 318. p. 231-237.

HYDRATION AND PROPERTIES OF BLENDED CEMENT SYSTEM INCORPORATING AEROGEL

Mohd Ikram Nul Hakim Bin Baharom and Che Rozid Bin Mamat
Department of Chemistry, Faculty of Science, Universiti Teknologi Malaysia, 81310 Johor Bahru.

Abstract

The utilization of supplementary cementing materials (SCMs) to produce economical cement that is cheaper and greener is an ongoing issue. The objectives of this study are to determine the effect of SCMs on the hydration and properties of blended cement. In this study, OPC was improvised by addition of GGBS and RHA with different weight percentages. Both types of respective were added with 1%, 2% and 3% of aerogel to improve its strength and hydrated for 7 and 28 days. The specimens was characterized by using compressive strength test, FTIR, FESEM, XRD and TGA techniques. The compressive strength test show all specimens have increase in strength for 7 and 28 days in which the composition of OPC-GGBS with 1% aerogel shows the highest compressive strength at early hydration. FTIR shows the functional group present in the OPC- GGBS-Aerogel and OPC-RHA-Aerogel blended cement which are the water lattice of CH, CSH and CASH. The hydration product formed such as CH, CSH and ettringite were observed by using FESEM having plated shaped, foil honey-comb and fine needle-like crystal structure respectively. The formation of the hydrated was confirmed by XRD technique. The TGA technique indicates that there were 3 stages of percentage decomposition of weight loss occur on both type of specimens associated with aerogel.

Keywords: SCM, GGBS, RHA

INTRODUCTION

Cement have many properties that contribute to its strength setting and quality. These properties is assessed and control by measuring the parameter involved such as compressive strength of cement , surface area, particle size distribution, fineness and mineral composition. The production of cement is very expensive nowadays. The rapid growth in construction industry increase the demand on cement production. The cement industry is considered to be one of the most energy consuming industries, with a high rate of carbon dioxide (CO_2) emissions. Every year, it is responsible for approximately 5% of the global manmade CO_2 emissions [1]. Supplementary cementing materials (SCMs) is a proven material addressing a climate change and clean air. SCMs can be divided into natural materials and artificially mades which both exhibit cementitious properties [2-3]. Some of these materials are called pozzolans (natural), which by themselves do not have any cementitious properties, but when used with portland cement, react to form cementitious compounds. Artificial SCMs have been investigated before, such as fly ash, rice husk ash, and silica fume. Their utilization has been an interesting subject of research for economic, environmental and technical reasons. When different material replaced, each materials possess different chemical and mineralogical compositions as well as different particle characteristics that have various effect on the properties of cement and concrete [4].

EXPERIMENTAL

Materials

The material that used in this study were Type 1 OPC, manufactured by Tasek Cement Corporation Berhad with 340 m2/kg specific surface. GGBS with 465 m2/kg specific surface area manufactured by YTL Cement Berhad. RHA that have been burn at 650-700 °C with excess air. Aerogel was synthesized by sol gel method followed by supercritical carbon dioxide drying.

Characterization of Blended Cement

Compressive Test Machine

The mixture of different composition blended cement were prepared by 50 mm x 50 mm x 50 mm cubes. The compressive strength test was done in accordance with ASTM C109/C109M [35]. After 24 hours, the test specimens were demolded and then cured in water. Three cubic test specimens were made from each mixture, covering two different ages of 7 and 28 days.

X-Ray Diffraction (XRD)

Phase purity and crystallinity of the samples were determined by XRD using a powder diffractometer with Cu K_α as the radiation source with λ = 1.5418Å. The X-ray tube voltage and current were fixed at 40 kV and 40 mA, respectively. The scan step size was 2θ in the range from 5° to 80° and the reflection position and δ-spacing were calculated from the raw data using automated data analysis programs.

Fourier Transform Infrared Spectroscopy (FTIR)

KBr technique was used. About 1/100 of sample to KBr ratio was taken by using microspatula and teaspoons respectively. Next mix both throughly in a mortar while grinding with the pestle. A force of approximately 10 ton was applied under vacuum for 2 minutes to form transparent pellet. Then, the pellet formed was inserted in the pellet holder and go into the sample chamber. Lastly the measurement was performed and the IR spectra was observed.

Field Emission Scanning Electron Microscope with Energy Dispersive X-ray spectroscopy (FESEM-EDX)

FESEM equipped with energy dispersive X-ray spectroscopy (EDX) was used to analyze the surface morphology and elemental information of the cement paste. A small fractured sample was soaked in acetone to stop hydration and dried at 80°C for 2 h. Then the sample was coated with 20 nm of gold to make it conductive. The accelerating voltage was set at 10 kV.

Thermogravimetry Analysis (TGA/DTA)

The percentage decomposition OPC-GGBS-aerogel and OPC-RHA aerogel for 28 day was determined using TGA/DTA. The parameter used to operate the TGA was heating rate 20 °C/min under nitrogen atmosphere. The temperature range was 50-900°C.

RESULTS AND DISCUSSION

Compressive Strength Test

The compressive strength of cement paste containing OPC-GGBS-aerogel 1% was greater than others composition due to the high pozzolanic reaction at early age. But when compared to control mix at 28 days the strength of other mix was lesser, this decline was result of low pozzolanic reaction of the SCMs
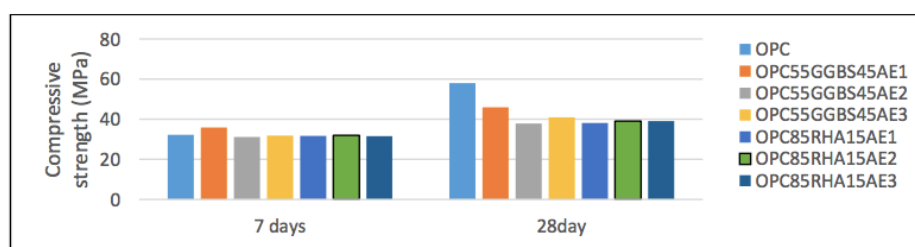

Figure 1 : Compressive strength development for 7 and 28 days

Determination of functional group in blended cement

The broad bands located at 3434 cm^{-1} and 1643 cm^{-1} are assigned to the stretching and bending vibrations of water lattice in CSH, CAH and hydrated calcium sulfoaluminates (CASH) hydrates. The band that appeared around 970 cm^{-1} is attributed to CSH.
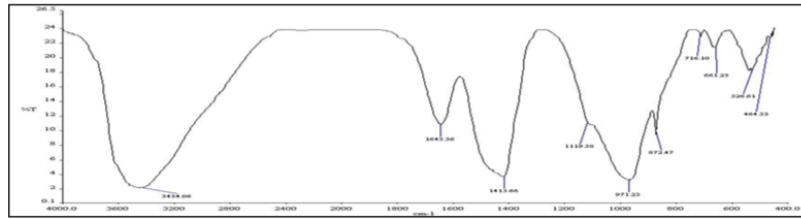
154

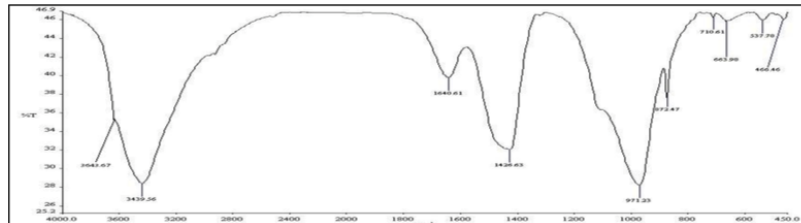**Figure 2** : FTIR spectra of OPC-GGBS-Aerogel 1%

Figure 3 : FTIR spectra of OPC-**RHA-Aerogel 2%**

Morphology Characteristic

There were great deals of plated shaped of CH (a) formed at 28 day. A foil honey-comb structure of CSH are present in the micrograph (b). It is indicate that the hydration reaction occurring. Some of the hydrated product are still surrounded by fine needle-like crystal which reveal a clear improvement in the performance characteristic of cement paste in (d). A large hexagonal shaped crystal CH present that contribute to higher strength in (e)

(a)

(b)
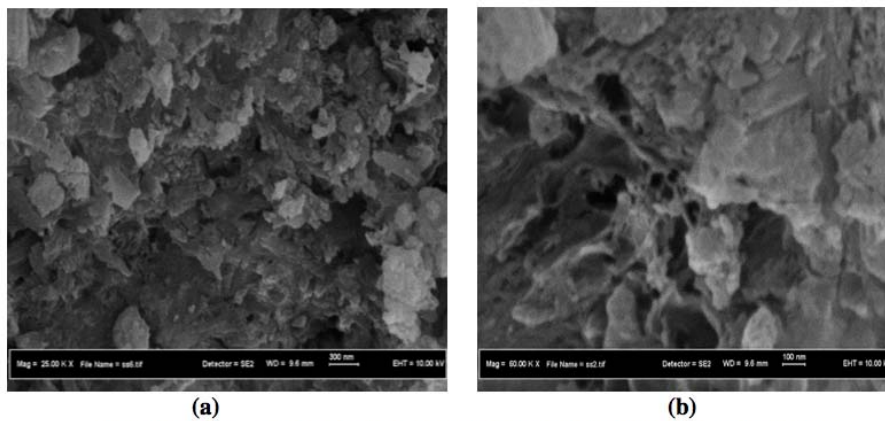
Figure 4 : (a) and **(b)** FESEM images of OPC-RHA-Aerogel 2% at 28 days
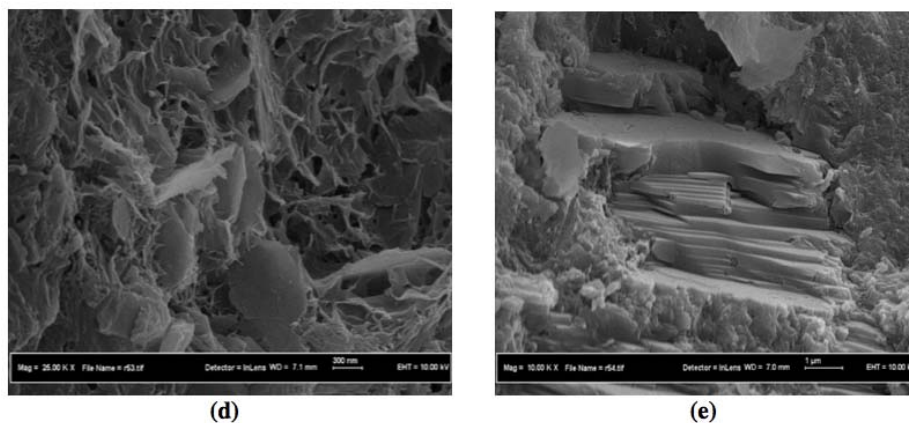

(d)

(e)

Figure 5 : (d) and **(e)** FESEM images of OPC-GGBS-aerogel (1%) at 28 days
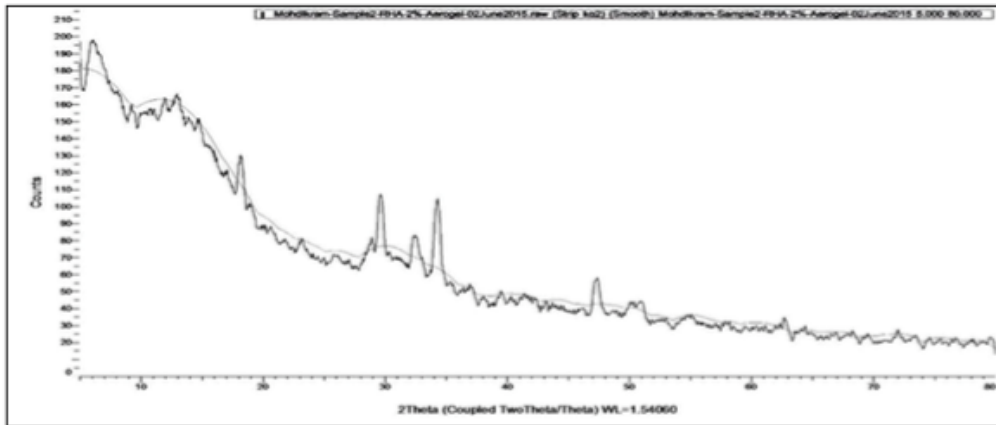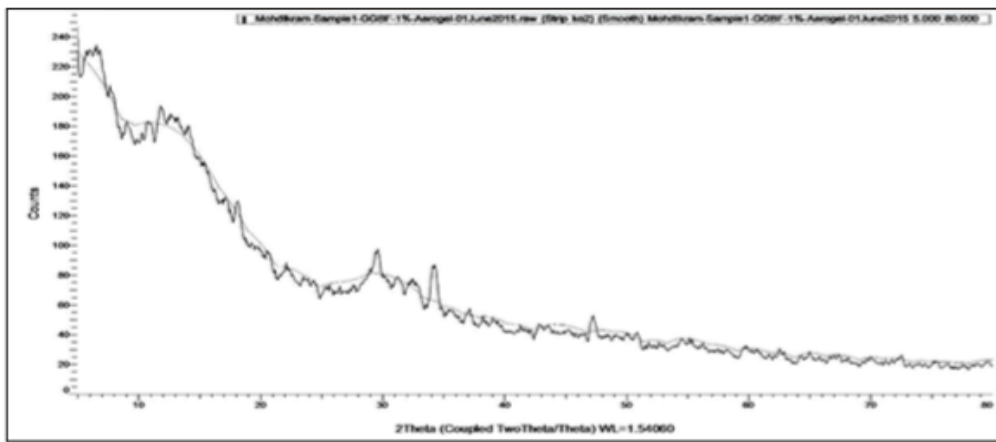
Figure 6 : OPC-RHA-Aerogel 1%

Figure 7 : OPC-GGBS-aerogel 1%

Calcium hydroxide, also known as portlandite (CH), presented at 34.259°, 18.133°, 47.358° and 34.213°, 18.133°, 47.282° in Figure 6 and Figure 7 respectively. The low intensity peak of CH in Figure 7 is due to pozzolanic reaction of the active silica and alumina of the GGBS during hydration to form CSH.

Percentage decomposition of blended cement

The first weight loss for OPC-GGBS-Aerogel 1% was lower than OPC-RHA-Aerogel 2% by 2.51%. This indicate that the amount hydrated product like water, ettringite or CSH was higher. The second weight loss is due to the decomposition of CH. Based on the table, OPC-GGBS- Aerogel 2% has the highest weight loss that is 2.74% that can relate to its strength. Due to the low third weight loss, it can be proved that OPC-RHA-Aerogel 2% has carbonate ion but the amount was low.

Table 1 : Weights loss of sample

Sample	Weight Loss (%)			
	First	Second	Third	Total
OPC-GGBS-Aerogel 1%	21.24	2.74	0.87	24.85
OPC-RHA-Aerogel 2%	23.75	1.86	0.28	25.89

156

CONCLUSION

The uses of SCMs have been experimentally proven to give some effect on the blended cement paste. In this study, OPC have been partially substituted with GGBS and RHA which the percentage of aerogel for both specimen were 1%, 2% and 3%. The sample were characterized by using variety of instruments. From the compressive strength test, all the specimen have increase in strength with curing time. OPC-GGBS-Aerogel 1% has higher strength at early hydration than other mix. Based on the IR spectrum, the main bands located at 3440 cm^{-1} and 1640 cm^{-1} related to the stretching and bending vibrations of water lattice in CSH, CAH and CASH. Another main band appeared around 970 cm^{-1} which attributed to the present of CSH. It is observed from the spectrum that the hydration product are formed. In FESEM images, the structure of hydration product observed. At 28 days, a fine needle-like ettringite was observed followed by hexagonal plate-like crystal that is CH or portlandite. The CSH structure was present as foil honey-comb. In the XRD pattern fine crystalline formation was observed that are CH, CSH and C_3S. Based on the weight loss from TGA, there are 3 main decomposition occur with first decomposition are continuous weight loss start at 100-300°C followed by 450-550°C and lastly 650-900°C. CH decomposition start in the range of 450–550°C. It is proven that GGBS, RHA and addition of aerogel has pazzolanic effect in the cement paste which provide positive result on physical properties of the blended cement.

REFERENCES

1.   Shen, L., Gao, T., Zhao, J., Wang, L., et al. (2014). Factory-level measurements on CO2 emission factors of cement production in China. Renewal. Sustainable. Energy Reviews. 34, 337–349.
2.   V. G. Papadakis, S. Tsimas. (2005). Greek supplementary cementing materials and their incorporation in concrete. Cement & Concrete Composites. 27, 223–230.
3.   V. G. Papadakis, S. Tsimas. (2002). Supplementary cementing materials in concrete Part I: efficiency and design. Cement and Concrete Research. 32, 1525–1532.
4.   S. Targana, A. Olgunb, Y. Erdoganb, V. Sevinc. (2002). Effects of supplementary cementing materials on the properties of cement and concrete. Cement and Concrete Research. 32, 1551–1558.